Evaluation of ultrasonic shear wave propagation in cortical bone by axial transmission technique

Leslie Vanessa Bustamante Diaz

Doshisha University

Graduate School of Science and Engineering

June 2020

ABSTRACT

In developed countries with rapidly aging populations, secondary to diabetes mellitus (DM) and chronic kidney diseases (CKD), fractures due to osteoporosis are on the rise. In 2015, the number of patients with osteoporosis in the country will exceed 12.8 million. Osteoporosis fractures in the elderly people require nursing care most of the time. The total cost of medical and nursing care is 700 billion yen per year. Since, fractures induce a decline in the physical function, it affects not only the motor function but also the internal organ function, and in some cases it is accompanied by a decrease in the bone metabolism. Thus, osteoporosis is likely to lead to a reduction in the quality of life (QOL). Therefore, for a "extension of healthy life expectancy", more accurate diagnosis of "bone strength and stiffness" is required. Here, we developed a simple and safe ultrasonic system for bone assessment that can be used to evaluate in vivo human bone.

Bone deterioration, weakness, and consequent fracture caused by bone diseases, such us Osteoporosis is currently evaluated by measurements of the bone mineral density BMD by energy X-ray absorptiometry (DXA). However, actual bone strength, which is a main factor in the bone fractures, cannot be determined by the amount of bone mineral content in the bones alone. As noted by the National Institutes of Health (NIH), the assessment of bone strength includes bone suppleness, microfractures. The concept of "bone quality", which comprehensively reflects the material properties of bone, is also important. In addition, the early stages of osteoporosis are unconscious, and X-ray methods, which can only be performed in a medical institution, cannot be used and a frequent exposure to radiation is unavoidable to evaluate the progression of osteoporosis. There is a need to quantitatively measure bone data to extract and determine important bone mechanical properties that will lead to understand the bone fracture mechanism and therefore, improve the current in vivo bone evaluation. Since patients with osteoporosis usually have no symptoms before fracture, early diagnosis, and treatment of the disease are of great importance. Bone fractures principally in long bones reduce the life quality of the individuals and could lead to disability.

Noninvasive ultrasonic techniques are ideal for bone evaluation, they are harmless, easy to use, and cost-effective. Ultrasound waves propagating in the bone structure

contain important information closely related to the mechanical properties and bone geometries, for these reasons, they are a great option to quantitatively evaluate bone biomechanical strength.

Importantly, shear wave measurements in bone have not been extensively reported, although such measurements are necessary for a complete bone evaluation. Commonly, loads applied on the skeleton are not only compressive loads (in the direction of the body weigh). Torsion and bending are also observed. Mechanical properties of bone such as shear modulus and torsional strength are related to shear waves and therefore are necessary to know when a bone fracture is suspected. The possibility of measuring shear waves in the cortical bone may yield additional diagnostic information of the material and geometric characteristics of bone.

In this thesis work, Quantitative Ultrasound (QUS) techniques with the advantages of an axial transmission measurement were applied to implement an ultrasonic system for cortical bone evaluation. This evaluation is focused on the measurement and characterization of shear waves propagating in the axial direction of the cortical layer of bone. In order to understand the wave propagation phenomenon, and predict experimental results, simulations using the elastic Finite-difference-time-domain (FDTD) method were implemented. Additionally, shear wave velocities were verified by a simple thought transmission measurement.

Axial transmission experiments were designed to evaluate ultrasonic waves from a very simplified bone geometry to a much closer bone model that considers real features of human long bones. Shear waves were evaluated in bone plates with regular thicknesses, bone tubes with regular thicknesses, and bone samples with irregular shape and thickness with the aim to determine the impact of bone shape, surrounding medium and irregular cortical thickness on the measurements of the shear wave velocity. On the other hand, 2D-FDTD and 3D-FDTD simulations considering isotropic and anisotropic conditions were interrogated as a reliable computational method to simulate the wave propagation and extract precise bone information.

Additionally, the obtained waves from experimental measurements and FDTD simulations were farther analyzed in the frequency domain using the 2D-FFT method.

It was found that wave characterization depended on the incident angle at which the ultrasound was radiated. This dependency is based on Snell's Law. Shear waves were not affected and consistently observed using our method at incident angles larger than 50°, with their measured velocities being highly reproducible despite the bone shape, surrounding medium, and the irregular bone thickness. At the same time, wave velocities were in good agreement to transverse transmission measurements performed in the same samples. Simulations in isotropic and anisotropic models showed to be a reliable approximation to estimate mechanical properties and could be used for bone evaluation. The wave characterization also suggested that apparent longitudinal waves are more sensitive to changes in the cortical bone thickness and bone shape.

The 2D-FFT was able to identify Lamb modes propagating in the plate samples however when the shape and cortical thickness changed these modes were difficult to identify especially, in the experiments.

In this thesis manuscript, principles, basic concepts, techniques, methods, and experimental and simulations results are provided in detail, as well as, discussion of the results and the emerging conclusions.

Chapter II describes the basic principles and properties of long bones used in this work. The complex structure of bone, pointing its mechanical properties is explained. Additionally, the influence of soft-tissue surrounding the bone and the substitute phantoms for ultrasound measurement are analyzed. Osteoporosis epidemiology and the importance of this work is further discussed.

Chapter III intents to give a review of the physics of the waves, focusing on the wave propagation phenomenon in bone and soft-tissue, principally at the interface of these two mediums. Surface and guided waves observed in this work are described.

Chapter IV describes the potential of QUS techniques for clinical application in osteoporosis assessment. Current devices using ultrasound techniques and the advantages of using the axial transmission method are presented. A general description of our system, the measurement method, and signal processing are detailed.

Chapter V focuses on the description of the Finite-Difference Time-Domain method used to simulate the wave propagation. Fundamental equations, simulation conditions necessary to build an FDTD simulation is explained. A general description of the constructions of the 2D and 3D models considering isotropic and anisotropic mediums implemented in this work is detailed.

Chapter VI describes the results of preliminary measurements that were necessary to validate the first hypotheses of this work.

In Chapter VII the evaluation of shear waves in plate samples is presented and the first conclusions of the effective angle for shear wave detection and angle dependence is discussed. Experimental measurements and simulations of the wave propagation in a 2D model considering bone as an isotropic material are compared and discussed. In Chapter VIII we present results of the evaluation of Shear wave velocity in Tube samples, this time the impact of the bone shape and the addition of a mimicking soft-tissue layer is interrogated and compared with plate samples. The simulation is upgraded and present a 3D bone model considering isotropic conditions. Chapter IX presents the results of the evaluation of the shear wave in the case of long bones considering real human bone characteristics. This time the 3D simulation model introduces the bone heterogeneity and anisotropy using computed tomography structures of the bone samples. Conclusion of the impact of bone irregular structure and irregular cortical thickness on the wave velocity are discussed.

Finally, in Chapter X, general conclusions considering the findings in plates, tube bones as well as the long bones are explained. The effectiveness of this proposed method and the evaluation system is discussed.

Results presented in this thesis work suggested the implementation of shear wave measurements for in vivo bone evaluation for a complete and reliable bone diagnosis.

ACKNOWLEDGMENTS

TABLE OF CONTENTS

CHAPTER I GENERAL INTRODUCTION

1.1 BACKGROUND AND MOTIVATION

Bone is a complex solid living material mainly composed of cortical and cancellous bone. Cortical human bone is a shell of anisotropic material, with a heterogeneous and geometrically irregular structure and, an internal hollow filled with bone marrow [1.1]. It is naturally surrounded by soft-tissue, which is highly deformable, and its mechanical properties vary significantly from one person to another.

Bone deterioration, weakness and consequent facture caused by bone diseases, such us Osteoporosis is evaluated mostly relying on X-ray based techniques, which evaluate the bone mineral density (BMD), although BMD methods are good predictors of bone strength, this technique still present problems in determining risk of fracture in certain group of individuals [1.2-1.3]. The importance of bone quality has been highlighted by the National Institutes of Health (NIH). Additional factors are necessary to describe bone elasticity and strength that may be related to properties of the tissue and the bone microstructure itself. According to the World Health Organization (WHO) [1.4] osteoporosis-induced fractures rates increase rapidly with age and are more prone in elderly woman. Osteoporosis is considered as a major public health problem since it affects a large number or individuals. There is a need to quantitatively measure bone data to determine important bone properties that will lead to understand the bone fracture mechanism. In this context, bone structure evaluation is essential to understand the impact of cortical bone loss and therefore prevent an imminent osteoporotic fracture. Bone fractures strongly affect the quality of life of the patient and could lead to disability.

Noninvasive ultrasonic techniques are ideal for bone evaluation, they are harmless, easy to use, and cost-effective. Ultrasound waves propagating in the bone structure contain important information closely related to the mechanical properties and bone geometries, for these reasons, they are a great option to quantitatively evaluate bone biomechanical strength.

In recent years, Quantitative Ultrasound (QUS) techniques have become an effective technique for the evaluation of long bone sites such as radius [1.5-1.8], tibia [1.9-1.10],

femur [1.10-1.11], phalanges [1.12-1.14]. Basically, QUS techniques consist in the estimation of the speed of sound (SOS) and the broadband ultrasound attenuation (BUA) of an ultrasonic wave propagating in bone. Most of the current clinical devices for bone evaluation have been implemented using transverse transmission techniques [1.15-1.17]. However, transverse transmission techniques require a two-sided configuration with transducers placed at opposite sides of the bone, making difficult the measurement of the bone. In contrast, axial transmission (AT) techniques only require a one-sided transducer configuration and can therefore be used to evaluate a greater number of skeletal sites, especially long bones [1.18-1.22].

AT techniques measuring the speed of sound (SOS) of the first arriving signal (FAS) [1.23-1.26] were initially used to characterize bone properties, such as cortical thickness [1.27-1.29] and porosity [1.22, 1.29]. However, FAS velocity was found to be highly dependent on the cortical bone thickness [1.27-1.30]. Therefore, irregular bone structure and thickness could modify the wave propagation and subsequently lead to measurement errors. The FAS velocity was also shown to be affected by thick soft-tissue structures [1.31].

The problem of a fluid-solid layer in terms of guided waves has been numerically studied for a water-aluminum bilayer [1.32]. At the interface of these two mediums, the energy of guided waves leaks from the solid to the fluid in the form of leaky waves. Leaky waves reflecting back at the top boundary of the fluid layer and propagating back to the solid medium are believed to propagate in the whole bilayer structure and consequently change the dispersion characteristics of the guided waves. However, material property characterization has been possible to extract from the bone samples tested [1.33]. Although, water-bone interface differs from the soft tissue-bone interface since water does not sustain the shear stresses whereas soft-tissue does. It has been demonstrated in some studies that both layers of the interface can be considered as independent waveguide structures [1.33-1.34].

Simulations using two- and three-dimensional models, as well as measurements using phantoms, have shown that the wave velocity in bone depends on its thickness relative to the wavelength. When the cortical bone thickness exceeds the longitudinal wavelength in the bone, the FAS corresponds to the lateral wave [1.23, 1.30]. Conversely, the FAS waves can be viewed as a guided S0 Lamb mode when the wavelength is much

greater than the plate thickness [1.30, 1.35]. Under these conditions, the FAS becomes sensitive to the surrounding geometry and is affected by the boundaries of the cortical layer. Additionally, an energetically slower signal arriving after the FAS has been observed to be consistent with the antisymmetric A0 mode [1.36]. For intermediate cases, a complex interference of several types of waves is observed [1.27,1.30]. Importantly, the AT measurements performed in these studies used transducers normal to the bone surface. Moreover, it has been found in several clinical studies that FAS velocity discriminates healthy patient from osteoporotic ones [1.7-1.8].

The possibility of measuring ultrasonic wave modes other than the FAS in cortical bone has been investigated in the last years. [1.37-1.41]

More importantly, measurements related to the shear wave in bone have not been extensively reported although shear waves are necessary for a complete bone evaluation. Commonly, loads applied on the skeleton are not only compressive loads (in the direction of the body weigh). Torsion and bending are also observed. Mechanical properties of bone such as shear modulus and torsional strength are related to shear waves and therefore are necessary to know when a bone fracture has occurred. The possibility of measuring shear waves in cortical bone could yield additional diagnostic information of the material and geometric characteristics of bone.

Simplified geometrical models of bone under ideal conditions are certainly a good approach to understand the actual problem in the human bone evaluation and are useful to give an idea and establish guidelines on how to approach the problem. However, it is important to consider that wave propagation could be affected by the actual bone geometries, the surrounding environment and cortical bone irregularities.

Different axial transmission measurement setups present different sensitivities to this bilayer problem, depending on the frequency bandwidth and other factors not fully understood yet. Therefore, more studies and supportive measurements that consider the impact of bone shape, surrounding medium, irregular cortical bone surface and thickness are required to understand the effects on the wave propagation as it occurs in vivo measurements.

Furthermore, the use of numerical simulations as a surrogate of an in vitro experiment can be an accurate solution to validate experimental observations. The feasibility of model bone geometries, mediums, mechanical properties etc. make

numerical simulations more attractive and extremely useful to guide the interpretation of the wave propagation and the complex ultrasonic signals. Compared to the experimental methods, numerical methods are more versatile and flexible, any configuration or conditions could be tested. Finite difference time domain (FDTD) methods for acoustic wave propagation have been extensible developed for seismic wave simulation [1.1]. The FDTD method consist in obtaining discrete equations whose unknowns are elements of a regular mesh. This method has been used successfully for a wide range of geometrical and material configuration [1.27, 1.30]. However, there is still a lack of geometrical flexibility and the need to search other additional methods to build complicated geometries and introduce heterogeneity [1.42].

This study proposes the implementation of an ultrasonic system based on the axial transmission technique for the evaluation of shear waves in the cortical layer of long bones. The main purposes of this study are to investigate the impact of bone curvature, bone surrounded medium and irregular thickness, on the shear wave velocities measured along the axial direction of the bone. To understand these effects, waves were characterized and the wave velocities were determined in bone samples using the advantages of an axial transmission technique. Additionally, wave velocities were verified through a transverse transmission measurement. For these purposes, experiments were performed in various samples, bone plates with regular thickness, bone tubes with regular thickness and bone samples with irregular shape and thickness.

Subsequently, in order to validate the experimental measurements and study the wave propagation in several types of bone models, 2D and 3D simulations based on the elastic Finite-difference time-domain (FDTD) method were implemented. To verify the efficacy of the FDTD method, simulations in isotropic and anisotropic bone models were compared and analyzed in each case, considering similar bone geometries and conditions used in these experiments.

Furthermore, waves from experiments and simulations were analyzed and characterized in the frequency domain using the 2D-FFT. Results were compared with theoretical dispersion curves of guided waves.

This thesis work presents a complete analysis on the viability of implementing shear wave measurements for in vivo bone evaluation.

1.2   OBJECTIVE AND APPROACH

The main objective of this thesis work is to analyze the feasibility of the implementation of an ultrasonic axial transmission system for in vivo measurement of shear waves in cortical layer of long human bones with the aim to improve considerably the current bone evaluation. Several approaches have been considered to overcome the problems in the current evaluation methods and are described below.

To detect ultrasonic shear waves in the axial direction of bone samples using an axial transmission technique. AT techniques has been demonstrated have several advantages compared to the traditional transverse transmission technique, additionally, AT techniques are ideal for bone evaluation in long bones.

To evaluate the impact of bone shape, bone surrounding medium and irregular thickness of the cortical layer of bone on the wave velocities measured in bone plates, bone cylinders and the complete diaphysis of bone samples. Bone irregular shape, structure and anisotropy is believed to affect the ultrasound propagation, therefore, it is important to evaluate the measurement under this conditions to verify its efficacy.

To verify wave velocity measurement using the through transmission technique. The transverse transmission technique has been largely used and implemented in several clinical devices, and could be a good method to verify the measurements obtained using the axial transmission technique.

To validate the experimental measurements and understand the wave propagation in isotropic and anisotropic bone models by the elastic-FDTD method and using several types of bone models. The wave propagation in models with different geometrical characteristics can be better understood using the simulations. Although, the flexibility to model complex geometries is limited, complex geometries and heterogeneity can be introduced by considering the bone HR pQCT data.

To validate simulations in isotropic and anisotropic models respect to the experimental measurements. It is important to understand how accurate the simulations can be in order to determine the effectiveness of these methods for more complex models and conditions.

REFERENCES

[1.1] P. Laugier, G. Haiat eds., "Bone Quantitative Ultrasound", *Dordrecht: Springer*, vol. 576, 2011.

[1.2] E. Siris, Y. Chen, T. Abbott, E. Connor, P. Miller, L. Wehren, M. Berger, "Bone Mineral Density Thresholds for Pharmacological Intervention to Prevent Fractures", *Arch Intern Med.*, vol. 164, no. 10, pp.1108-1112, 2004.

[1.3] E. Siris, P. Miller, E. Connor, K. Faulkner, L. Wehren, T. Abbott, M. Berger, A. Santora, L. Sherwood, "Identification and fracture outcomes of undiagnosed low bone mineral density in postmenopausal women: results from the National Osteoporosis Risk Assessment", *JAMA*, vol. 286, no. 22, pp. 2815-2822, 2001.

[1.4] WHO Scientific Group on Prevention, Management of Osteoporosis, and World Health Organization, *Prevention and management of osteoporosis: report of a WHO scientific group* (No. 921), World Health Organization, 2003.

[1.5] S. Gnudi, C. Ripamonti, N. Malavolta, "Quantitative Ultrasound and Bone Densitometry to Evaluate the Risk of Nonspine Fractures: A Prospective Study", *Osteoporos Int.*, vol. 11, pp. 518-523, 2000.

[1.6] V. Kilappa, P. Moilanen, L. Xu, P. H. F. Nicholson, J. Timonen, S. Cheng, "Low-frequency axial ultrasound velocity correlates with bone mineral density and cortical thickness in the radius and tibia in pre-and postmenopausal women", Osteoporosis international, vol. 22, no. 4, pp. 1103-1113, 2011.

[1.7] M. Weiss, A. Ben-Shlomo, P. Hagag, S. Ish-Shalom, "Discrimination of proximal hip fracture by quantitative ultrasound measurement at the radius," *Osteoporos Int.*, vol. 11, no. 15, pp. 411-416, 2000.

[1.8] M. Talmant, S. Kolta, C. Roux, D. Haguenauer, I. Vedel, B. Cassou, P. Laugier, "In vivo performance evaluation of bi-directional ultrasonic axial transmission for cortical bone assessment", Ultrasound in medicine and biology, vol. 35, no. 6, pp. 912-919, 2009.

[1.9] J. Foldes, A. Rimon, D. D. Keinan, and M. M. Popovtzer, "Quantitative ultrasound of the tibia: a novel approach assessment of bone status," *Bone*, 17(4), 363–367, 1995.

[1.10] M. Määttä, P. Moilanen, P. Nicholson, S. Cheng, J. Timonen, T. Jämsä, "Correlation of tibial low-frequency ultrasound velocity with femoral radiographic measurements and BMD in elderly women", *Ultrasound in medicine and biology*, vol. 35, no. 6, pp. 903-911, 2009.

[1.11] R. Barkmann, P. Laugier, U. Moser, S. Dencks, M. Klausner, F. Padilla, G. Haiat, M. Heller, C. C. Glüer, "In vivo measurements of ultrasound transmission through the human proximal femur," *Ultrasound Med Biol*, vol. 34, no. 7, pp. 1186–1190, 2008.

[1.12] K. E. Fredfeldt, "Sound velocity in the middle phalanges of the human hand," *Acta Radiol Diagn*, 27, 95–96, 1986.

[1.13] C.V. Albanese, F. De Terlizzi, R. Passariello, "Quantitative ultrasound of the phalanges and DXA of the lumbar spine and proximal femur in evaluating the risk of osteoporotic vertebral fracture in postmenopausal women," *Radiol med*, vol. 116, pp. 92–101, 2011.

[1.14] K. E. Fredfeldt, "Sound velocity in the middle phalanges of the human hand," *Acta Radiol Diagn*, vol. 27, pp. 95-96, 1986.

[1.15] E. M. Stein, F. Rosete, P. Young, M. Kamanda-Kosseh, D. McMahon, G. Luo, R. Siffert, *Ultrasound in medicine and biology*, vol. 39, no. 3, pp. 388-395, 2013.

[1.16] K. Mano, H. Horii, T. Hagino, M. Miki, M. Matsukawa, and T. Otani, Journal of *Medical Ultrasonics, 42*, (3), 315-322, 2015.

[1.17] M. L. Bouxsein, B. S. Coan, and S. C. Lee, "Prediction of the strength of the elderly proximal femur by bone mineral density and quantitative ultrasound measurements of the heel and tibia," *Bone*, 25(1), 49–54, 1999.

[1.18] R. Barkmann, E. Kantorovich, C. Singal, D. Hans, H. K. Genant, M. Heller, C. C., Glüer, "A new method for quantitative ultrasound measurements at multiple skeletal sites: first results of precision and fracture discrimination," *Journal of Clinical Densitometry*, *3*(1), 1-7, 2000.

[1.19] C. F. Njeh, I. Saeed, M. Grigorian, D. L. Kendler, B. Fan, J. Shepherd, H. K. Genant, "Assessment of bone status using speed of sound at multiple anatomical sites," *Ultrasound in medicine and biology*, vol. 27, no.10, pp. 1337-1345, 2001.

[1.20] H. Sievänen, S. Cheng, S. Ollikainen, K. Uusi-Rasi, "Ultrasound velocity and cortical bone characteristics in vivo," *Osteoporosis International*, vol. 12, no. 5, pp. 399-405, 2001.

[1.21] M. Sasso, G. Haiat, M. Talmant, P. Laugier, and S. Naili, "SVD-based algorithm for axial transmission ultrasound technique application to cortical bone characterization," *IEEE Trans Ultrason Ferroelectr Freq Control*, vol. 55, no. 6, pp. 1328-1332, 2008.

[1.22] J. Schneider, G. Iori, D. Ramiandrisoa, M. Hammami, M. Gräsel, C. Chappard, R. Barkmann, P. Laugier, Q. Grimal, JG. Minonzio, K. Raum, "Ex vivo cortical porosity and thickness predictions at the tibia using full-spectrum ultrasonic guided-wave analysis," *Arch Osteoporos*, vol. 14, no. 21, 2019.

[1.23] E. Camus, M. Talmant, G. Berger, P. Laugier, "Analysis of the axial transmission technique for the assessment of skeletal status," *The Journal of the Acoustical Society of America*, vol. 108, no. 6, pp. 3058-3065, 2000.

[1.24] E. Bossy, M. Talmant, F. Peyrin, L. Akrout, P. Cloetens, P. Laugier, "An in vitro study of the ultrasonic axial transmission technique at the radius: 1-MHz velocity measurements are sensitive to both mineralization and intracortical porosity," *Journal of Bone and Mineral Research*, vol. 19, no. 9, pp. 1548-1556, 2004.

[1.25] T. Otani, "Quantitative estimation of bone density and bone quality using acoustic parameters of cancellous bone for fast and slow waves," *Jpn J Appl Phys*, vol. 44, no. 6S, 4578-4582, 2005.

[1.26] T. Nakatsuji, K. Yamamoto, D. Suga, T. Yanagitani, M. Matsukawa, K. Yamazaki, Y. Matsuyama, "Three dimensional anisotropy of ultrasonic wave velocity in bovine cortical bone: effects of hydroxyapatite crystallites orientation and microstructure," *Japanese Journal of Applied Physics*, vol. 50, no. 7S, 2011.

[1.27] E. Bossy, M. Talmant, P. Laugier, "Three-dimensional simulations of ultrasonic axial transmission velocity measurement on cortical bone models," *The Journal of the Acoustical Society of America*, vol. 115, no. 5, pp. 2314-2324, 2004.

[1.28] P. Moilanen, V. Kilappa, P. H. Nicholson, J. Timonen, and S. Cheng, "Thickness sensitivity of ultrasound velocity in long bone phantoms," *Ultrasound in medicine and biology*, vol. 30, no. 11, pp. 1517-1521, 2004.

[1.29] J. Minonzio, N. Bochud, Q. Vallet, Y. Bala, D. Ramiandrisoa, H. Follet, P. Laugier, "Bone cortical thickness and porosity assessment using ultrasound guided waves: An ex vivo validation study," *Bone*, vol. 116, pp. 111-119, 2018.

[1.30] E. Bossy, M. Talmant, P. Laugier, "Effect of bone cortical thickness on velocity measurements using ultrasonic axial transmission: A 2D simulation study," *The Journal of the Acoustical Society of America*, vol. 112, no.1, pp. 297-307, 2002.

[1.31] F. Lefebvre, Y. Deblock, P. Campistron, D. Ahite, and J. J. Fabre, "Development of a new ultrasonic technique for bone and biomaterials in vitro characterization," *Journal of Biomedical Materials Research*, vol. 63, no. 4, pp. 441-446, 2002.

[1.32] C. L. Yapura, and V. K. Kinra, "Guided waves in a fluid-solid bilayer," *Wave motion*, 21, 35-46, 1995.

[1.33] N. Bochud, Q. Vallet, J. G. Minonzio, and P. Laugier, "Predicting bone strength with ultrasonic guided waves," *Scientific reports*, vol. 7, no. 43628, 2017.

[1.34] J. Chen, J. Foiret, J. G. Minonzio, M. Talmant, Z. Su, L. Cheng and P. Laugier, *Physics in Medicine and Biology,* 57, 3025, 2012.

[1.35] P. H. Nicholson, P. Moilanen, T. Kärkkäinen, J. Timonen, S. Cheng, "Guided ultrasonic waves in long bones: modelling, experiment and in vivo application," *Physiological measurement*, vol. 23, no. 4, pp. 755, 2002.

[1.36] P. Moilanen, P. H. Nicholson, V. Kilappa, S. Cheng, and J. Timonen, "Assessment of the cortical bone thickness using ultrasonic guided waves: modelling and in vitro study," *Ultrasound Med Biol*, vol. 33, no. 2, pp. 254-262, 2007.

[1.37] K. I. Lee, and S. W. Yoon, "Feasibility of bone assessment with leaky Lamb waves in bone phantoms and a bovine tibia," *The Journal of the Acoustical Society of America*, vol. 115, no. 6, pp. 3210-3217, 2004.

[1.38] V. C. Protopappas, D. I. Fotiadis, and K. N. Malizos, "Guided ultrasound wave propagation in intact and healing long bones," *Ultrasound in medicine and biology*, vol. 32, no. 5, pp. 693-708, 2006.

[1.39] Q. Vallet, N. Bochud, C. Chappard, P. Laugier, and J. Minonzio, "In vivo characterization of cortical bone using guided waves measured by axial transmission," IEEE transactions on ultrasonics, ferroelectrics, and frequency control, vol. 63, no. 9, pp. 1361-1371, 2016.

[1.40] P. Moilanen, "Ultrasonic guided waves in bone," *IEEE transactions on ultrasonics, ferroelectrics, and frequency control*, vol. 55, no. 6, pp. 1277-1286, 2008.

[1.41] S. Okumura, V. H. Nguyen, H. Taki, G. Haiat, S. Naili, and T. Sato, "Phase velocity estimation technique based on adaptive beamforming for ultrasonic guided waves propagating along cortical long bones," *Japanese Journal of Applied Physics*, vol. 56, no. 7S1, 2017.

[1.42] M. Saeki, L. Bustamante, T. Misaki, K. Chiba, I. Mano, Y. Nagatani, M. Matsukawa, "FDTD simulation study of ultrasonic wave propagation in human radius model generated from 3D HR-pQCT images," *Physics in Medicine*, 100029, 2020.

CHAPTER II BONE BASIC PRINCIPLES AND OSTEO-POROSIS

2.1 LONG BONES

Bone is a heterogeneous anisotropic hard tissue that constitutes part of the vertebrate skeleton and sustain loads caused by external actions and forces such us gravity or muscular movements. Under these effects, bones adapt their shape and structure to their mechanical environment inclusive of strain magnitude, rate, frequency, distribution and deformation mode (Wolff's Law 1892) [2.1]. Commonly, loads applied on the skeleton are not only compressive loads (in the direction of the body weigh). Torsion and bending are also observed.

Bone structure extends over several organization levels, containing approximately 70% of minerals (hydroxyapatite), 22% of proteins (collagen) and 8% water (by weight) [2.2]. Bone is composed mainly by cortical and cancellous bone. The basic organization of bone is made by collagen molecules that conform the fibril which are arranged in fibers. Mineralized fibers are aligned to form bone lamellae. The bone structural unit in cortical bone is called osteon and it consists on several lamellae and is surrounded a Harversian canal. Harversian canal forms networks inside the bone to interconnect the vessels and nerves [2.3].

The cortical bone is an external layer that covers the bone. At the macroscopic level has a compact appearance. Cortical bone presents a dense structure with a typical porosity of less of the 15%. [2.3]

The cancellous bone o trabecular bone constitutes the inner part of the bone. Contrary to cortical bone, the cancellous bone present high porosity. The structure formed by the cancellous bone is called trabeculae and are filled with bone marrow. A basic scheme of the long bone structure is shown in Fig. 2.1. Additionally, acoustic properties of cortical and cancellous bone are detailed in Table 2.1.
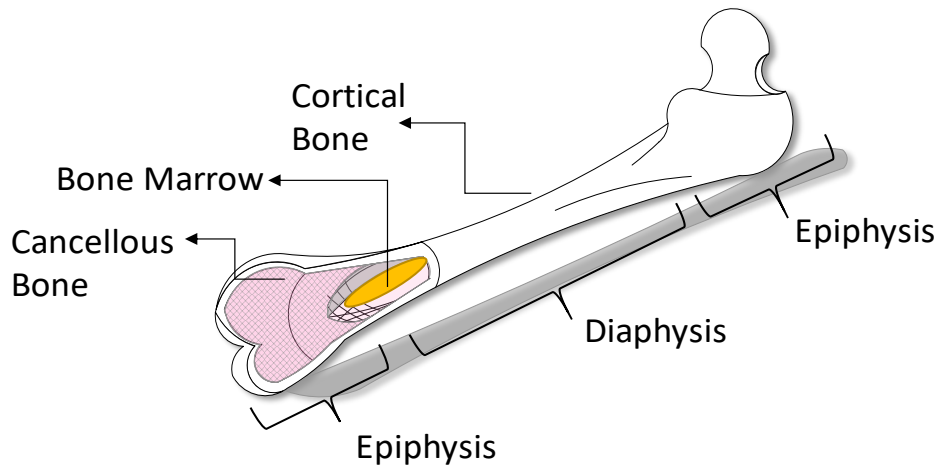
Figure 2.1 Scheme of long bone structure.

Table 2.1 Acoustic Properties of cortical and cancellous bone

Material	Velocity (m/s)	Density (kg/m³)	Attenuation (dB/cm MHz)	Acoustic Impedance (MRayl)
Cortical Bone [2.4]	3476	1055	6.9	7.38
Cancellous Bone [2.5]	1886	1040	9.94	1.45

2.1.1 ELASTIC COEFFICIENTS OF LONG BONES

The degree of anisotropy for bone is that of orthotropic material symmetry which means that the properties differ according to orthogonal directions. An orthotropic material is characterized elastically by nine independent elastic constants. Cortical and cancellous bone are considered to be transversally isotropic in its material symmetry [2.3, 2.6]. Therefore, a transversally isotropic bone has five independent elastic constants. The matrix of elastic coefficients, shown in Eq. (2.1), for an orthotropic material is written as follows:

$$[c_{ij}] = \begin{bmatrix} c_{11} & c_{12} & c_{13} & 0 & 0 & 0 \\ c_{12} & c_{22} & c_{23} & 0 & 0 & 0 \\ c_{13} & c_{23} & c_{33} & 0 & 0 & 0 \\ 0 & 0 & 0 & c_{44} & 0 & 0 \\ 0 & 0 & 0 & 0 & c_{55} & 0 \\ 0 & 0 & 0 & 0 & 0 & c_{66} \end{bmatrix} \qquad (2.1)$$

Where, C is the elastic tensor and C_{ij} are the elastic coefficients.

For a transversely isotropic material the matrix of the elastic coefficients would have the following form shown in Eq. (2.2):

$$[c_{ij}] = \begin{bmatrix} c_{11} & c_{12} & c_{13} & 0 & 0 & 0 \\ c_{12} & c_{11} & c_{13} & 0 & 0 & 0 \\ c_{13} & c_{13} & c_{33} & 0 & 0 & 0 \\ 0 & 0 & 0 & c_{44} & 0 & 0 \\ 0 & 0 & 0 & 0 & c_{44} & 0 \\ 0 & 0 & 0 & 0 & 0 & c_{66} \end{bmatrix} \qquad (2.2)$$

2.1.2 BONE MECHANICAL PROPERTIES IN HUMAN

The mechanical properties of the cortical layer of a human bone at the mesoscopic level taken from literature are summarized in Table 2.2.

Table 2.2 Mechanical properties of the cortical layer of a human bone [2.7].

Property	Cortical bone
Young's modulus (longitudinal), E_L	17400 MPa
Young's modulus (transverse), E_T	9600 MPa
Poison's coefficient, ν	0.22-0.42 (Femur)
Shear modulus, G	3510

Mechanical properties of biomaterials such as bone are characterized by stress-strain curves produced by progressive tensile and compressive loads. According to these curves, the bone is a brittle material, if the total strain produced by an external load, exceeds the

elastic limit of the strained bone, the bone suffers plastic deformation, and exceeding the strength limit leads to bone fracture. The strength and tensile-compressive moduli of cortical bone along the longitudinal direction are greater than those along the radial and circumferential directions [2.8] (Table 2.2). However, bone can resist to higher compression loads than tension loads and to higher tension loads than shear loads [2.9-2.10].

2.2 SOFT-TISSUE

Soft-tissue are tissues that connect, support, or surround other structures and organs of the body. Soft-tissue includes tendons, ligaments, fascia, skin, fibrous tissues, fat, synovial membrane, muscles, nerves and blood vessels. Bone is naturally surrounded by soft-tissue. Human soft-tissue is highly deformable, and its mechanical properties vary significantly from one person to another. Table 2.3 summarizes the acoustic properties of tissues of typical values found in literature.

Table 2.3 Acoustic Properties of tissues

Material	Velocity (m/s)	Density (kg/m^3)	Attenuation (dB/cm MHz)	Acoustic Impedance (MRayl)
Fat [2.11]	1478	950	0.48	1.4
Muscle [2.11]	1547	1050	1.09	1.62
Soft-tissue (avg.) [2.11]	1561	1043	0.54	1.63
Water	1480	1000	0.0022	1.48

2.2.1 SOFT-TISSUE PHANTOMS FOR ULTRASOUND EVALUATION

Water and water-based acoustic scanning gels are the simplest tissue substitutes for medical ultrasound measurements. Water and water-based materials are also known to have a strong dependence on temperature, with the speed of sound in water varying as

much as 50 m/s over the temperature range between 20–40 °C [2.12]. Despite these limitations, water is a great soft-tissue substitute because of its ease of use and the prevalence of immersion transducers and test tanks.

On the other hand, agarose-based tissue substitutes provide another alternative to the use of graphite powders to achieve sufficient attenuation and scattering properties, as well as improved temperature resistance and particle suspension [2.13]. Agarose-based techniques are the most widely used of the soft-tissue substitute preparation techniques. The broad use of agarose-based substitutes is a result of their well characterized performance, the ease of fabrication (the mixture can be heated in a microwave) and the flexibility that the process provides, allowing the incorporation of additional ingredients to achieve a range of acoustic properties. Table 2.4 summarizes some important acoustic properties of soft-tissue substitutes used as mimicking layers of soft-tissue.

Table 2.4 Acoustic Properties of soft-tissue substitutes

Phantom	Velocity (m/s)	Density (kg/m³)	Attenuation (dB/cm MHz)	Acoustic Impedance (MRayl)
Agarose-based [2.14]	1498-1600	1016-1100	0.04-1.40	1.52-1.76
Water-based gels [2.15]	1518-1574	1000		1.48-1.60

2.3 OSTEOPOROSIS

Osteoporosis is a bone disease in which bone density and bone quality are significantly reduced, leading to weakness of the skeleton and consequently, the risk of bone fracture increases. Osteoporosis is considered as a major public health problem since it reduces the life quality of large number or individuals. According to the World Health

Organization (WHO) Osteoporosis-induced fractures rates increase primarily as a result of normal ageing, but can arise as a result of impaired development of peak bone mass or excessive bone loss during adulthood, and are more prone in elderly woman [2.16].

Hip fractures are the most common, as they nearly always result in hospitalization and could produce permanent disability and are fatal about 20% of the time [2.16]. The lifetime risk of fracture in 50 year-old women is about 40%[2.17], and 15%-30% [2.18] of men will sustain bone fragility in the rest of their life. In 1990, there were 1.7 million hip fractures alone worldwide, this number is expected to rise to 6 million by 2050 [2.16].

2.3.1 OSTEOPOROSIS DIAGNOSIS

Clinical diagnosis of Osteoporosis relies on the measurement of the bone mineral density (BMD). The BDM value of a patience is expressed in terms of T-score, the number of standard deviations from the mean BMD of healthy reference population. The World Health Organization (WHO) uses a BMDa to categorize a patient into one of four groups (Normal, Low bone mass or Osteopenia, Osteoporosis, Established osteoporosis). However, a significant overlap exists between the BMDa values of non-fractured and fractured patients. In other words, bone fracture cannot be precisely predicted by BMD [2.19-2.21].

Treatments for osteoporosis are available nowadays, these can effectively reduce the risk of bone fractures [2.22]. However, this does not explain the fracture mechanism. The quality of a healthy or osteoporotic bone can be determined by the biomechanical characteristics. Noninvasive ultrasonic techniques are ideal for bone evaluation, they are harmless, easy to use, and cost-effective. Ultrasound waves propagating in the bone structure contain important information closely related to the mechanical properties and bone geometries, for these reasons, they are a great option to quantitatively evaluate bone biomechanical strength.

2.4 SUMMARY

Bone is a heterogeneous anisotropic hard tissue that constitutes part of the vertebrate skeleton and sustain loads. If the total strain produced by an external load, exceeds the strength limit this leads to bone fracture. Commonly, loads applied on the skeleton are not only compressive loads. Torsion and bending are also observed. The degree of anisotropy for bone is that of orthotropic material symmetry. Cortical bone is considered to be transversally isotropic in its material symmetry, having five independent elastic constants.

Bone deterioration and weakness is caused by Osteoporosis, which reduce the bone density and bone quality, consequently, the risk of bone fracture increases. Osteoporosis is considered as a major public health problem since it reduces the life quality of large number or individuals. Treatments for osteoporosis are available nowadays, these can effectively reduce the risk of bone fractures. However, this does not explain the fracture mechanism. Noninvasive ultrasonic techniques are ideal for bone evaluation, they are harmless, easy to use, and cost-effective. a great option to quantitatively evaluate bone biomechanical strength.

REFERENCES

[2.1] J. Stock, "Wolff's law (bone functional adaptation)", *The International Encyclopedia of Biological Anthropology*, 1-2, 2018.

[2.2] P. Augat, and S. Schorlemmer, "The role of cortical bone and its microstructure in bone strength", *Age and ageing*, *35*(suppl_2), ii27-ii31, 2006.

[2.3] P. Laugier, G. Haiat eds., "Bone Quantitative Ultrasound", Dordrecht: Springer, vol. 576, 2011.

[2.4] B.K. Hoffmeister, S.R. Smith, S.M. Handley, J. Y. Rho, "Anisotropy of Young's modulus of human tibial cortical bone," *Medical and Biological Engineering and Computing*, vol. 38, pp. 333–338, 2000.

[2.5] K. A. Wear, "Frequency dependence of ultrasonic backscatter from human trabecular bone: Theory and experiment," *The Journal of the Acoustical Society of America*, 106(6), 3659-3664, 1999.

[2.6] R. B. Ashman, S. C. Cowin, W. C. Van Buskirk, J.C. Rice, "A continuous wave technique for the measurement of the elastic properties of cortical bone," *Journal of biomechanics*, vol. 17, no. 5, pp. 349-361,1984.

[2.7] S. Cowin, *Bone mechanics handbook* (CRC Press, Boca Raton, FL), 2001.

[2.8] Morgan, E. F., Unnikrisnan, G. U., and Hussein, A. I., "Bone mechanical properties in healthy and diseased states," *Annual review of biomedical engineering*, *20*, 119-143, 2018.

[2.9] J. Galante, W. Rostoker, R.D. Ray "Physical properties of trabecular bone," *Calcif Tissue Res*, 1970; 5:236–46.

[2.10] W.T. Dempster, R.T. Liddicoat. "Compact bone as a non-isotropic material," *Am J Anat*, 91(3), 331-362, 1952.

[2.11] T. D. Mast, "Empirical relationships between acoustic parameters in human soft tissues," *Acoustics Research Letters Online*, *1*(2), 37-42, 2000.

[2.12] J. Chavaudra, "Last ICRU recommendations for the prescription, recording and reporting of external bean therapy," *Cancer radiotherapie: journal de la Societe francaise de radiotherapie oncologique*, *2*(5), 607-614, 1998.

[2.13] E. L. Madsen, G. R. Frank, and F. Dong, "Liquid or solid ultrasonically tissue-mimicking materials with very low scatter," *Ultrasound in medicine and biology*, *24*(4), 535-542, 1998.

[2.14] M. Burlew, E. Madsen, J. A. Zagzebski, R. A. Banjavic, and S. W. Sum, "A new ultrasound tissue-equivalent material," *Radiology*, *134*(2), 517-520, 1980.

[2.15] A. Giacomini, "Ultrasonic Velocity in Ethanol-Water Mixtures," *The Journal of the Acoustical Society of America*, *19*(4), 701-702, 1947.

[2.16] WHO Scientific Group on Prevention, Management of Osteoporosis, and World Health Organization. (2003). *Prevention and management of osteoporosis: report of a WHO scientific group* (No. 921). World Health Organization.

[2.17] Melton III, J. L. (1995). "Perspectives: how many women have osteoporosis now?," *Journal of Bone and Mineral Research*, *10*(2), 175-177.

[2.18] A. Randell, P. N. Sambrook, T. V. Nguyen, H. Lapsley, G. Jones, P. J., Kelly, J. A. Eisman "Direct clinical and welfare costs of osteoporotic fractures in elderly men and women," *Osteoporosis International*, *5*(6), 427-432, 1995.

[2.19] J. J. Stepan, D. B. Burr, I. Pavo, A. Sipos, D. Michalska, J.Li, and M. Sato, "Low bone mineral density is associated with bone microdamage accumulation in postmenopausal women with osteoporosis," *Bone*, *41*(3), 378-385, 2007.

[2.20] J. Balseiro, F. H. Fahey, H. A. Ziessman, T. V. Le, "Comparison of bone mineral density in both hips," *Radiology*, *167*(1), 151-153, 1988.

[2.21] X. D. Wang, N. S. Masilamani, J. D. Mabrey, M. E. Alder, C. M. Agrawal, "Changes in the fracture toughness of bone may not be reflected in its mineral density, porosity, and tensile properties," *Bone*, 23(1), 67-72, 1998.

[2.22] P. J. Meunier, C. Roux, S. Ortolani, M. Diaz-Curiel, J. Compston, P. Marquis, C. Cormier, G. Isaia, J. Badurski, J. D. Wark, J. Collette, and J. Y. Reginster, "Effects of long-term strontium ranelate treatment on vertebral fracture risk in postmenopausal women with osteoporosis," *Osteoporos Int*, 20(10), 1663–1673 2009.

CHAPTER III ULTRASONIC WAVE PHYSICS

Ultrasound corresponds to a mechanical wave propagating at frequencies above the range of human hearing (>20kHz). Ultrasound waves propagates in fluids and solids. The wave propagation depends on the intrinsic elastic properties of the medium and its mass density. Several types of waves with particular characteristics have been observed in fluids and solids.

3.1   SURFACE ACOUSTIC WAVES

Surface waves are modes of propagation of elastic energy along the free surface of an infinite half-space in which the displacement amplitudes of the propagating waves decays exponentially with depth under the surface, so all the associated energy is concentrated in a small region near the surface at approximately one wavelength depth from where it was excited [3.1]. The particle motion on the surface and at each depth is elliptical.

Rayleigh waves, is type of surface wave, that include longitudinal and transverse motions that decrease exponentially in amplitude as distance from the surface increases. There is a phase difference between these component motions. The existence of Rayleigh waves was predicted in 1885 by Lord Rayleigh [3.2]. In isotropic solids these waves cause the surface particles to move in ellipses in planes normal to the surface and parallel to the direction of propagation (Fig. 3.1). The motion amplitude decays and the eccentricity changes as the depth into the material increases. Rayleigh waves have a speed slightly less than shear waves by a factor dependent on the elastic constants of the material.
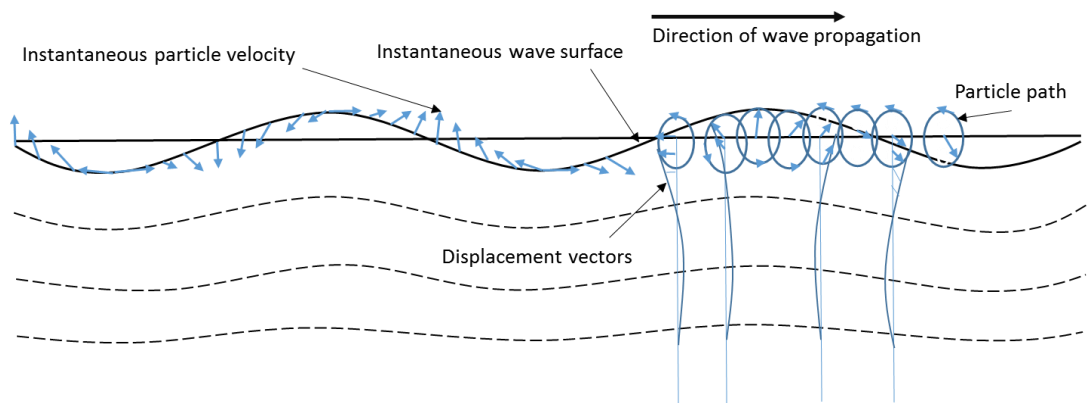
Figure 3.1 Rayleigh waves propagation.

3.2 LONGITUDINAL AND SHEAR WAVES IN THE SOLID AND LIQUID MEDIA

Longitudinal and shear wave are the most common type of surface waves that can be generated on the interface of two mediums. In the longitudinal waves, the oscillations occur in the longitudinal direction or the direction of wave propagation. Since compressional and dilatational forces are active in these waves, they are also called pressure or compressional waves. On the other hand, in the transverse or shear wave, the particles oscillate at a right angle or transverse to the direction of propagation (Fig. 3.2). Shear waves generation is relatively weak when compared to longitudinal waves. In fact, shear waves are usually generated in materials using some of the energy from longitudinal waves [3.3].

Perfect fluids and solids support the propagation of longitudinal waves only, however, in solids unlike in fluids, a produced shearing strain can be transmitted to adjacent layers by the strong biding between particles, this phenomenon generates transverse waves or shear waves [3.4].

Biological tissues are viscoelastic solids, where longitudinal and shear waves can propagate [3.5-3.7]. However, ultrasound shear waves are commonly neglected in tissues because these waves are highly attenuated at ultrasonic frequencies. In the case of hard tissues like, cortical bone, both waves could be considered. Wave propagation follows the elastic character of Eq. (2.2).
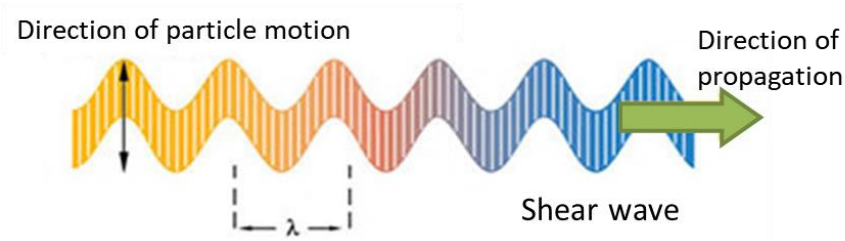
Figure 3.2 Shear waves propagation.

3.3 DETERMINATION OF THE SPEED OF SOUND

3.3.1 ISOTROPIC HOMOGENEOUS ELASTIC SOLIDS

In an infinite isotropic homogeneous solid body, with no interactions with the boundaries, the longitudinal and shear propagation velocity c_l and c_s are given by Eqs. (3.1-3.2) [3.8]:

$$c_l = \sqrt{\frac{\lambda + 2\mu}{\rho}} = \sqrt{\frac{c_{11}}{\rho}} = \sqrt{\frac{E(1 - \nu)}{\rho(1 + \nu)(1 - 2\nu)}} \tag{3.1}$$

$$c_s = \sqrt{\frac{\mu}{\rho}} = \sqrt{\frac{c_{11} - c_{12}}{2\rho}} = \sqrt{\frac{E}{\rho(1 + \nu)}} \tag{3.2}$$

3.4 GUIDED WAVES

Lamb waves are elastic waves that propagate in solid materials in the plane direction of propagation. Contrary to the surface waves, when the propagation medium is thinner compared to the wavelength λ and the two boundaries are sufficiently close together, the continuous motion of the two surfaces will produce multiple reflections, mode conversions and interference of the longitudinal and shear waves inside the boundaries. This phenomenon originates a wave guide character. The sound perturbations can be represented as superposition of resonant guided wave modes. Guided wave modes which

exist in plates are known as Lamb waves which are complex waves traveling through the entire plate [3.9]. The two basic Lamb modes are anti-symmetrical and symmetrical to whether the displacements on the two surfaces are in phase or anti-phase. Figure 3.3 shows a representation of the displacement of these modes. The phase velocity of these particular modes depends mainly on the thickness, the elastic properties of the material, density and the frequency. Different frequencies travel at different phase velocities, making these wave modes highly dispersive. The number of symmetric and antisymmetric modes that a plate can display depends on the frequency-thickness product. For a selected frequency, the number of modes will increase with the thickness of the plate [3.10].
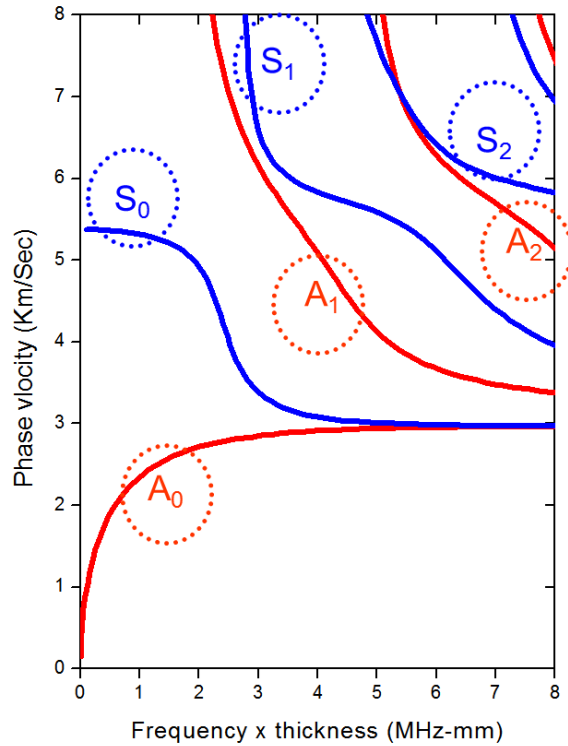
Figure 3.3 Lamb wave dispersion curves.

The symmetrical and anti-symmetric zero-order modes are the most important since they exist over the entire frequency spectrum from zero to indefinitely high frequencies

and they carry more energy than the higher-order modes [3.11]. The flexural mode (antisymmetric) is more easily excited of the two and often carries most of the energy.

3.4.1 DISPERSION RELATIONS OF LAMB MODES

Dispersion curves graphs show relationship between wave velocity, wavelength and frequency in dispersive systems. The dispersion relations for a linear, homogeneous, elastic isotropic plate under traction free surface boundary conditions in z axis and motion taking place in x and y axes; were effectively derived by Lamb [3.12] and are described as follow:

When the motion is symmetrical with respect to the plane $y = 0$. Equation (3.3) describes this relation.

$$\frac{\tanh \beta f}{\tanh \alpha f} = \frac{4\xi^2 \alpha \beta}{(\xi^2 + \beta^2)^2} \tag{3.3}$$

When the motion is anti-symmetrical with respect to the plane $y = 0$. Equation (3.4) describes this relation.

$$\frac{\tanh \beta f}{\tanh \alpha f} = \frac{(\xi^2 + \beta^2)^2}{4\xi^2 \alpha \beta} \tag{3.4}$$

The terms alpha and beta in Eq. (2.5) and Eq. (2.6) are given by the Eqs. (3.5-3.6)

$$\propto^2 = \frac{\omega}{C_L^2} - \xi^2 \tag{3.5}$$

$$\beta^2 = \frac{\omega}{C_S^2} - \xi^2 \tag{3.6}$$

Where: C_L is longitudinal wave velocity $[m/s]$; C_S is shear wave velocity $[m/s]$; ω is angular frequency $[rad/s]$; ξ is wavenumber $[rad/s]$.

The theoretical dispersion curves of phase velocity versus frequency or wave number, can be calculated and plotted using Eqs. (3.3-3.6). In Fig. 3.3 a representation of symmetric and anti-symmetric Lamb modes employing these equations was shown. The

x-axis shows the product of angular frequency ω and plate thickness normalized by the shear wave velocity, C_{SH}. The y-axis shows the phase velocity C_{Ph} of the Lamb wave normalized by the shear wave velocity, C_{SH}.

3.5   THE INTERFACE PHENOMENON

In a fluid-fluid interface, if a plane wave impinges on a plane interface a reflected and a transmitted wave will be generated. In a fluid medium only longitudinal waves can exit therefore the refracted and reflected waves are naturally longitudinal waves, as shown in Fig. 3.4 (a). According to Snell's Law, the reflection angle θ_1 is equal to the angle of the incident wave and, the transmitted wave is refracted away from the direction of the incident wave at a refraction angle θ_2 [3.8]. This is given by Eq. (3.7)

$$\frac{\sin \theta_1}{c_1} = \frac{\sin \theta_2}{c_2} \tag{3.7}$$

Where c_1 and c_2 are the wave velocities of the first and second medium.
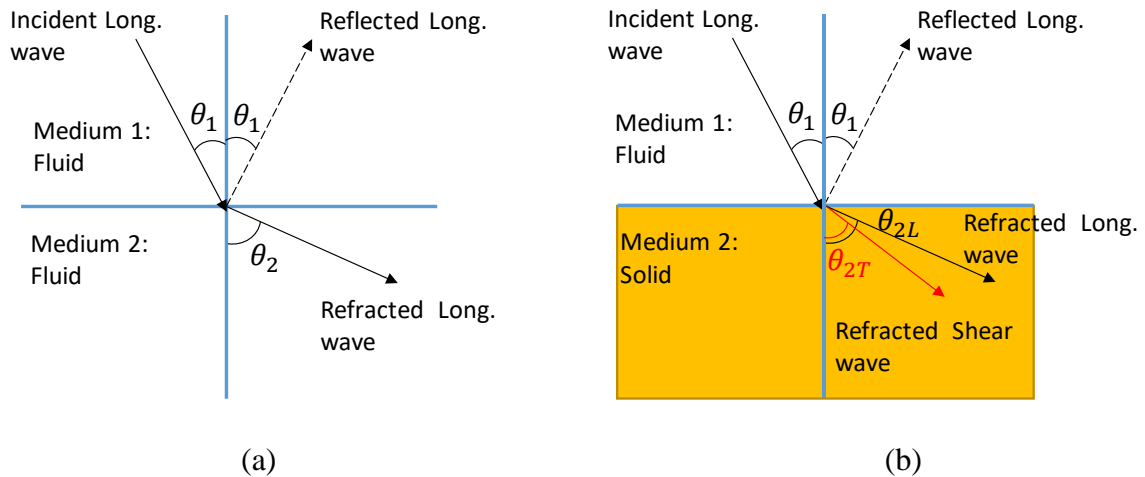
Figure 3.4 Refraction Law in (a) fluid-fluid interface and, (b) fluid-solid interface.

In a fluid-solid interface, when the second medium is a solid material such as cortical bone, approximately less than a half of the total energy is transferred to the reflected wave

and only 50-75% to the refracted longitudinal wave. The refracted longitudinal wave is partially converted into shear wave, as shown in Fig. 3.4 (b). As generally longitudinal waves in solids propagates at greater velocity than in fluids, the refraction angle θ_{2L} is larger than the angle of incidence θ_1. When θ_1 is larger than the critical angle θ_c the longitudinal wave is no longer transmitted. The corresponding critical angle θ_c is defined by Eq. (3.8).

$$\sin \theta_c = \frac{c_1}{c_{2L}} \qquad\qquad (3.8)$$

The problem of a fluid-solid bilayer in terms of guided waves has been numerically studied for a water-aluminum bilayer [3.5]. At the interface of these two mediums, the energy of guided waves leaks from the solid to the fluid in the form of leaky waves. Leaky waves reflecting back at the top boundary of the fluid layer and propagating back to the solid medium are believed to propagate in the whole bilayer structure and consequently change the dispersion characteristics of the guided waves. On the other hand, it has been demonstrated also that both layers of the interface can be considered as independent waveguide structures [3.6-3.7].

REFERENCES

[3.1] A. A. Oliner, Acoustic surface waves, Berlin and New York, Springer-Verlag, Topics in Applied Physics, vol. 24, 1978.

[3.2] L. Rayleigh, "On waves propagated along the plane surface of an elastic solid," *Proceedings of the London mathematical Society*, 1(1), pp. 4-11, 1985.

[3.3] D. Belgroune, J. F. de Belleval, H. and Djelouah, "A theoretical study of ultrasonic wave transmission through a fluid–solid interface," *Ultrasonics*, 48(3), 220-230, 2008.

[3.4] H. J. McSkimin, "Propagation of longitudinal waves and shear waves in cylindrical rods at high frequencies," *The Journal of the Acoustical Society of America,* 28(3), 484-494, 1956.

[3.5] C. L. Yapura, and V. K. Kinra, "Guided waves in a fluid-solid bilayer," *Wave motion*, 21, 35-46, 1995.

[3.6] N. Bochud, Q. Vallet, J. G. Minonzio, and P. Laugier, "Predicting bone strength with ultrasonic guided waves," *Scientific reports*, vol. 7, no. 43628, 2017.

[3.7] J. Chen, J. Foiret, J. G. Minonzio, M. Talmant, Z. Su, L. Cheng and P. Laugier, Physics in Medicine and Biology, 57, 3025, 2012.

[3.8] P. Laugier, G. Haiat eds., "Bone Quantitative Ultrasound", Dordrecht: Springer, vol. 576, 2011.

[3.9] D. E. Chimenti, "Guided waves in plates and their use in materials characterization," 1997.

[3.10] D. E. Chimenti, A. H. Nayfeh, "Leaky Lamb waves in fibrous composite laminates,". *Journal of applied physics*, 58(12), 4531-4538, 1985.

[3.11] A. Abdelrahman, U. Amjad, D. Jha, K. S. Tarar, W. Grill, Zero order mode selective excitation and highly resolved observations of lamb waves," In Health

Monitoring of Structural and Biological Systems 2011, vol. 7984, p.p. 798413, *International Society for Optics and Photonics*, 2011.

[3.12] H. Lamb, "On waves in an elastic plate," *Proc. R. Soc. Lond. A*, vol. 93, no. 648, pp. 114-128, 1917.

CHAPTER IV QUANTITATIVE ULTRASOUND TECHNIQUES (QUS)

Quantitative ultrasound techniques (QUS), using ultrasound technology, are relatively new methods for bone evaluation. This technique focus on the measurement of quantitative variables by which to asses bone mechanical properties. However, QUS techniques are not widely accepted because of technical immaturity and lack of standardization. Other techniques such as, patient-specific finite element analysis (QCT-based) [4.1- 4.4] are new alternatives that could offer an improved risk facture assessment in the near future but they need more research.

QUS methods have been investigated for in vivo diagnosis of bone. These techniques have several advantages such as it is non-invasive, no hazard involved compared to X-ray densitometry techniques, portable and inexpensive. QUS techniques are used to quantitatively measure variables by which to assets bone mechanical properties [4.5- 4.6]. QUS techniques to assess bone quality have demonstrated potential to predict risk of fracture by providing measurements of ultrasonic parameters of cortical or cancellous bone sites [4.7- 4.14]. QUS is already being used in clinical practice [4.15] and new methods are being developed to enable multisite QUS assessment [4.16- 4.17]. The main clinical field of application is fracture risk prediction and it is also used for healing [4.18- 4.19]. In vivo bone assessment uses different devices and configurations. It is common to classify the different approaches in two: the transverse transmission technique and the axial transmission technique. Other in vivo approaches based on ultrasound reflection [4.20] or backscatter are still being investigated.

4.1   IN VIVO CLINICAL DEVICES USING QUS
4.1.1   FOREARM DEVICE LD-100

QUS technologies has been applied for the development of the in vivo device, LD-100 (OYO Electric) to evaluate the cancellous part at the distal portion of the radius. These evaluation is based on the measurement of the fast and slow waves investigated in

a several in vivo studies by Otani et al. [4.21- 4.22]. The systems basically present a transverse transmission configuration for the measurement of ultrasonic waves. A pair of broadband focused transducers (diameter 20 mm, and focal point of 40 mm) at 1MHz are aligned and moves simultaneously through water bags covering the transducer and used as the coupling material, during the scan.

LD-100, shown in Fig. 4.1, estimates several parameters such as cancellous bone mineral density (BMD) and elasticity, cortical bone thickness by making use of several echo modes in the observed signals. LD-100 offers a good concordance with the BMD obtained by pQCT.

Figure 4.1 LD-100 (OYO Electrics) and Doshisha U.

4.1.2   HEEL DEVICES

Heel devices also uses a transversal transmission configuration, with planar or focused transducers with a center frequency of 0.5 MHz. Most heel devices use a fixed flat-surface unfocused transducers. The speed of sound is measured through a scan (in modern devices) that includes the back and bottom edges of the heel bone. The device automatically searches for the planar and posterior acoustic edges. The signal processing

allows detecting the proximity to an edge of the calcaneus bone. After the identification of this part of the bone, the transducer moves to the target location to scan 1 cm^2.

4.2   AXIAL TRANSMISSION TECHNIQUE

QUS axial transmission measurements were initially studied for the fracture healing in bone and to determine the velocity of the first arriving signals (FAS) in bone [4.23]. In this technique the transmitter and received are placed in the same side of the bone to measure the arrival time of an ultrasonic wave propagating along the cortical bone layer parallel to its long axis. Contrary to the Transverse transmission techniques, which configuration requires a two-sided configuration with transducers placed at opposite sides of the bone making difficult the measurement. Axial transmission configuration is especially useful to evaluate long bones. Axial transmission technique is one of the novel promising techniques for assessment of long cortical bones, such as radius or tibia.

AT techniques measurements of the SOS of the First Arriving Signal (FAS) [4.24- 4.27] have been used to characterize bone properties, such us cortical thickness [4.28- 4.29], porosity [4.30] depending on the wavelength used. However, the FAS velocity measurements showed to have a significant impact depending on the cortical bone thickness [4.28- 4.31]. Therefore, the bone irregular structure and thickness could modify the wave propagation and subsequently lead to errors in the measurement expected.
FAS velocity can be also affected by the soft-tissue which allows the propagations of waves that could be erroneously assumed as the waves propagating in bone [4.32- 4.33]. Additional guided modes and small modifications in the mode trajectory have been observed [4.34] as a result of the wave overlapping in bilayer phantoms with especially large soft-tissue thickness

Simulation studies in 2D and 3D models as well as, measurements in phantoms using the axial transmission technique have shown a relation between wavelength-thickness on the wave velocity in the bone. When the cortical bone thickness is larger than one wavelength, the FAS corresponds to the measurement of the lateral wave [4.24, 4.31]. FAS waves can also be seen as guided S0 Lamb mode, according to simulations and studies [4.31, 4.35] that showed the increment of the velocity of the FAS at wavelengths

greater than the plate thickness. Under these conditions, the FAS becomes sensitive to the surrounding geometry and is affected by the boundaries of the cortical layer. Additionally, an energetic slower signal component arriving after the FAS has been observed to be consistent with the antisymmetric A0 mode [4.36]. For intermediate cases, a complex interference of several types of waves [4.28, 4.31] has been observed. It is important to point out that the axial transmission measurements performed in these studies considered transducers normal to the bone surface. Moreover, it has been found in several clinical studies that FAS velocity discriminates healthy patient from osteoporotic ones [4.9, 4.17].

4.3 PROPOSED SHEAR WAVE AXIAL TRANSMISSION SYSTEM

4.3.1 SHEAR WAVE AXIAL TRANSMISSION ME-ASUREMENT IMPORTANCE

The possibility of measuring axial ultrasonic wave modes other than the FAS in cortical bone has been investigated in the last years. [4.36- 4.41]
Importantly, measurements related to the shear wave in bone using the axial transmission technique have not been extensively reported although shear waves are necessary for a complete bone evaluation. Commonly, loads applied on the skeleton are not only compressive loads (in the direction of the body weight or axial direction of the bone). Torsion and bending are also observed. Mechanical properties of bone such as shear modulus and torsional strength are related to shear waves and therefore are necessary to know when a bone fracture has occurred. The possibility of measuring shear waves in cortical bone could yield additional diagnostic information of the material and geometric characteristics of bone.

4.3.2 METHOD DESCRIPTION

The method proposed in this thesis work is based on the generation of ultrasonic waves at different incident angles, determined by the Snell's Law and, the detection of the resulting waves leaking from the surface of the bone into the water medium (and thought soft-tissue in following experiments) by using an axial transmission configuration

of the transducers. Water was selected as the surrounding medium since its bulk velocity is close to that in soft-tissue and is typically used for these purposes [4.28- 4.31]. In the experiments with soft-tissue, an additional layer of mimicking Agarose tissue [4.42] will be used to cover the surface of the cortical bone. The methods, a general system description and measurement process is detailed as follows.

4.3.3   SYSTEM DESCRIPTION

The experimental system used an axial transmission measurement method which is briefly described below. For every specific case of the samples, which have different shapes, the exact geometries of the experimental configuration will be described in the following sections.

In general, experimental measurements were performed in degassed water tank at room temperature. The bone samples were also degassed using a vacuum degassing chamber. The system uses an axial transmission configuration of two thickness-mode transducers, one acting as the transmitter and one as the receiver. Both transducers were set at the same angle and were separated a distance from 40 mm to 45 mm approximately far from each other (depending on the sample) and were aligned to the axial direction (the main axis of the bone). Experiments were performed at incident angles (θ) between 15º and 60º. The geometry conditions, shown in the corresponding measurement case were maintained in each measurement of the incident angle. The angles were decided according to the law of refraction or Snell's law and relation Eq. (3.7). In each case of the measurement, existing waves leaking at the same or close to the incident angle will be more easily detected while, other waves leaking at different angles will be attenuated. In order to avoid as possible, the detection of specular reflections from the surface of the sample and signals traveling directly from the transmitter to the receiver, a spongy block was placed between the transmitter and receiver.

4.3.4   EQUIPMENT, ELECTRONICS AND MEASURE-MENT METHOD

One cycle sinusoidal electrical signal with a frequency of 1 MHz (frequency commonly used in current clinical devices of this type [4.44]) is generated using a function generator (Agilent Technologies, 33250). After that, the signal was amplified 10 times from 7 Vp-p to 70 Vp-p using an amplifier (NF, HSA4101). The amplified signal, excited the transmitter, a commercial composite transducer (Japan Probe), flat type with a diameter of 13 mm. The transmitter scanned a distance of 10 mm along the axial direction of the bone sample at a step size of 0.1 mm. The receiver, a homemade PVDF transducer (Fig. 4.2), flat type and with a diameter of 10 mm, detected the waves leaking into the water medium. A sampling frequency equal or above 500 MHz was selected to record the temporal signals received at every step (while moving the transmitter). After that, a pre-amplifier (NF, BX-31A) was used to amplify the detected signals. The signals were observed in an Oscilloscope (Tektronix, DPO7104C) and a NI data acquisition card was used to transfer acquired signals averaged 1024 times to a portable computer. Applications created in MATLAB were used for the subsequent signal processing.

The electronic system setup and the axial transmission configuration is shown in Fig. 4.3.
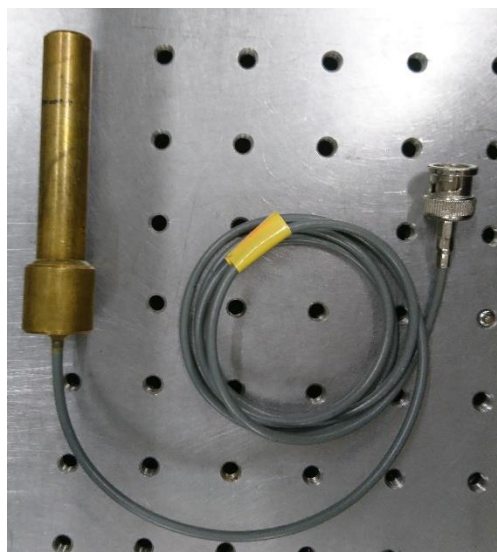
Figure 4.2 Homemade PVDF transducer used as receiver.
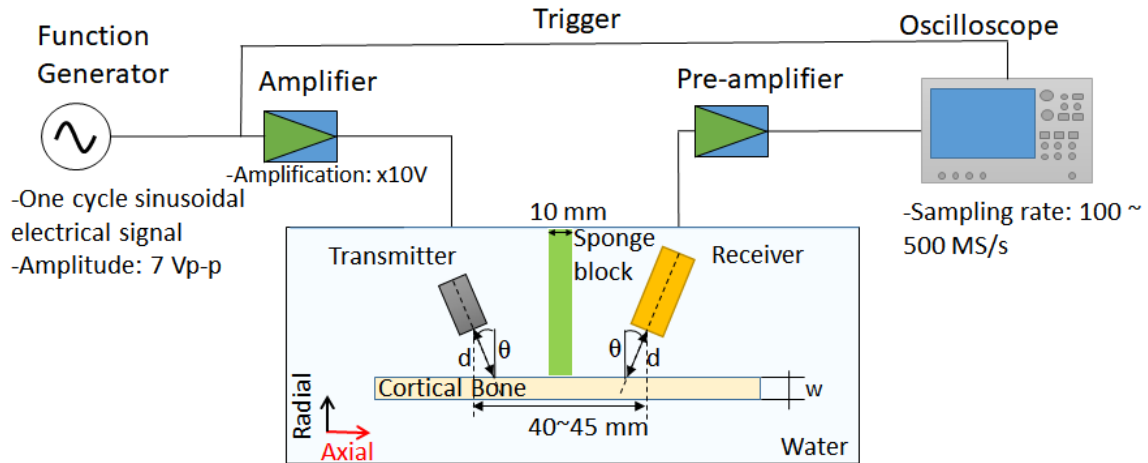
Figure 4.3 General setup of the axial transmission measurement system.

4.3.5   SIGNAL PROCESSING

The true path followed by a wave propagating from the transmitter to the receiver was difficult to determine because it involved reflections from the boundaries of the irregular bone shell. A time-of-flight technique (ToF) was therefore used, whereby the time taken for a signal to travel the known distance from the transmitter to the receiver is measured [4.31, 4.43]. With this technique, the time that took a signal to fly between the transmitter to the receiver (whose distance is known) was measured instead. Various criteria are used to estimate ToF, for example the fists arriving point, first zero crossing point, a fixed threshold etc. In here, we used four different peak points obtained from the target waves of each case.

B-scans (plots of scanned distance vs. time) were constructed at each incident angle from the temporal signals detected at every step. Four peaks from the target waves were selected and the wave velocities were estimated using a least-squares fit of all the values determined from the time rate of change of the peak signal while moving the transmitter at the step size.

In some cases, the estimation of the wave velocity may be significantly affected by the irregular bone shape, especially for waves traveling a relatively long path through the bone. Considering the possibility of measuring mixed waves, the estimated wave velocities will therefore be referred to as apparent wave velocities.

4.4   TWO-DIMENSIONAL FAST FOURIER TRANSFORM (2D-FFT)

Conventional time domain methods of measuring the amplitudes and velocities of stress waves generally require minimal signal processing and are easy to implement. However, the time record is usually composed of a number of superposed wave packets, difficult to be resolved separately from every single mode. Then, the measurement of the amplitudes or group velocity cannot be determined. Studies have demonstrated that transforming the time domain data to the frequency domain, the data interpretation may be easier to measure phase and group velocity [4.44]. Analysis in the frequency domain using spectral methods were initially applied in the nondestructive testing for measurement of Lamb waves in plates. Since then, various numerical methods have been proposed to measure the dispersion curves of leaky Lamb waves for property characterization in different models.

The two-dimensional Fourier transform (2D-FFT) technique is an alternative method of measuring the dispersion curves of Lamb waves quantitatively and it overcomes the problems of multiple modes and dispersion by transforming the received amplitude-time records to amplitude-wave-number records at discrete frequencies, where individual Lamb waves may be resolved and their amplitudes measured [4.45].

4.4.1   2D-FFT FROM ACQUIRED DATA

Broadband excitation signals from transducers of finite dimensions generally excite more than one propagating mode. Propagating Lamb waves are sinusoidal in both the frequency and spatial domains. Therefore, a temporal Fourier transform is carried out to go from the time to frequency domain, then a spatial Fourier transform is applied to go to the frequency wavenumber domain, where the amplitudes and wave numbers of individual modes can be measured.

Experimentally and numerically acquired data is two-dimensional Fourier transformed using Eq. (4.1)

$$H(k,f) = \int_{-\infty}^{+\infty} \int_{-\infty}^{+\infty} u(x,t)e^{-i(kx+\omega t)} \, dx \, dt \qquad (\mathbf{4.1})$$

Where, $u(x,t)$ is the wave displacement on a surface, $\omega = 2\pi f$ is the angular frequency, the wave number $k = \omega/c$, and c as the phase velocity.

The result of this transformation is a two-dimensional array of amplitudes at discrete frequencies and wavenumbers. To avoid aliasing the data must be sampled at sufficiently high frequency in time and wave number in space. Usually the signal will not be periodic within the temporal and spatial sampling windows and leakage will occur. Window functions such as the Hanning window may be used to reduce this leakage, and zeros may be padded to the end of the signal to enable the frequency and wave number of the maximum amplitude to be determined more accurately.

4.4.2   APPLICATION OF THE 2D-FFT FOR DISPERSION CURVES OBTAINING

For the estimation of the dispersion curves from data experimentally or numerically calculated a two-dimensional Fourier transform was used. Temporal signals were first transformed from the time to frequency domain, then the second transform was applied to go to the frequency wavenumber domain using Eq. (4.1).

For each case the corresponding values of sampling frequency and step size (spatial) at which the signals were acquired, were considered for the transform. Once the graph phase velocity vs frequency-wave number was obtained, a threshold was used on the extraction of the highest amplitudes of the ridge line. The threshold level must be balanced against the possibility of a false peak due to the noise. Dispersion curves extracted from the experimental measurements and simulation data considering the region of the selected target waves.

On the other hand, the theoretical dispersion curves were calculated by finding the solutions of the Lamb wave equation for the antisymmetric, Eq. (3.3) and, symmetric modes, Eq. (3.4) [4.46]. By plotting the solutions, a graph of the phase velocities as function of the frequency-thickness product was obtained. The theoretical curves consider the corresponding thickness w of the sample and were calculated assuming a longitudinal

wave velocity of 4000 m/s and a shear wave velocity of 1800 m/s, typical values found in literature [4.47].

REFERENCES

[4.1] J. H. Keyak, S. Sigurdsson, G. Karlsdottir, D. Oskarsdottir, A. Sigmarsdottir, S. Zhao, K. Siggeirsdottir, "Male–female differences in the association between incident hip fracture and proximal femoral strength: a finite element analysis study," *Bone*, *48*(6), 1239-1245, 2011.

[4.2] L. Duchemin, D. Mitton, E. Jolivet, V. Bousson, J. D. Laredo, and W. Skalli, "An anatomical subject-specific FE-model for hip fracture load prediction," *Comput Methods Biomech Biomed Engin*, 11(2), 105–111 2008.

[4.3] E. Schileo, F. Taddei, L. Cristofolini, and M. Viceconti, "Subject-specific finite element models implementing a maximum principal strain criterion are able to estimate failure risk and fracture location on human femurs tested *in vitro*," *J Biomech* 41(2), 356–367, 2008.

[4.4] T. M. Keaveny, "Biomechanical computed tomography—noninvasive bone strength analysis using clinical computed tomography scans," *Annals of the New York Academy of Sciences*, 1192(1), 57-65, 2010.

[4.5] M. L. Bouxsein, S. E. Radloff, "Quantitative ultrasound of the calcaneus reflects the mechanical properties of calcaneal trabecular bone," *Journal of Bone and Mineral Research*, *12*(5), 839-846, 1997.

[4.6] J. J. Kaufman, T. A. Einhorn, "Perspectives: Ultrasound assessment of bone," *Journal of Bone and Mineral Research*, *8*(5), 517-525, 1993.

[4.7] S. Gnudi, C. Ripamonti, N. Malavolta, "Quantitative Ultrasound and Bone Densitometry to Evaluate the Risk of Nonspine Fractures: A Prospective Study", *Osteoporos Int.*, vol. 11, pp. 518-523, 2000.

[4.8] V. Kilappa, P. Moilanen, L. Xu, P. H. F. Nicholson, J. Timonen, S. Cheng, "Low-frequency axial ultrasound velocity correlates with bone mineral density and cortical thickness in the radius and tibia in pre-and postmenopausal women", *Osteoporosis international*, vol. 22, no. 4, pp. 1103-1113, 2011.

[4.9] M. Talmant, S. Kolta, C. Roux, D. Haguenauer, I. Vedel, B. Cassou, P. Laugier, "In vivo performance evaluation of bi-directional ultrasonic axial transmission for cortical bone assessment", *Ultrasound in medicine and biology*, vol. 35, no. 6, pp. 912-919, 2009.

[4.10] A. J. Foldes, A. Rimon, D. D. Keinan, and M. M. Popovtzer, "Quantitative ultrasound of the tibia: a novel approach assessment of bone status," *Bone*, 17(4), 363–367, 1995.

[4.11] M. Määttä, P. Moilanen, P. Nicholson, S. Cheng, J. Timonen, T. Jämsä, "Correlation of tibial low-frequency ultrasound velocity with femoral radiographic measurements and BMD in elderly women", *Ultrasound in medicine and biology*, vol. 35, no. 6, pp. 903-911, 2009.

[4.12] R. Barkmann, P. Laugier, U. Moser, S. Dencks, M. Klausner, F. Padilla, G. Haiat, M. Heller, C. C. Glüer, "In vivo measurements of ultrasound transmission through the human proximal femur," *Ultrasound Med Biol*, vol. 34, no. 7, pp. 1186–1190, 2008.

[4.13] K. E. Fredfeldt, "Sound velocity in the middle phalanges of the human hand," *Acta Radiol Diagn,* 27, 95–96, 1986.

[4.14] C.V.Albanese, F. De Terlizzi, R. Passariello, "Quantitative ultrasound of the phalanges and DXA of the lumbar spine and proximal femur in evaluating the risk of osteoporotic vertebral fracture in postmenopausal women," *Radiol med*, vol. 116, pp. 92–101, 2011.

[4.15] I. Mano, K. Horii, H. Hagino, T. Miki, M. Matsukawa, and T. Otani, *Journal of Medical Ultrasonics*, 42, (3), 315-322, 2015.

[4.16] J. P. Karjalainen, O. Riekkinen, J. Töyräs, M. Hakulinen, H. Kröger, T. Rikkonen, and J. S. Jurvelin, "Multi-site bone ultrasound measurements in elderly women with and without previous hip fractures," *Osteoporosis international*, 23(4), 1287-1295, 2012.

[4.17] M. Weiss, A. Ben-Shlomo, P. Hagag, S. Ish-Shalom, "Discrimination of proximal hip fracture by quantitative ultrasound measurement at the radius," *Osteoporos Int.*, vol. 11, no. 15, pp. 411-416, 2000.

[4.18] C. F. Njeh, J. R. Kearton, D. Hans, C. M. Boivin, "The use of quantitative ultrasound to monitor fracture healing: a feasibility study using phantoms," *Medical engineering and physics*, 20(10), 781-786, 1999.

[4.19] V. C. Protopappas, D. I. Fotiadis, and K. N. Malizos, "Guided ultrasound wave propagation in intact and healing long bones," *Ultrasound in medicine and biology*, vol. 32, no. 5, pp. 693-708, 2006.

[4.20] A. Hosokawa "Numerical investigation of ultrasound reflection and backscatter measurements in cancellous bone on various receiving areas," *Ultrasonics*, 54(5), 1237-1244, 2014.

[4.21] T. Otani, "Quantitative estimation of bone density and bone quality using acoustic parameters of cancellous bone for fast and slow waves," *Japanese journal of applied physics*, 44(6S), 4578, 2005.

[4.22] A. Hosokawa, T. Otani, "Acoustic anisotropy in bovine cancellous bone," *The Journal of the Acoustical Society of America*, 103(5), 2718-2722, 1998.

[4.23] M. Muller, P. Moilanen, E. Bossy, P. Nicholson, V. Kilappa, J. Timonen, M. Talmant, S. Cheng, and P. Laugier, "Comparison of three ultrasonic axial transmission methods for bone assessment," *Ultrasound Med Biol,* 31(5), 633–642, 2005.

[4.24] E. Camus, M. Talmant, G. Berger, P. Laugier, "Analysis of the axial transmission technique for the assessment of skeletal status," *The Journal of the Acoustical Society of America*, vol. 108, no. 6, pp. 3058-3065, 2000.

[4.25] E. Bossy, M. Talmant, F. Peyrin, L. Akrout, P. Cloetens, P. Laugier, "An in vitro study of the ultrasonic axial transmission technique at the radius: 1-MHz velocity

measurements are sensitive to both mineralization and intracortical porosity," *Journal of Bone and Mineral Research*, vol. 19, no. 9, pp. 1548-1556, 2004.

[4.26] T. Otani, "Quantitative estimation of bone density and bone quality using acoustic parameters of cancellous bone for fast and slow waves," *Jpn J Appl Phys*, vol. 44, no. 6S, 4578-4582, 2005.

[4.27] T. Nakatsuji, K. Yamamoto, D. Suga, T. Yanagitani, M. Matsukawa, K. Yamazaki, Y. Matsuyama, "Three dimensional anisotropy of ultrasonic wave velocity in bovine cortical bone: effects of hydroxyapatite crystallites orientation and microstructure," *Japanese Journal of Applied Physics*, vol. 50, no. 7S, 2011.

[4.28] E. Bossy, M. Talmant, P. Laugier, "Three-dimensional simulations of ultrasonic axial transmission velocity measurement on cortical bone models," *The Journal of the Acoustical Society of America*, vol. 115, no. 5, pp. 2314-2324, 2004.

[4.29] P. Moilanen, V. Kilappa, P. H. Nicholson, J. Timonen, and S. Cheng, "Thickness sensitivity of ultrasound velocity in long bone phantoms," *Ultrasound in medicine and biology*, vol. 30, no. 11, pp. 1517-1521, 2004.

[4.30] J. Minonzio, N. Bochud, Q. Vallet, Y. Bala, D. Ramiandrisoa, H. Follet, P. Laugier, "Bone cortical thickness and porosity assessment using ultrasound guided waves: An ex vivo validation study," *Bone*, vol. 116, pp. 111-119, 2018.

[4.31] E. Bossy, M. Talmant, P. Laugier, "Effect of bone cortical thickness on velocity measurements using ultrasonic axial transmission: A 2D simulation study," The Journal of the Acoustical Society of America, vol. 112, no.1, pp. 297-307, 2002.

[4.32] P. Moilanen, "Ultrasonic guided waves in bone," *IEEE transactions on ultrasonics, ferroelectrics, and frequency control*, vol. 55, no. 6, pp. 1277-1286, 2008.

[4.33] N. Bochud, Q. Vallet, J. G. Minonzio, and P. Laugier, "Predicting bone strength with ultrasonic guided waves," *Scientific reports*, vol. 7, no. 43628, 2017.

[4.34] F. Lefebvre, Y. Deblock, P. Campistron, D. Ahite, and J. J. Fabre, "Development of a new ultrasonic technique for bone and biomaterials in vitro characterization," *Journal of Biomedical Materials Research*, vol. 63, no. 4, pp. 441-446, 2002.

[4.35] P. H. Nicholson, P. Moilanen, T. Kärkkäinen, J. Timonen, S. Cheng, "Guided ultrasonic waves in long bones: modelling, experiment and in vivo application," *Physiological measurement*, vol. 23, no. 4, pp. 755, 2002.

[4.36] P. Moilanen, P. H. Nicholson, V. Kilappa, S. Cheng, and J. Timonen, "Assessment of the cortical bone thickness using ultrasonic guided waves: modelling and in vitro study," *Ultrasound Med Biol*, vol. 33, no. 2, pp. 254-262, 2007.

[4.37] K. I. Lee, and S. W. Yoon, "Feasibility of bone assessment with leaky Lamb waves in bone phantoms and a bovine tibia," *The Journal of the Acoustical Society of America*, vol. 115, no. 6, pp. 3210-3217, 2004.

[4.38] V. C. Protopappas, D. I. Fotiadis, and K. N. Malizos, "Guided ultrasound wave propagation in intact and healing long bones," *Ultrasound in medicine and biology*, vol. 32, no. 5, pp. 693-708, 2006.

[4.39] Q. Vallet, N. Bochud, C. Chappard, P. Laugier, and J. Minonzio, "In vivo characterization of cortical bone using guided waves measured by axial transmission," *IEEE transactions on ultrasonics, ferroelectrics, and frequency control*, vol. 63, no. 9, pp. 1361-1371, 2016.

[4.40] P. Moilanen, "Ultrasonic guided waves in bone," *IEEE transactions on ultrasonics, ferroelectrics, and frequency control*, vol. 55, no. 6, pp. 1277-1286, 2008.

[4.41] S. Okumura, V. H. Nguyen, H. Taki, G. Haiat, S. Naili, and T. Sato, "Phase velocity estimation technique based on adaptive beamforming for ultrasonic guided waves propagating along cortical long bones," *Japanese Journal of Applied Physics*, vol. 56, no. 7S1, 2017.

[4.42] E. L. Madsen, G. R. Frank, and F. Dong, "Liquid or solid ultrasonically tissue-mimicking materials with very low scatter," *Ultrasound in medicine and biology*, *24*(4), 535-542, 1998.

[4.43] P. Laugier, G. Haiat eds., "Bone Quantitative Ultrasound", Dordrecht: Springer, vol. 576, 2011.

[4.44] D. N. Alleyne, P. Cawley, "A 2-dimensional Fourier transform method for the quantitative measurement of Lamb modes,". *IEEE Symposium on Ultrasonics* , pp. 1143-1146, 1990.

[4.45] P. Moilanen, V. Kilappa, J. Timonen, A. Salmi, P. Karppinen, E. Hæggström, R. Myllylä, "Photo-acoustic phase-delayed excitation of guided waves in coated bone phantoms. *In 2013 IEEE International Ultrasonics Symposium (IUS)*, pp. 2080-2083, 2013.

[4.46] H. Lamb, "On waves in an elastic plate," Proc. R. Soc. Lond. A, vol. 93, no. 648, pp. 114-128, 1917.

[4.47] Y. Yamato, M. Matsukawa, T. Otani, K. Yamazaki, A. Nagano, "Distribution of longitudinal wave properties in bovine cortical bone in vitro," *Ultrasonics*, vol. 44, pp. e233-e237, 2006.

CHAPTER V FINITE-DIFFERENCE TIME-DOMAIN (FDTD)

Finite difference schemes for time-dependent partial differential equations have been employed in computational fluid dynamics for several years. However, in 1966 was further developed by Yee [5.1] who presented a FDTD numerical technique for solving Maxwell's curl equations on grids staggered in space and time, since then, FDTD method has become very popular because of its effectiveness and easiness and it has been largely used in several fields such as, electromagnetics [5.2-5.4], geophysics [5.5] and ultrasound [5.6].

The finite-difference time-domain is a numerical method grid-based differential numerical modeling that approximates a differential equation defined over a continuous domain by a finite number of equations defined at the point of a mesh [5.3]. The vector components in a volume of space are solved at a given instant in time; then the vector components in the same spatial volume are solved at the next instant in time; and the process is repeated over and over.

In ultrasound, FDTD is commonly used to simulate the sound wave propagation, as demonstrated in several studies of the wave propagation in bone [5.7-5.9]. Recently, an improved FDTD, one-step leapfrog FDTD method has been originated from the conventional FDTD but with no mid-time computation needed, therefore it has higher computational efficiency than the other unconditionally stable FDTD methods [5.2].

5.1 ELASTIC FDTD FOR WAVE PROPAGATION

The elastic FDTD method consider the sound propagation in solid media, where longitudinal waves as well as shear waves can propagate.

In the elastic FDTD method, particle velocity, normal stress, and shear stress (vector values) in the simulation field are aligned alternately. Then, stresses and particle velocity are updated alternately, as is seen in Fig. 5.1.
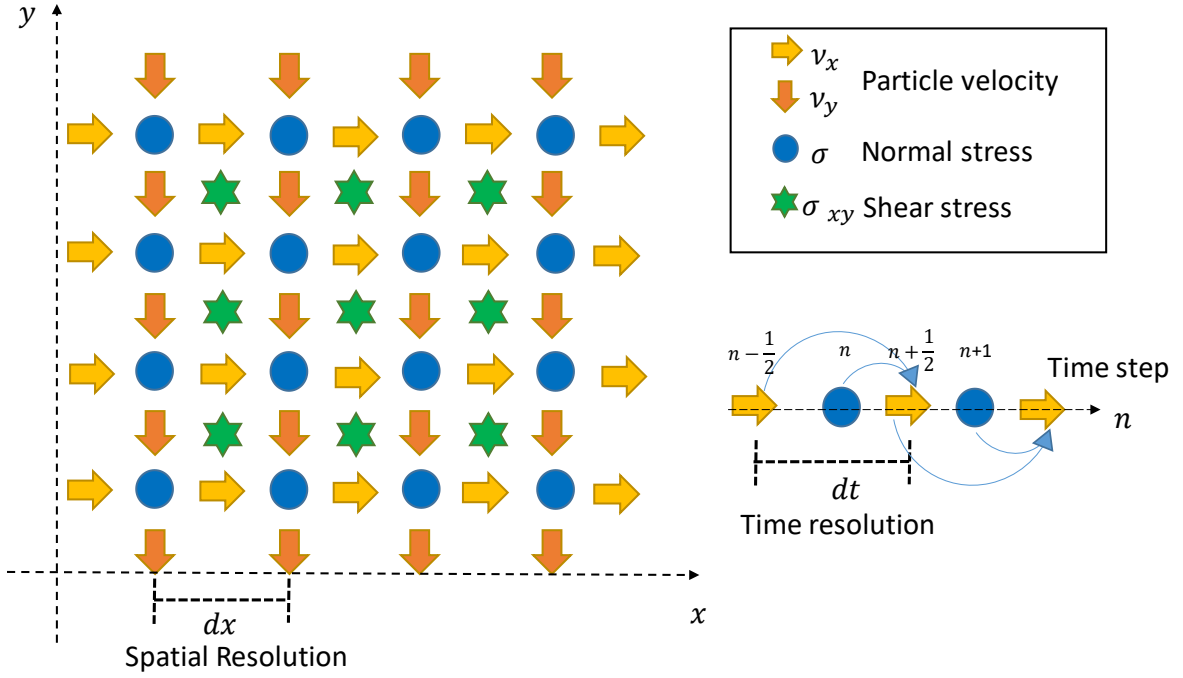
Figure 5.1 Simulation field of the FDTD method.

5.2 FUNDAMENTAL EQUATIONS

The fundamental equations for the simulation of the wave propagation are described in Eqs. (5.1-5.6), as follows.

2D case:

$$\frac{\partial \sigma_{xx}}{\partial t} = (\lambda + 2\mu)\frac{\partial v_x}{\partial x} + \lambda\left(\frac{\partial v_y}{\partial y}\right) \tag{5.1}$$

$$\frac{\partial \sigma_{xy}}{\partial t} = \frac{\partial \sigma_{yx}}{\partial t} = \mu\left(\frac{\partial v_x}{\partial y} + \frac{\partial v_y}{\partial x}\right) \tag{5.2}$$

$$\frac{\partial v_x}{\partial t} = \frac{1}{\rho}\left(\frac{\partial \sigma_{xx}}{\partial x} + \frac{\partial \sigma_{xy}}{\partial y}\right) \tag{5.3}$$

3D case:

$$\frac{\partial \sigma_{xx}}{\partial t} = (\lambda + 2\mu)\frac{\partial v_x}{\partial x} + \lambda\left(\frac{\partial v_y}{\partial y} + \frac{\partial v_z}{\partial z}\right) \tag{5.4}$$

$$\frac{\partial \sigma_{xy}}{\partial t} = \frac{\partial \sigma_{yx}}{\partial t} = \mu \left(\frac{\partial v_x}{\partial y} + \frac{\partial v_y}{\partial x} \right) \quad\quad (5.5)$$

$$\frac{\partial v_x}{\partial t} = \frac{1}{\rho} \left(\frac{\partial \sigma_{xx}}{\partial x} + \frac{\partial \sigma_{xy}}{\partial y} + \frac{\partial \sigma_{zx}}{\partial z} \right) \quad\quad (5.6)$$

Where σ, is the normal and shear stress, ν is the particle velocity, ρ is the density and; λ and μ are the Lame's coefficients [5.10].

5.3   STABILITY CONDITIONS OF THE FDTD-METHOD

Since the FDTD method discretizes spatial and temporal domains over grids, defined by spatial resolution Δx or Δy and time resolution Δt. The good selection of these parameters is crucial to provide smooth representation of the discretized field [5.7-5.8]. Its selection depends on the stability condition.

The stability condition CFL (Courant, Friedrichs, Levy) [5.11] depends on the numerical scheme and guaranties that the computed fields are stable. For wave propagation, the CFL condition has generally the next form shown in Eq. (5.7):

$$c \frac{\Delta t}{dx} \leq \alpha_d \quad\quad (5.7)$$

Where α_d is some dimensionless constant, which depends on the space dimension d, c is the wave velocity. When several wave velocity values are involved, as the case for heterogeneous medium, the largest wave velocity value is used. Therefore, the CFL condition is given by Eq. (5.8):

$$c \frac{\Delta t}{dx} \leq \frac{1}{\sqrt{d}} \qu\quad (5.8)$$

For second order FDTD, a minimum spatial resolution size of $\lambda/10$ is needed, the selection of the spatial resolution will depends on the desired accuracy and other factors related with the simulation itself.

5.4   IMPLEMENTATION OF THE FDTD METHOD FOR AXIALLY TRANSMITTED WAVE PROPAGATION

Simulations of the wave propagation consider the shape and geometries of every sample tested. In the plate samples a simplified 2D-simulation with isotropic conditions was implemented. In the tube samples the simulation was upgraded to a 3D model and considered isotropic conditions of the mediums. In the simulation for the wave propagation in long bones the model considered the heterogeneity and anisotropy of real bone, using data of the structural models built from high-resolution peripheral quantitative computed tomography (HR-pQCT) images. In this case a 3D-simulation with anisotropic conditions was implemented. Details of the simulation and conditions are presented in the corresponding section. Here, general considerations are explained.

5.4.1   SIMULATION CONDITIONS

In order to simulate the longitudinal and shear wave propagation along bone, a custom-developed elastic FDTD code presented in previous studies [5.7, 5.12-5.13] was rebuilt and implemented for these application. In these simulations, the sound attenuation was not considered. To avoid reflections coming from the end faces of the simulation volume, a Higdon's second order absorption boundary condition [5.14] was implemented. During the simulation, the values taken by the voxels of each receiver were averaged at every loop and then recorded.

5.4.2   MODEL CONSTRUCTION

2D and 3D-bone models were reconstructed considering the corresponding geometries of the sample, in the case of the isotropic simulations, and from the bone HR pQCT data, in the case of anisotropic simulations. The simulation geometries will be described in each case depending on the sample, Fig. 5.2 shows two views of a general representation of a 3D-model for simulation. Wave propagation in complex materials could turn out to be very complicated, therefore, some assumptions were made. Conditions close to the actual human bone measurements were gradually considered while simulating the wave propagations in the different sample cases. The transmitter and

receivers consisted of a set of voxels (of the 3D-simulation matrix) or pixels (of the 2D-simulation matrix) in a defined circumference of diameter 10 mm and 13 mm (the same diameter of the transducers used in the experimental measurements) respectively. One set of voxels as the transmitter and fifty sets of voxels as the receiver array, in an axial transmission configuration, were positioned at angles between 15º and 60º. A vacuum block was placed between the transducers in the model, working in the same way as the sponge block in the experimental measurements. The simulation geometries will be described for each sample in the corresponding section. In general, the bone surrounding medium, water or soft-tissue layer, were considered isotropic and homogeneous. Additionally, the sound velocity in water was defined as 1500 m/s and a water density of 1000 kg/m^3. A single sinusoidal wave with a Hann window at 1 MHz was used as the transmitted signal. The spatial resolution and time resolution were defined in each case in order to satisfy the Courant's stability condition [5.11].

For the isotropic and homogeneous models, longitudinal and shear wave velocities were assumed from values found in literature [5.15]. For the anisotropic and heterogeneous models, the bone mass density was estimated from the HR pQCT data of the bone samples [5.16] as in explained in the following sections.
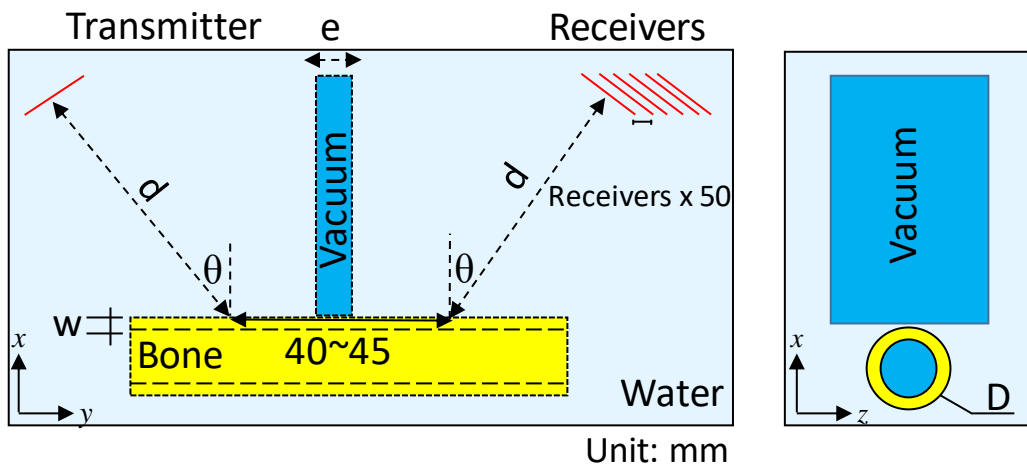
Figure 5.2 General representation of a 3D-model for simulation

REFERENCES

[5.1] K. S. Yee, J. S. Chen, A. H. Chang, "Conformal finite difference time domain (FDTD) with overlapping grids," *IEEE Antennas and Propagation Society International Symposium 1992 Digest*, pp. 1949-1952, 1992.

[5.2] E. L. Tan, "Fundamental schemes for efficient unconditionally stable implicit finite-difference time-domain methods," *IEEE Trans. Antenn. Propag.* 56(1), 170–177, 2008.

[5.3] D. M. Sullivan "Electromagnetic simulation using the FDTD method," *John Wiley and Sons*, 2013.

[5.4] A. Z. Elsherbeni, V. Demir, "The finite-difference time-domain method for electromagnetics with MATLAB simulations," 2009.

[5.5] P. B. Wong, G. L. Tyler, J. E. Baron, E. M. Gurrola, R. A. Simpson, "A three-wave FDTD approach to surface scattering with applications to remote sensing of geophysical surfaces," *IEEE Transactions on Antennas and Propagation*, *44*(4), 504-514, 1996.

[5.6] I. M. Hallaj, R. O. Cleveland "FDTD simulation of finite-amplitude pressure and temperature fields for biomedical ultrasound," *The Journal of the Acoustical Society of America*, *105*(5), L7-L12, 1999.

[5.7] Y. Nagatani, H. Imaizumi, T. Fukuda, M. Matsukawa, Y. Watanabe, and T. Otani, "Applicability of finite-difference time-domain method to simulation of wave propagation in cancellous bone," *Japanese Journal of Applied Physics*, vol. 45, no. 9R, 2006.

[5.8] A. Hosokawa, "Numerical analysis of variability in ultrasound propagation properties induced by trabecular microstructure in cancellous bone," *IEEE transactions on ultrasonics, ferroelectrics, and frequency control*, 56(4), 738-747, 2009.

[5.9] E. Bossy, M. Talmant, P. Laugier, "Three-dimensional simulations of ultrasonic axial transmission velocity measurement on cortical bone models," *The Journal of the Acoustical Society of America*, vol. 115, no. 5, pp. 2314-2324, 2004.

[5.10] B. A. Auld, "Acoustic Fields and Waves in Solids," *Krieger Publishing Co. Malabar*, vol.1, 1973.

[5.11] R. Courant, K. Friedrichs, and H. Lewy, "On the partial difference equations of mathematical physics," *IBM Journal of Research and Development*, vol. 11, no. 2, pp. 215-234, 1967.

[5.12] Y. Nagatani, K. Mizuno, T. Saeki, M. Matsukawa, T. Sakaguchi, H. Hosoi, "Numerical and experimental study on the wave attenuation in bone–FDTD simulation of ultrasound propagation in cancellous bone," *Ultrasonics,* vol. 48, no. 6-7, pp. 607-612, 2008.

[5.13] K. Takano, Y. Nagatani, and M. Matsukawa, "Simulation study of axial ultrasound transmission in heterogeneous cortical bone model," *Japanese Journal of Applied Physics*, vol. 56, no. 7S1, 2017.

[5.14] R. L. Higdon, "Numerical absorbing boundary conditions for the wave equation. Mathematics of computation," *Mathematics of computation*, vol. 49, no. 179, pp. 65-90, 1987.

[5.15] Y. Yamato, M. Matsukawa, T. Otani, K. Yamazaki, A. Nagano, "Distribution of longitudinal wave properties in bovine cortical bone in vitro," *Ultrasonics*, vol. 44, pp. e233-e237, 2006.

[5.16] M. Saeki, L. Bustamante, T. Misaki, K. Chiba, I. Mano, Y. Nagatani, M. Matsukawa, "FDTD simulation study of ultrasonic wave propagation in human radius model generated from 3D HR-pQCT images," *Physics in Medicine*, 100029, 2020.

CHAPTER VI PRELIMINARY MEASUREMENTS IN CORTICAL BONE

In this part of the thesis work, a preliminary measurement in plate samples was performed to validate the proposed system, the angle configuration of the transducers, and principally it is focused on the errors of the sample position or misalignment in the experimental axial transmission configuration and the consequent effects of the bone anisotropy on the wave velocity measurements. Several factors contribute to the mechanical anisotropy of bone such as the orientation of the osteons, lamellae and the alignment of the of the collagen fibers and hydroxyapatite [6.1, 6.2]. It is known that wave velocities are affected by bone anisotropy as demonstrated by Yamato et. al [6.3- 6.4]. In this research, longitudinal wave was measured in a ball made of cortical bovine bone in all the directions and at different angles. It was found, in the first place, that longitudinal wave velocity depended on the bone direction (axial, transversal or radial), being axial direction where the highest longitudinal wave velocities were measured. It also demonstrated that depending on the angle, the longitudinal wave velocity changes and this change was attributed to the orientation of the crystallites and bone microstructure. Bone anisotropy is not fully understood but it is believed to affect the ultrasound propagation, therefore, it is important to evaluate shear waves, which have a different wave propagation compared to longitudinal wave, and investigate the anisotropy effects on these measurements.

The objective of this measurement is to understand the effect of misalignment of the sample position, that may be caused by the bone anisotropy, when it is rotated few degrees clockwise and anticlockwise, on the wave velocity determination using the axial transmission technique. This evaluation of the wave velocities in each case will help to understand how experimental errors in the sample placement can affect the measurement.

6.1   SAMPLES

One cortical bone plate obtained from the cortical bone of a bovine femora was used for this measurement. The thickness of the sample was 1.6 mm [6.5] and a length of approximately, 60 mm. The bone sample was degassed using a vacuum degassing chamber, and immersed in degassed water.

6.2   EXPERIMENT DESCRIPTION

The experimental setup of the axial transmission configuration and geometries for the evaluation of bone plate is shown in Fig. 6.1. In this case, the transducers were separated 40 mm, approximately; and were aligned to the axial direction (the main axis) of the bone. The lift-off distance was 40 mm with respect to the sample surface. Experiments were performed at incident angles (θ) from 10º to 60º (each 10º) keeping the same geometries in each measurement. Here, a sampling frequency of 100 MHz was selected to record the temporal signals, averaged 1024 times by hardware. And spongy block of 10 mm of thickness was placed between the transducers to avoid the detection of specular reflections. The electronic equipment is the same described in the previous section and uses the same configurations described in previous sections.
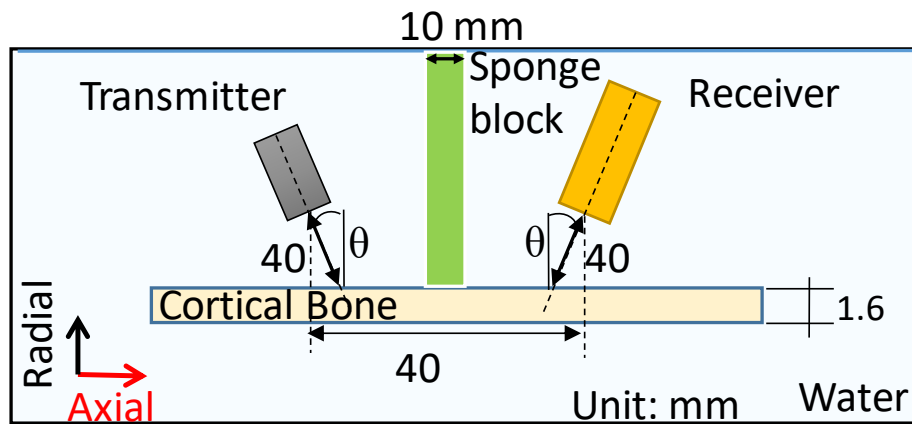
Figure 6.1 System setup for bone plates evaluation.

The sample was aligned with the transducers fixed in an initial position shown in the top view Fig. 6.2 a) position o'-o', after this, the position of the sample was rotated +20° to a position, b) a'-a' and finally, it was rotated to the opposite direction and placed in a position -20°, c) b'-b'. These three positions of the sample were used for measurements of the wave transmitted and received at different incident angles. Wave velocities were estimated as was described in the signal processing method in Chapter IV, after that, wave velocities at the three different positions were compared.
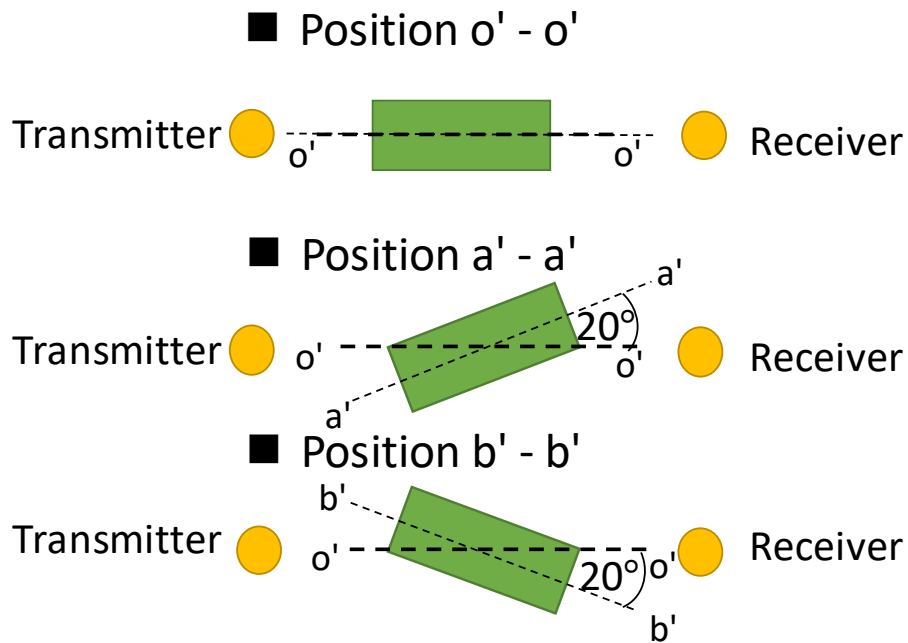
Figure 6.2 Top view of the sample positions considered for the measurement of the wave velocity.

6.3 RESULTS AND DISCUSSION

Waveforms of the bone sample in the position a'-a' are at 60° shown in Fig.6.3. Wave velocities measured at different incident angles with the plate sample being placed at different positions (o'-o', a'-a', b'-b') are shown in Fig. 6.4. In regard to the position of the sample in this measurement, wave velocities measured at incident angles $\theta < 30°$, were more affected by the orientation of the sample in the axial measurement, when it is not aligned to the initial position o'-o'. Wave velocities measured at different positions, with a misalignment of 20°, showed a reduction on the wave velocity values. On the other hand, at incident angles $\theta > 30°$, the sample position did not significantly influenced the wave velocity measurement at this range. The estimated wave velocities were quite similar in all the sample positions.

Regarding to the incident angles, as seen in the results (Fig. 6.4), two main wave velocities were observed depending on the angle of the ultrasound radiation. In the first range a

velocity of approximately 3500 m/s and in the other range, a velocity of 1750 m/s is mainly observed. Wave velocities found in literature and Snell's Law relations, indicates the possibility of the measurement of longitudinal wave when the incident angle is $\theta < 30°$, and shear wave when the incident angle is $\theta > 30°$.

Figure 6.3 Waveforms observed at different time in the position a'-a'
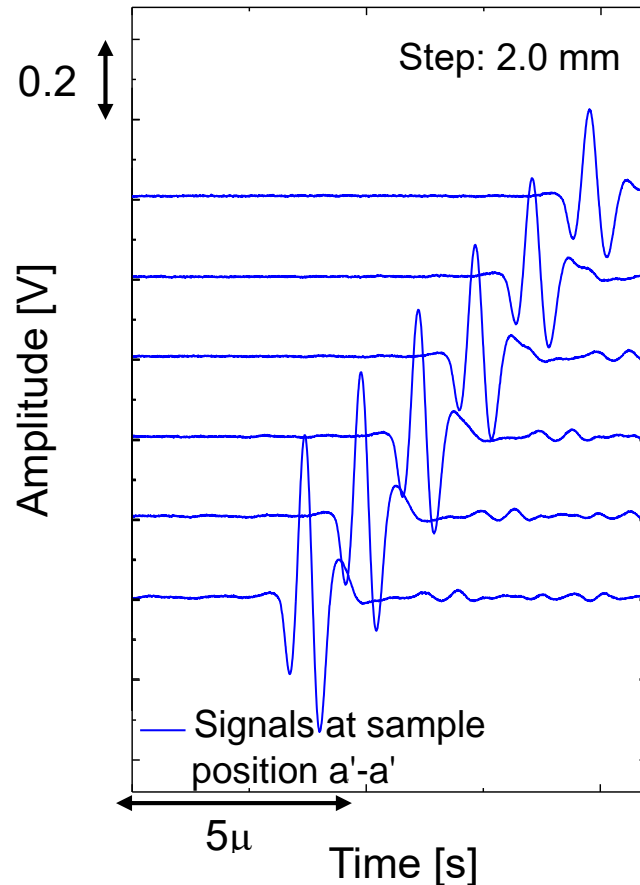
Assuming this is true, it is valid to say that the longitudinal wave velocity is more significantly affected by misalignment of the sample. Whereas, shear wave velocity is almost not affected by any change in the position of the sample, conserving the same range of values of the wave velocity.
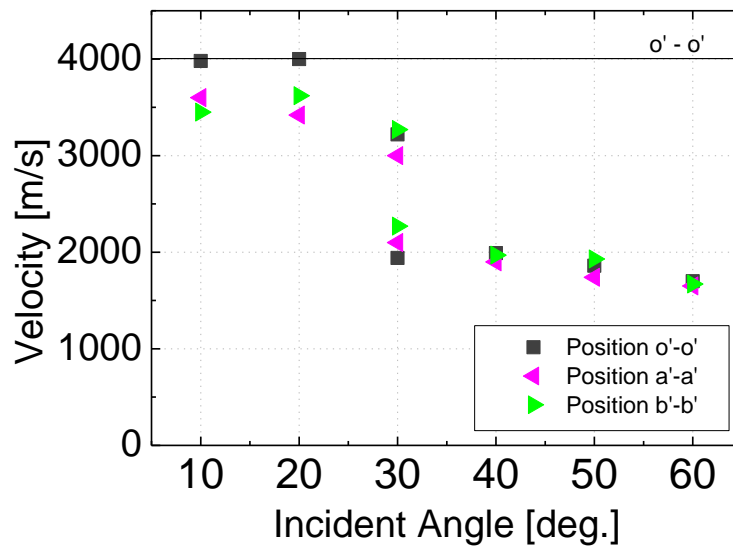
Figure 6.4 Wave velocities obtained at different angles of the sample evaluated at different orientations.

6.4 SUMMARY

A preliminary measurement in plate samples was performed to validate the system, the angle configuration. The measurement was focused on the experimental errors that could happens when the sample is placed causing a misalignment in the experimental axial transmission configuration. Here, the consequent effects on the shear wave velocity were analyzed in order to understand the bone anisotropy. Shear wave velocity was not affected by the bone misalignment of the experimental setup, whereas longitudinal wave velocity was significantly affected by the sample misalignment.

6.5 CONCLUSIONS

This preliminary measurement verified the good functioning of the system and the method proposed for the measurement of ultrasonic waves in bone samples using the axial transmission technique.

A plate sample was tested in three different positions to verify experimental errors of misalignment when the sample is placed. These measurements were performed in the axial direction of the bone sample.

Depending on the incident angle configuration, the system observed two possible waves with velocities similar to the longitudinal and shear waves. These findings were compared with theoretical values of the wave velocity and Snell's Law relations.

Finally, it was concluded that depending on the type of ultrasonic wave, the sample position and misalignment has more or less impact in the wave velocity. Therefore, this preliminary measurement suggest that shear wave velocity seems to be not affected by the bone misalignment of the experimental setup, whereas longitudinal wave velocity could be significantly affected by the sample position. These changes in the measurement of the wave velocity are attributed to the bone anisotropy. Measurements considering different waves, which propagation is different from one to another, are important to understand the effects of anisotropy in cortical bone and how these change the ultrasound propagation. This understanding may allow to improve the precision of current clinical devices using ultrasound.

REFERENCES

[6.1] P. Laugier, G. Haiat eds., "Bone Quantitative Ultrasound", Dordrecht: Springer, vol. 576, 2011.

[6.2] S. F. Lipson, J. L. Katz, "The relationship between elastic properties and microstructure of bovine cortical bone", *Journal of biomechanics*, *17*(4), 231-240, 1984.

[6.3] Y. Yamato, M. Matsukawa, T. Otani, K. Yamazaki, A. Nagano, "Distribution of longitudinal wave properties in bovine cortical bone in vitro," *Ultrasonics*, vol. 44, pp. e233-e237, 2006.

[6.4] B.K. Hoffmeister, S.R. Smith, S.M. Handley, J. Y. Rho, "Anisotropy of Young's modulus of human tibial cortical bone," *Medical and Biological Engineering and Computing*, vol. 38, pp. 333–338, 2000.

[6.5] H. Sai, G. Iguchi, T. Tobimatsu, K. Takahashi, T. Otani, K. Horii, and K. Yoh, "Novel ultrasonic bone densitometry based on two longitudinal waves: significant correlation with pQCT measurement values and age-related changes in trabecular bone density, cortical thickness, and elastic modulus of trabecular bone in a normal Japanese population," *Osteoporosis international*, 21, (10), 1781-1790, 2010.

CHAPTER VII EVALUATION OF WAVE VELOCITY IN BONE PLATES

This part of the thesis work focuses on the detection of axially transmitted shear waves and finding the effective incident angle for an efficient shear wave detection in plate samples of different bones. In the experimental measurements, ultrasonic waves radiated at different incident angles along the axial direction of the bone were characterized in thin cortical bone plates considering typical thicknesses values of osteoporotic cortical bone in humans. Only one transmitter and one receiver, in an axial transmission configuration, were necessary for the determination of the wave velocity using the time of flight technique (TOF) [7.1]. Similar experimental conditions were modeled and the wave propagation was simulated using the Finite-difference time-domain method (FDTD) [7.2-7.3]. Isotropic 2D-simulations were compared with the experimental measurements performed in the anisotropic medium of the bone. These results were discussed, considerations observed in the simulations of the wave propagation were made in order to understand the complicated waveforms in this case. The identification of target waves for the wave velocity calculation is explained in plate samples. Generated waves on the plate surface of the bone plate were characterized and the corresponding dispersion curves were extracted using an enhanced two-dimensional spatio-temporal Fourier transform (2D-FFT) [7.4]. The 2D-FFT was applied at the effective angles for longitudinal and shear wave detection, consequently longitudinal, as well as, shear waves were observed and successfully characterized.

7.1 SAMPLES

In order to represent a simplified but sufficient model of human bone that be suitable for experimental measurements and provides the information aimed to achieve through this experiment, plate samples were extracted from the cortical bone of bovine femora. The ages of the bovines ranged between 27 to 32 months. Previous studies have demonstrated the applicability of plate models as a satisfactory approximation of the curved shaped surface of the cortical bone [7.5- 7.7], additionally similarities between the wave velocities measured in plate and tube bone samples has been investigated [7.8]. The

samples were prepared as is shown in Fig. 7.1 in order to perform measurements in the axial direction of the bone plate. The corresponding thicknesses of the fabricated bone plates are w = 1.0 mm, 1.6 mm and 2.0 mm which are typical values of human bone thicknesses [7.9]. Cortical bone thickness in the range of 1.4 ~ 2.0 mm are normally measured in an osteoporotic elderly person [7.10]. Sample geometries are also represented in Fig. 7.1. A picture of the actual samples is show in Fig. 7.2. And, Table 7.1 summarizes the fabricated plates, thicknesses and the corresponding density determined by a simple measurement of the weight and volume of the plate. Moreover, bone samples were immersed and tested in a water tank in order to simulate the surrounding soft-tissue.
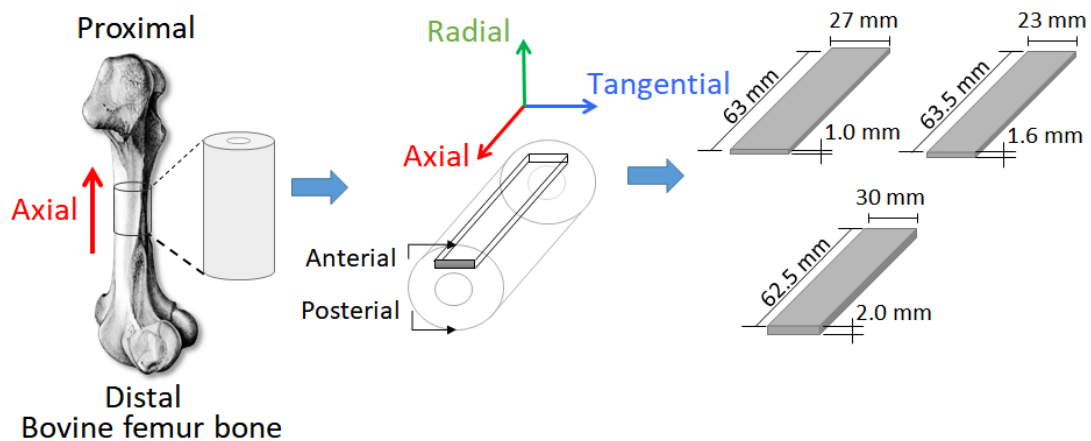
Figure 7.1 Samples obtaining and geometries of the fabricated bone samples plates.
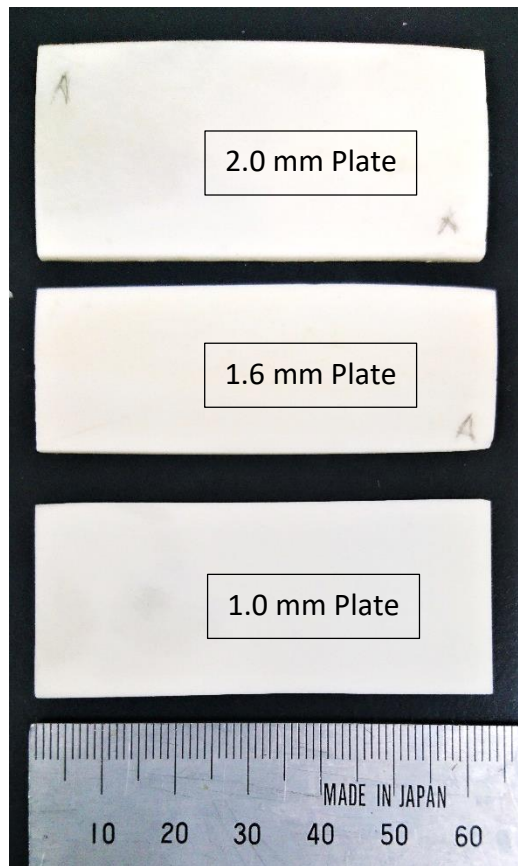
Figure 7.2 Image of the fabricated plate samples.

Table 7.1 Fabricated plate samples: thickness and density.

Sample	Thickness [mm] *w*	Density [kg/m³] (x 10³)
Plate 1	1.0	2.05
Plate 2	1.6	1.97
Plate 3	2.0	1.94

7.2 EXPERIMENT DESCRIPTION

Experimental measurements in this experiment uses the axial transmission configuration and geometries described in Fig. 7.3. Plate samples were evaluated at

incident angles (θ) from 10º to 60º (each 10º and 15º). Transmitter and receiver were separated 40 mm, approximately. The lift-off distance of the transducers with respect to the sample surface was defined in 50 mm, this distance was found to improve the signal response. The same geometries and configuration were maintained at each measurement at the corresponding incident angle.
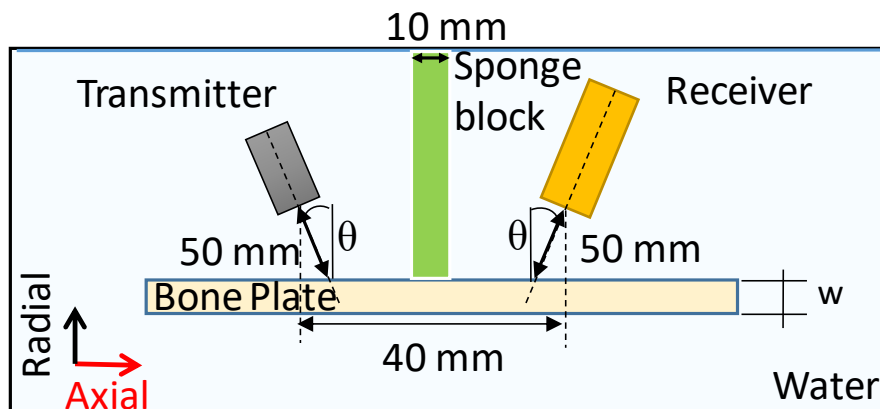
Figure 7.3. Experimental system using an axial transmission configuration for measurements along the axial direction of the bone plates samples.

The sampling frequency used in this experiment was 100 MHz, and temporal signals were averaged 1024 times by hardware. To avoid the detection of specular reflections and waves travelling in water directly a spongy block of 10 mm of thickness was placed between the transducers. For the frequency analysis, the 2D-FFT was performed using the temporal signals. The same sample frequency and the step size 0.1 mm used in the scan were used for the transform of the experimental signals.

7.2.1 ADDITIONAL EXPERIMENTS

Additional experiments using a transverse transmission measurement [7.11- 7.14] were carried out in the plate samples in order to compare the experimental results obtained from the axial transmission measurement [7.15- 7.18]. For the longitudinal wave measurement, a transmitter and a receiver were in contact with the lateral side of the bone and were aligned transversally in the axial direction of the bone. Fig. 7.4. shows a scheme

of this measurement. For the determination of the shear wave velocity, the bone sample was placed between the transducers and with the bone surfaces facing the surface of the transducers and was rotated around the *y*-axis (tangential direction) of the bone plate. Measurements were performed every $\alpha = 5°$ from 30° to 65°.
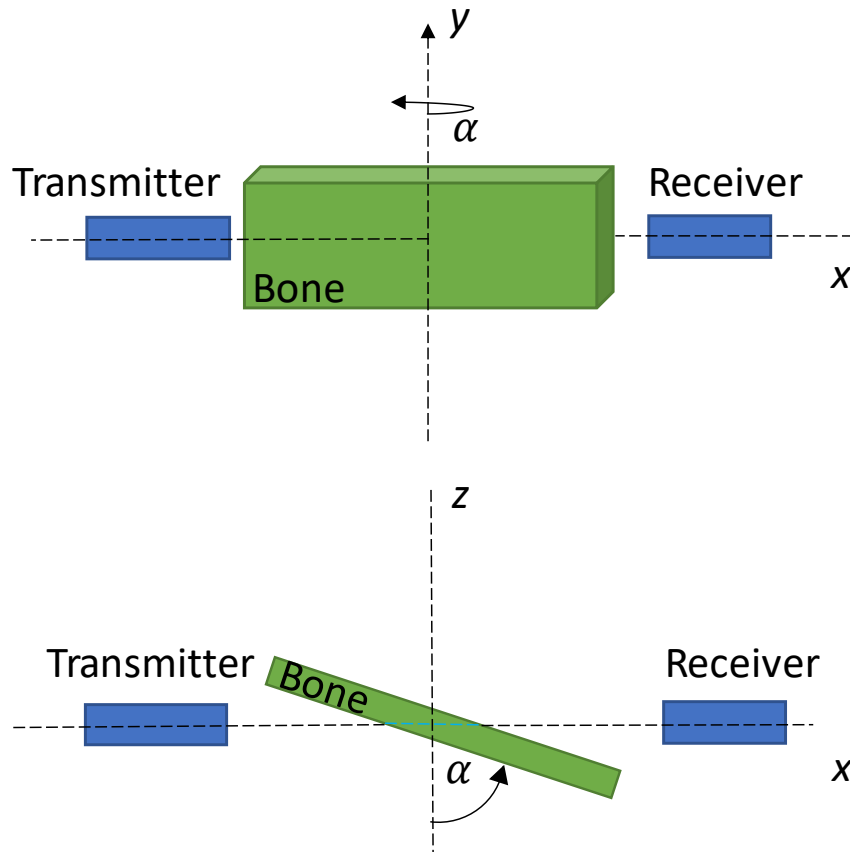
Figure 7.4 Transverse transmission setup for wave velocity measurement.

7.3   SIMULATION OF THE WAVE PROPAGATION

In order to understand the wave propagation in plate samples considering bone as an isotropic material, a simulation model using the 2D-FDTD method [7.2- 7.3] was implemented. The simulation geometries of the plate samples are shown in Fig. 7.5. For the model construction, some assumptions were made. The cortical bone is contemplated as a two dimensional transverse free plate. The plate model was considered as an isotropic and homogeneous material surrounded by an isotropic water medium. In this case, one transmitter and six receivers were considered, in an axial transmission configuration. The

receivers were separated 2.0 mm from each other were set at incident angles (θ) of 15º, 30º, 45º and 60º. The transmitter and receiver consisted in an array of pixels with the same length of the diameter of the transducers used in the experiments.
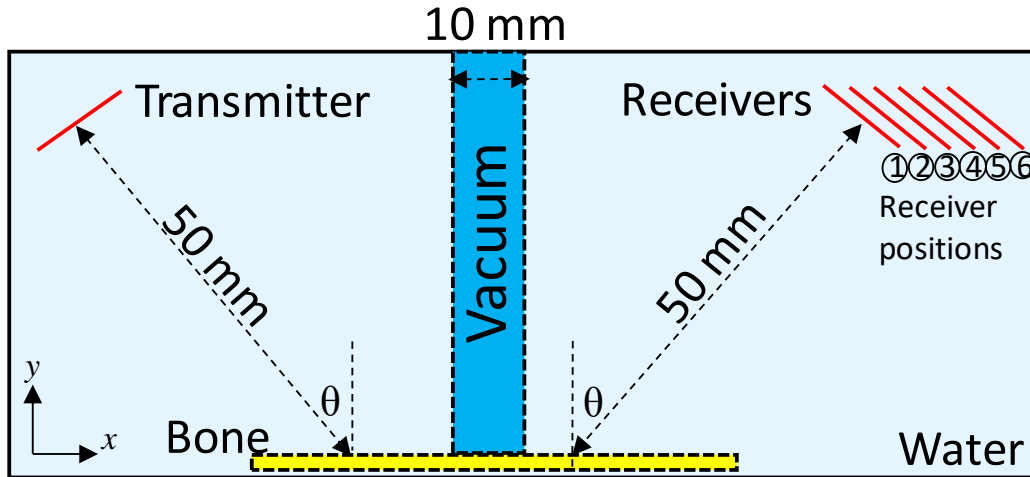
Figure 7.5 Simulation model and geometries.

Since the bone model is considered isotropic material, a longitudinal wave velocity of 4000 m/s and a shear wave velocity 1800 m/s was assumed following reference values of wave velocities measured in bovine bone [7.19]. The densities were defined using the same values of the fabricated bone plates, these values were shown in Table 6.1. Considering these parameters, a spatial resolution of 37.5 µm and a time resolution of 6.6 ns, both satisfying the Courant's stability condition [7.20], were established for the simulation. The Higdon's boundary condition [7.21] was implemented to avoid reflections from the edges of the simulation area. The simulation area has a matrix size of 1410×3700 pixels. The surrounding medium was considered isotropic, the sound velocity in water was defined as 1500 m/s and a density of 1000 kg/m^3. In this case, a vacuum block of 10 mm was set between the transducers working in the same way as the sponge block in the experimental measurements.

7.4   RESULTS AND DISCUSSION

The experimental signals obtained from the scan of the 1.0 mm plate at every step were stacked, the B-scans images at incident angles (θ) of 15º, 30º, 45º and 60º are shown

in Fig. 7.6. Waves arriving at different time, suggested the existence of basically two waves (longitudinal and shear waves among other attenuated waves). One detected at incident angles $\theta < 30°$ and another at incident angles $\theta > 30°$. The same can be seen in the simulation case, however, since the attenuation was not considered, multiple waves overlapping were observed. In order to determine the corresponding wave from where the wave velocities will be determined, the simulation of the waves propagating through the water-bone-water interface was carefully analyzed. Fig. 7.7 shows different instants of the wave propagation in the plate sample. The waves that are detected at the same incident angle (θ) at which it was generated, were selected. The first arriving waves at incident angles (θ) of 45° and 60° seem to come from the wave radiated from the edge of the transmitter and were therefore neglected. The waveform of the target waves, are indicated in Fig. 7.8, which are defined in a range between the dashed lines. In this graph, waves observed at incident angles (θ) of 15º, 30º, 45º and 60º in the simulation are displayed.
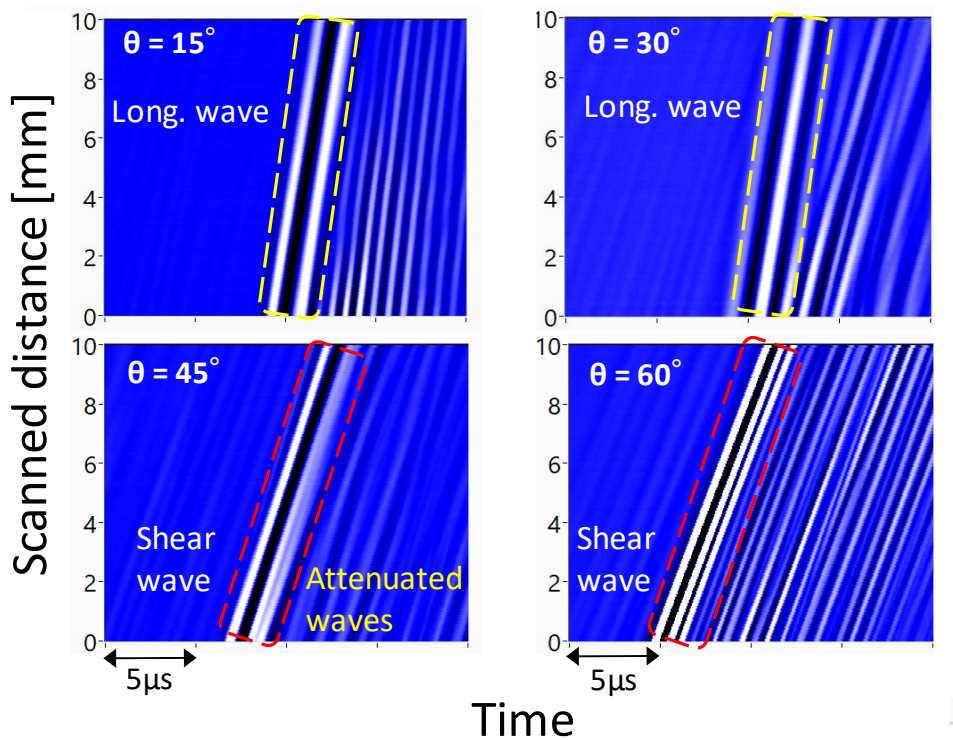
Figure 7.6 B-scan images of the experimental measurements.
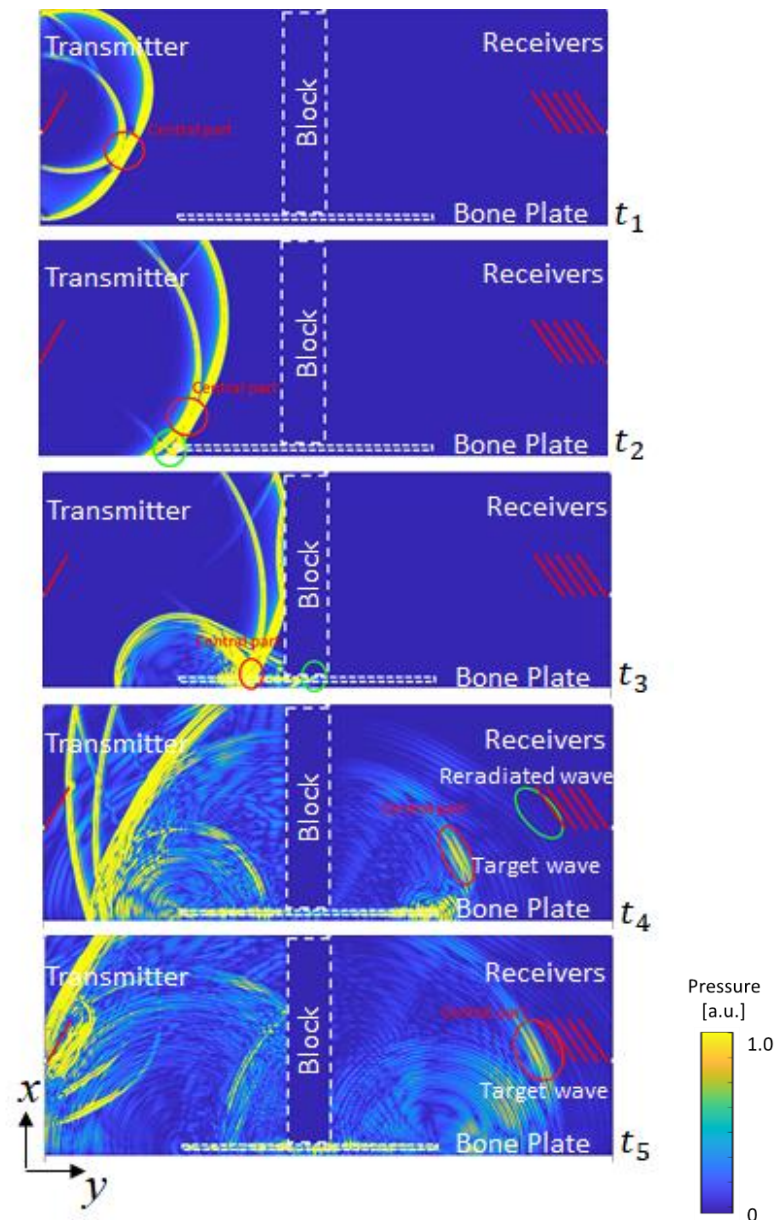
Figure 7.7 Instants of the simulation of the wave propagation in plate sample.
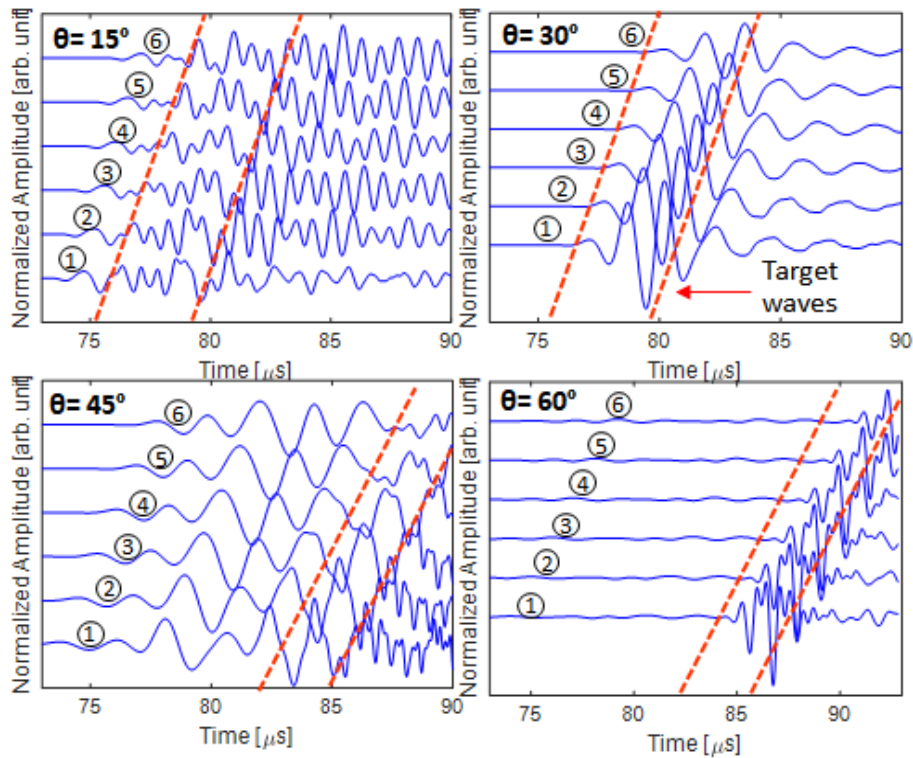
Figure 7.8 B-scan images of the experimental measurements.

The obtained wave velocities from the experimental measurements and simulation results, considering four distinct peak points of the wave are shown in Fig. 7.9. As it was predicted, two wave velocities were mainly observed. At incident angles $\theta < 30°$, close to the longitudinal wave critical angle $\theta_c = 22°$ (considering an isotropic medium) a velocity of 3840 m/s (experimental measurements) and 3680 m/s (simulation), corresponding to the longitudinal wave velocity was obtained. On the other hand, at incident angles $\theta > 30°$, close to the shear wave critical angle, $\theta_c = 56°$ (considering an isotropic medium) a velocity of 1850 m/s (experimental measurements) and 1840 m/s (simulation) corresponding to the shear wave velocity was determined. Finally, at incident angles $\theta = 30°$, both longitudinal and shear wave velocities were obtained. The values of these velocities represent the averaged values of velocities obtained at incident angles $\theta < 30°$ and incident angles $\theta > 30°$, respectively.
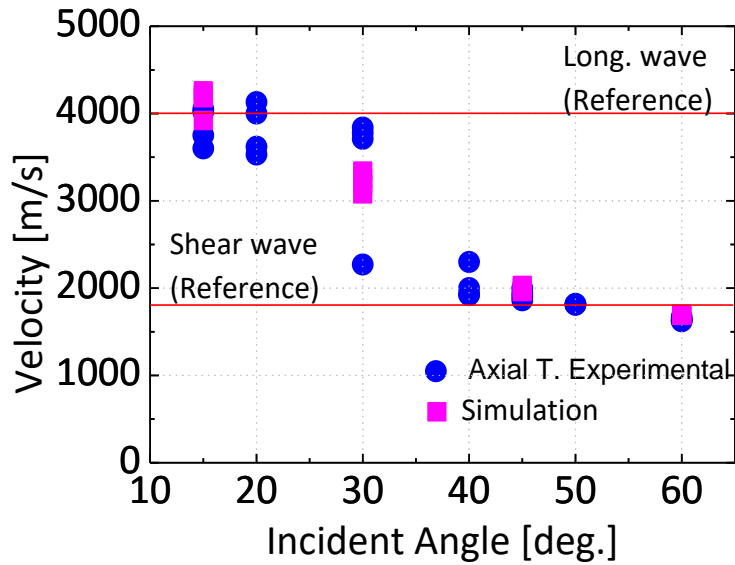
Figure 7.9 Obtained wave velocities from experimental measurements and simulations using axial transmission technique.

Similar results of shear wave velocities could be observed when comparing the axial transmission results with transverse transmission measurements, as is observer in Fig. 7.10. Additionally, a longitudinal wave velocity of approximately 3650 m/s was also confirmed with a transverse transmission measurement along the axial direction of the plate[31].
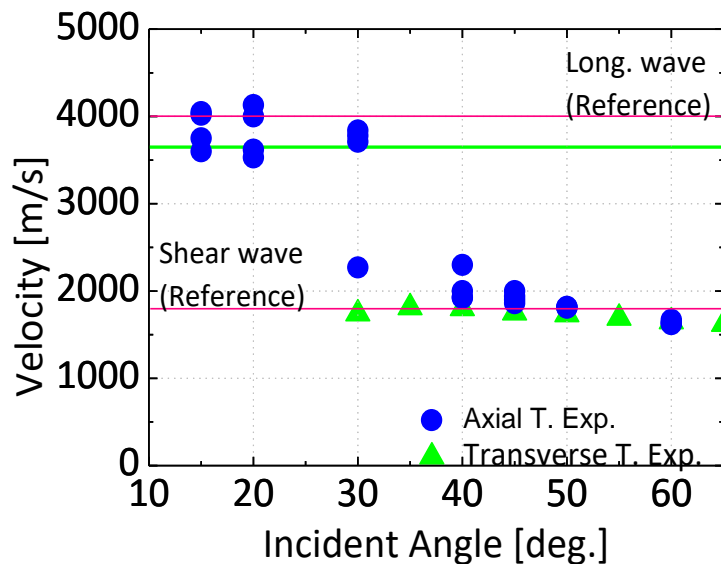
Figure 7.10 Obtained wave velocities from experimental measurements using axial and transverse transmission technique.

The obtained wave velocities are summarized in Table 7.2, Table 7.3 and Table 7.4 corresponding to the models with a plate thickness of 1.0 mm, 1.6 mm and 2.0 mm. As can be seen, results from the 2D-FDTD model shows good agreement with the experimental measurements in the anisotropic medium of the bone plate. Moreover, waveforms obtained in both, simulation and experiments revealed the existence of other waves travelling close and at different frequencies. In fact, these conditions are favorable to originate Lamb waves, especially in the 1.0 mm sample.

Table 7.2 Obtained velocities from the 1.0 mm sample. The values represent averaged values of all measurements at incident angles $\theta = 15 - 20°$ (Longitudinal wave velocity) and measurements at incident angles $\theta = 60°$ (Shear wave velocity).

	Experiments		Simulation	
Wave	**Transverse T.**	**Axial T.**	**Reference value**	**Axial T.**
Long. wave [10^3 m/s]	3.65	3.60-4.05	4.00	3.94-4.38
Shear wave [10^3 m/s]	1.67	1.62-1.67	1.80	1.69-1.70

Table 7.3 Obtained velocities from the 1.6 mm sample. The values represent averaged values of all measurements at incident angles $\theta = 15 - 20°$ (Longitudinal wave velocity) and measurements at incident angles $\theta = 60°$ (Shear wave velocity).

	Experiments		Simulation	
Wave	**Transverse T.**	**Axial T.**	**Reference value**	**Axial T.**
Long. wave [10^3 m/s]	3.45	3.20-4.07	4.00	4.06-4.30
Shear wave [10^3 m/s]	1.67	1.63-1.65	1.80	1.70

Table 7.4 Obtained velocities from the 2.0 mm sample. The values represent averaged values of all measurements at incident angles $\theta = 15 - 20°$ (Longitudinal wave velocity) and measurements at incident angles $\theta = 60°$ (Shear wave velocity).

	Experiments		Simulation	
Wave	**Transverse T.**	**Axial T.**	**Reference value**	**Axial T.**
Long. wave [10^3 m/s]	3.68	3.46-4.45	4.00	4.33-4.53
Shear wave [10^3 m/s]	1.60	1.63-1.65	1.80	1.70-1.75

Signals from the plate samples and simulations were analyzed in the frequency domain as a second approach. The relation between phase velocity and frequency-thickness was determined by the 2D-FFT method. Dispersion curves extracted from the

experimental measurements and simulation data considering the region of the selected target waves, as well as, the corresponding theoretical dispersion curves are presented in Fig. 7.11. The theoretical dispersion curves were calculated by finding the solutions of the Lamb wave equation for the antisymmetric, Eq. (3.3) and, symmetric modes, Eq. (3.4) [7.22- 7.23]. By plotting the solutions, a graph of the phase velocities as function of the frequency-thickness product was obtained. The theoretical curves consider the corresponding thickness t of the sample and were calculated assuming a longitudinal wave velocity of 4000 m/s and a shear wave velocity of 1800 m/s, typical values found in literature [7.19].
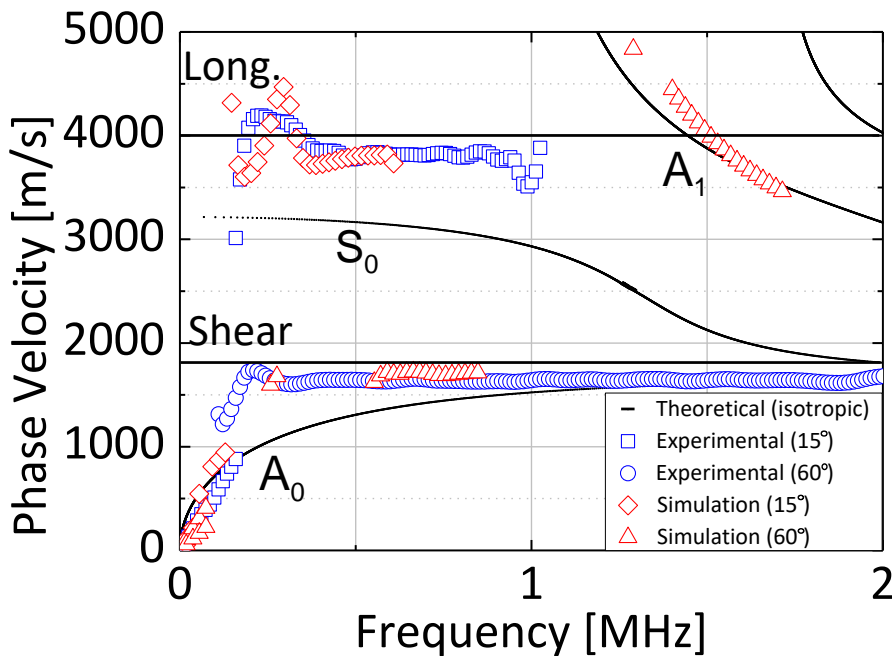
Figure 7.11 Extracted dispersion curves from experimental measurements and simulations.

In this plot, Fig. 7.11 longitudinal and shear waves were mainly characterized, the wave velocities were in good agreement to the wave velocity values previously determined. The use of few receivers in the simulation allowed that only few information about the sample be received. Under these conditions, apparent signs of the antisymmetric zero-order mode, A_0 and the A_1 mode were also observed in the simulation results.

While both, simulation and experimental results showed good agreement between each other, even though simulations consider an isotropic model, simulations curves do not perfectly match the theoretical dispersion curves. Theoretical curves that consider the Lamb equations only describe the wave propagation in solid mediums. However, simulations consider waves travelling in two different mediums liquid (water) and solid (bone).

It is presumable that the small difference between these two curves is caused by the bilayer condition, in this case water which mimics the soft-tissue may have some effects in the wave propagation from the liquid-solid and the solid-liquid medium, in other words, soft-tissue could affect the wave velocity when the wave is propagating in bone. However, this effects seems to be not very significant in this case. Indeed, a current challenge for clinical applications is to understand the influence of soft-tissue in the bone evaluation.

The use six receivers scanning a distance of 10 mm of the sample with a step size of 2.0 mm for the 2D-FFT analysis of the simulation signals, could be not enough to extract successfully the sample information due to the problems with the spatial resolution. As it was observed in Fig. 7.11 only few measurements are extracted in the simulation for the dispersion curves. In order to verify the information extracted from the 6 receivers, especially at the incident angle of 60° (for shear wave excitation). A simulation using 30 receivers and a simulation using 100 receivers were compared. This time considerations of the target waves were not considered and a wider range of waves were taking in account in order to verify the effectiveness of the 6 receivers against the addition of more receivers, as well as, to characterize all the waves detected at the 60° case. The 2D-FFT, wave number vs. frequency, intensity graphs were considered to improve the observability of the dispersion curves. These graphs were at the same time compared with the theoretical dispersion curves for a 1.0 mm plate. 2D-FFT intensity maps are shown in Fig. 7.12 a) using 6 receivers, step size: 2.0 mm, b) using 30 receivers, step size: 0.3 mm, c) using 100 receivers, step size: 0.15 mm and d) experimental data measured in 100 steps, with a sampling frequency of 151 MHz at which the signals were calculated in the simulation.
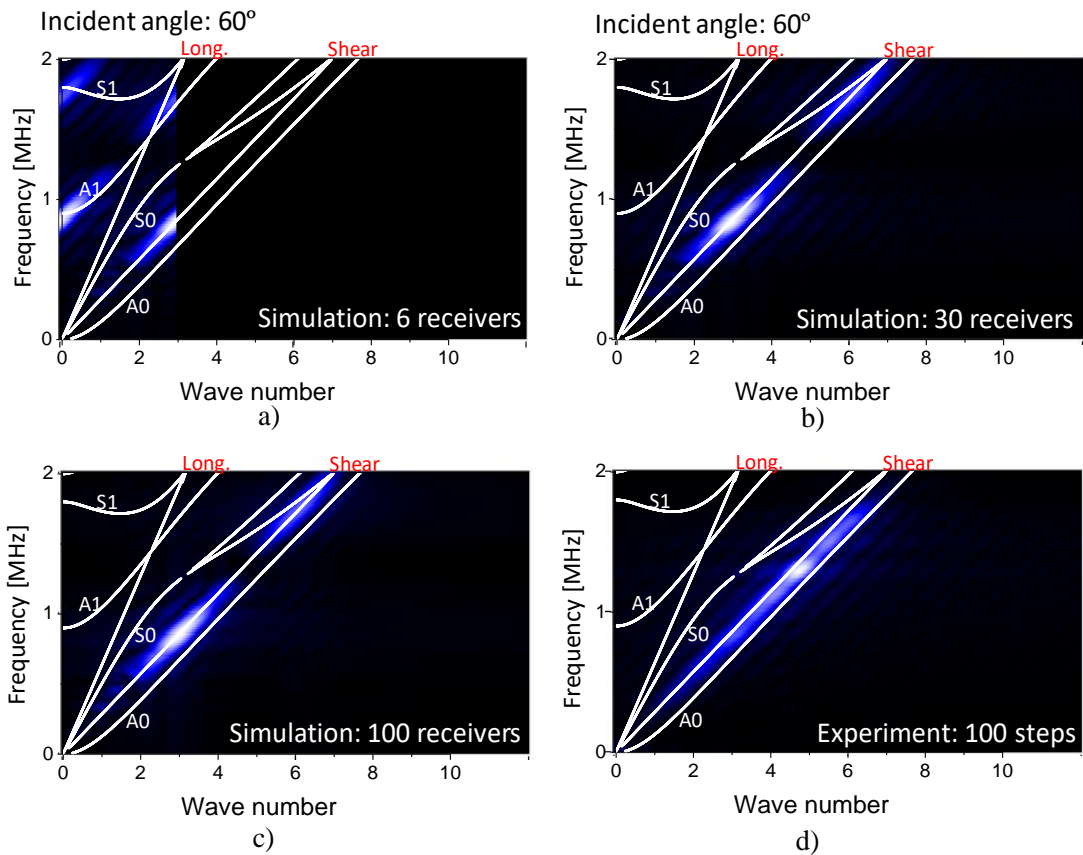
Figure 7.12 2D-FFT intensity maps of simulations using a) 6 receivers, b) 30 receivers, c) 100 receivers and d) experimental data measured in 100 steps.

The 2D-FFT intensity maps showed good agreement between the theoretical curves and the simulations using 6, 30 and 100. However, in the case of six receivers, no much information is showed to define clearly the shear wave in the dispersion curve. In the cases of 30 and 100 receivers, the wave is much precisely defined since more information was extracted by the implementation of several receivers and therefore improving the spatial resolution. Certainly, the implementation of several receivers scanning a larger area with a reduced spatial resolution will proportionally improve the information obtained from the sample however, in the real case this is not possible. The implementation of several transducers in medical devices for bone evaluation will increase significantly the cost of the device. Moreover, big or large devices may not be suitable for *in vivo* measurement of bones.

Improvements in the measurement techniques and signal analysis are rather required to process the information more efficiently. In this case, the wave selection by using a defined incident angle (using an axial transmission configuration) and a simple 2D-FFT allowed the observations of shear wave, in spite of few receivers were used. Lamb wave approaches using the same methods on the other hand, may not be suitable for mode identification, as was demonstrated in Fig. 7.12. This limitation of the 2D-FFT analysis for Lamb modes identifications can be overcome using a group-velocity filtering method to improve the 2D-FFT or enhancing the time domain signals using the singular value decomposition method (SVD) [7.23].

7.5   SUMMARY

An axial transmission measurement was applied in this measurement for the characterization of ultrasonic waves in plate samples fabricated from bovine bone. This study focused on the evaluation and effective detection of shear waves in bone plates. The wave propagation in a homogeneous and isotropic bone model was analyzed using the Finite-difference time-domain, (FDTD) method. A comparative analysis was presented between the experimental measurements and simulation results. Ultrasound generated and detected at different incident angles, revealed that longitudinal or shear waves can be observed depending on the angle. Wave velocity measurements in the anisotropic medium of the bone plate showed good agreement with the FDTD isotropic model results, suggesting that isotropic models could give a reliable estimation for measurements performed in the axial direction of the cortical bone. Finally, this study confirmed the possibility of shear wave detection using the axial transmission technique in plate samples of bovine bone.

7.6   CONCLUSIONS

In this section of the thesis work, shear waves were successfully measured in the axial direction of bone plates samples with regular thickness, using the axial transmission technique. The angle dependence of the wave propagation reveled that ultrasound

radiated at incident angles $\theta < 30°$, longitudinal wave were observed, on the other hand ultrasound radiated at incident angles $\theta > 30°$, shear wave were detected. Results of shear wave velocity at incident angles of $\theta = 60°$ showed great repeatability. In general, for an efficient wave detection and precise measurement of the wave velocity, the incident angle must be close or equal to the critical angle of the desired wave. Longitudinal and shear wave velocity values were approximately similar to reference values and they also were in good agreement to the wave velocities obtained in the transverse transmission measurement performed in the same bone samples. It was also concluded that measurements using the axial transmission technique are as efficient as the transverse transmission measurements. The wave propagation and the obtained signals in the bone plate were better understood using the FDTD method.

The comparative analysis of the wave velocities from isotropic simulation results showed good agreement with the experimental measurements performed in the anisotropic medium of the bone plate, it suggests that isotropic, homogeneous models can be used as a good approximation of bone properties.

In the second approach, longitudinal and shear wave were satisfyingly characterized in the frequency domain using the 2D-FFT method. Phase velocities had good agreement with the previous results. In this case, the employed measurement method, the proposed axial transmission configuration, and the wave selection were adequate to identify the desired waves by means of the 2D-FFT method independently of the number of receivers implemented in the simulations.

REFERENCES

[7.1] E. Bossy, M. Talmant, P. Laugier, "Effect of bone cortical thickness on velocity measurements using ultrasonic axial transmission: A 2D simulation study," *The Journal of the Acoustical Society of America*, vol. 112, no.1, pp. 297-307, 2002.

[7.2] Y. Nagatani, H. Imaizumi, T. Fukuda, M. Matsukawa, Y. Watanabe, and T. Otani, "Applicability of finite-difference time-domain method to simulation of wave propagation in cancellous bone," *Japanese Journal of Applied Physics*, vol. 45, no. 9R, 2006.

[7.3] Y. Nagatani, K. Mizuno, T. Saeki, M. Matsukawa, T. Sakaguchi, H. Hosoi, "Numerical and experimental study on the wave attenuation in bone–FDTD simulation of ultrasound propagation in cancellous bone," *Ultrasonics*, vol. 48, no. 6-7, pp. 607-612, 2008.

[7.4] P. Moilanen, V. Kilappa, J. Timonen, A. Salmi, P. Karppinen, E. Hæggström, R. Myllylä, "Photo-acoustic phase-delayed excitation of guided waves in coated bone phantoms. *In 2013 IEEE International Ultrasonics Symposium (IUS)*, pp. 2080-2083, 2013.

[7.5] P. H. Nicholson, P. Moilanen, T. Kärkkäinen, J. Timonen, S. Cheng, "Guided ultrasonic waves in long bones: modelling, experiment and in vivo application," *Physiological measurement*, vol. 23, no. 4, pp. 755, 2002.

[7.6] C. F. Njeh, J. R. Kearton, D. Hans, C. M. Boivin, "The use of quantitative ultrasound to monitor fracture healing: a feasibility study using phantoms," *Medical engineering and physics*, 20(10), 781-786, 1999.

[7.7] J. Foiret, J. Minonzio, C. Chappard, M. Talmant, and P. Laugier, *IEEE transactions on ultrasonics, ferroelectrics, and frequency control*, 61, (9), 1478-1488 (2014).

[7.8] E. Bossy, M. Talmant, F. Peyrin, L. Akrout, P. Cloetens, P. Laugier, "An in vitro study of the ultrasonic axial transmission technique at the radius: 1-MHz velocity

measurements are sensitive to both mineralization and intracortical porosity," *Journal of Bone and Mineral Research*, vol. 19, no. 9, pp. 1548-1556, 2004.

[7.9] C. F. Njeh, I. Saeed, M. Grigorian, D. L. Kendler, B. Fan, J. Shepherd, H. K. Genant, "Assessment of bone status using speed of sound at multiple anatomical sites," *Ultrasound in medicine and biology*, vol. 27, no.10, pp. 1337-1345, 2001.

[7.10] H. Sai, G. Iguchi, T. Tobimatsu, K. Takahashi, T. Otani, K. Horii, and K. Yoh, "Novel ultrasonic bone densitometry based on two longitudinal waves: significant correlation with pQCT measurement values and age-related changes in trabecular bone density, cortical thickness, and elastic modulus of trabecular bone in a normal Japanese population," *Osteoporosis international*, 21, (10), 1781-1790, 2010.

[7.11] T. Otani, "Quantitative estimation of bone density and bone quality using acoustic parameters of cancellous bone for fast and slow waves," *Jpn J Appl Phys*, vol. 44, no. 6S, 4578-4582, 2005.

[7.12] E. M. Stein, F. Rosete, P. Young, M. Kamanda-Kosseh, D. McMahon, G. Luo, R. Siffert, *Ultrasound in medicine and biology*, vol. 39, no. 3, pp. 388-395, 2013.

[7.13] K. Mano, H. Horii, T. Hagino, M. Miki, M. Matsukawa, and T. Otani, Journal of *Medical Ultrasonics, 42*, (3), 315-322, 2015.

[7.14] M. L. Bouxsein, B. S. Coan, and S. C. Lee, "Prediction of the strength of the elderly proximal femur by bone mineral density and quantitative ultrasound measurements of the heel and tibia," *Bone* **25**(1), 49–54 (1999).

[7.15] R. Barkmann, P. Laugier, U. Moser, S. Dencks, M. Klausner, F. Padilla, G. Haiat, M. Heller, C. C. Glüer, "In vivo measurements of ultrasound transmission through the human proximal femur," *Ultrasound Med Biol*, vol. 34, no. 7, pp. 1186–1190, 2008.

[7.16] H. Sievänen, S. Cheng, S. Ollikainen, K. Uusi-Rasi,"Ultrasound velocity and cortical bone characteristics in vivo," *Osteoporosis International*, vol. 12, no. 5, pp. 399-405, 2001.

[7.17] M. Sasso, G. Haiat, M. Talmant, P. Laugier, and S. Naili, "SVD-based algorithm for axial transmission ultrasound technique application to cortical bone characterization," *IEEE Trans Ultrason Ferroelectr Freq Control*, vol. 55, no. 6, pp. 1328-1332, 2008.

[7.18] J. Schneider, G. Iori, D. Ramiandrisoa, M. Hammami, M. Gräsel, C. Chappard, R. Barkmann, P. Laugier, Q. Grimal, JG. Minonzio, K. Raum, "Ex vivo cortical porosity and thickness predictions at the tibia using full-spectrum ultrasonic guided-wave analysis," *Arch Osteoporos*, vol. 14, no. 21, 2019.

[7.19] Y. Yamato, M. Matsukawa, T. Otani, K. Yamazaki, A. Nagano, "Distribution of longitudinal wave properties in bovine cortical bone in vitro," *Ultrasonics*, vol. 44, pp. e233-e237, 2006.

[7.20] R. Courant, K. Friedrichs, and H. Lewy, "On the partial difference equations of mathematical physics," *IBM Journal of Research and Development*, vol. 11, no. 2, pp. 215-234, 1967.

[7.21] R. L. Higdon, "Numerical absorbing boundary conditions for the wave equation. Mathematics of computation," *Mathematics of computation*, vol. 49, no. 179, pp. 65-90, 1987.

[7.22] H. Lamb, "On waves in an elastic plate," Proc. R. Soc. Lond. A, vol. 93, no. 648, pp. 114-128, 1917.

[7.23] P. Moilanen, "Ultrasonic guided waves in bone," *IEEE transactions on ultrasonics, ferroelectrics, and frequency control*, vol. 55, no. 6, pp. 1277-1286, 2008.

CHAPTER VIII EVALUATION OF WAVE VELOCITY IN BONE TUBES

This section of the thesis work focus on the application of an ultrasound axial transmission technique for the evaluation of shear wave velocities in cortical bone tube samples (bare bone) and bone tubes surrounded by a mimicking soft-tissue layer. Two different bare tube samples made of cortical bone and three soft-tissue mimicking layers of different thicknesses were tested. The main purposes of this study are to investigate the impact of bone curvature in tube samples and the impact of soft-tissues, on the shear wave velocities measured along the axial direction of the bone. Subsequently, 3D simulations based on the elastic Finite-difference time-domain (FDTD) method are used to validate the experimental measurements and study the wave propagation in homogeneous and isotropic bone models. Observed signals are analyzed in both, time and frequency domains. Results in bone tube samples are compared with previous measurements in bone plate samples. Isotropic 3D-bone models as a simplification of the actual problem are validated.

8.1 SAMPLES

Two hollow tube samples (Tube A and Tube B) were fabricated from the anterior part of the cortical bone of bovine femora. The samples were cut to such an extent that measurements can be performed in the axial direction of the bone tube. The thickness w, the difference between the outer and inner radius, was 1.6 mm in both cases. The thickness selection was based on the typical values measured in osteoporotic elderly people that are in the range of $1.4 \sim 2.0$ mm [8.1]. The length of the samples was 63 mm and the outer diameters were 11 mm (Tube A) and 12 mm (Tube B), other geometries are depicted in Fig. 8.1. An image of the samples can be observed in Fig. 8.2. Whereas, Table 8.1 summarizes these values and the corresponding densities that were determined by measuring the weight and volume of the cylinder.
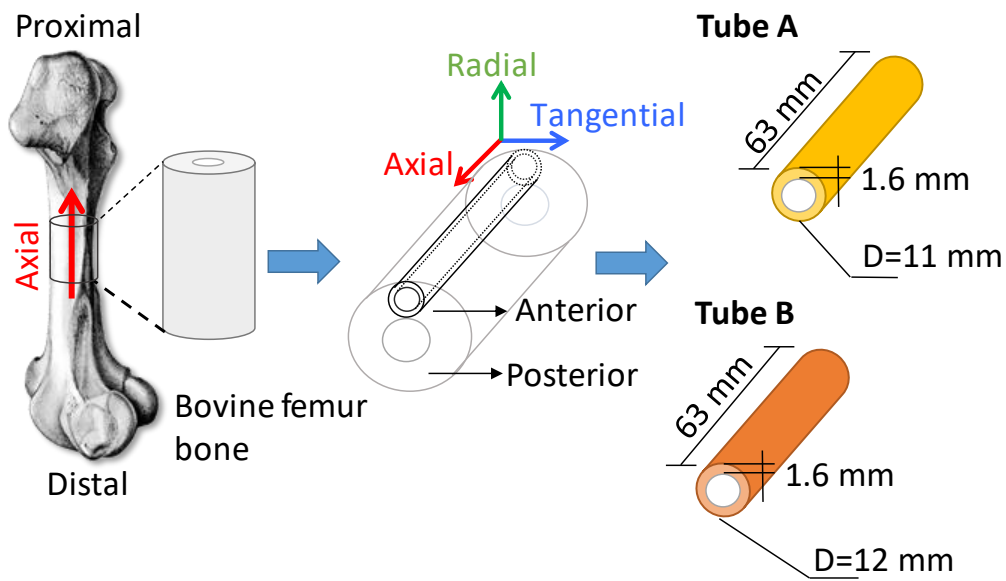
Figure 8.1 Fabricated bone samples and geometries.

Figure 8.2 Image of the fabricated bone samples.

Table 8.1. Fabricated bone samples: thickness and density

Sample	Thickness [mm]	Density [10^3 kg/m^3]
Tube A	1.6	1.75
Tube B	1.6	1.81

On the other hand, three soft-tissue mimicking layers were fabricated from a combination of Agar powder (10%, HPC Ind., Ltd.) and water [8.2- 8.4]. The fabricated layers had approximated thicknesses of 2.2 mm, 4.0 mm and 7.0 mm, these soft-tissue thicknesses can be expected at the distal end of the forearm [8.5]. Other properties are described in detail in Table 8.2.

Table 8.2. Properties of the soft-tissue mimicking layer.

Sample	Thickness [mm]	Density [10^3 kg/m^3]	Wave velocity [10^3 m/s]	Composition
Agar solid layer	1.6	1.05	1.75	10% agar powder 90% water

8.2   EXPERIMENT DESCRIPTION

The experimental method used in this section is similar to the experimental method described in previous experiments in plates. For the evaluation of tube samples without soft-tissue, water as the surrounding medium was selected because its bulk velocity is close to that in soft-tissue and is typically used for these purposes [8.6- 8.7]. On the other hand, a more accurate model using the mimicking soft-tissue layer covering the tube sample was also considered and which bulk velocity is closer to the real soft-tissue in humans. This process is detailed as follows.

For the axial transmission configuration, the transducers were set at the same incident angle and were separated 40 mm approximately, after that, the transducers and

sample were aligned to the axial direction and separated from the surface of the sample a lift-off distance of 50 mm. As explained before, the angle selection will overcome the difficulty in the identification of the waves due to a complex interference of several waves pointed in reference [8.6], especially in this case where a more complex geometry is tested. The incident angles (θ) used were in a range from 10º to 60º (each 10º in the case of bare bone and each 15º in the case of bone with soft-tissue layer). The experimental system configuration and the geometries used are displayed in Fig. 8.3. In this Figure a representation of the axial transmission configuration used for the evaluation of bone tube sample covered with a mimicking soft-tissue layer is shown. For the case of the bare bone, when the sample is not covered by the soft-tissue layer, the geometries and configurations are similar to the ones presented in Fig. 8.3, now considering the bone surface as the reference surface to place the transducers.
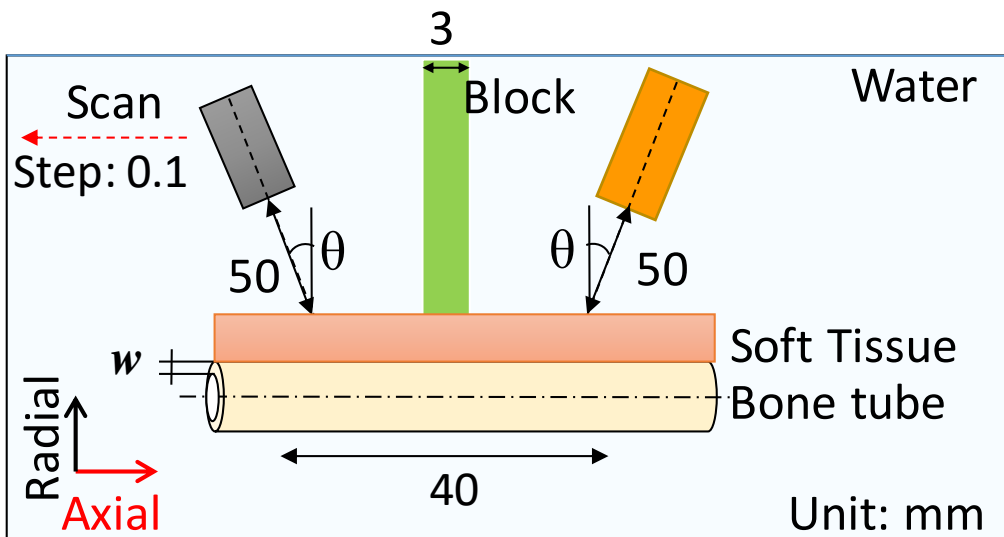
Figure 8.3 Experimental system configuration using the axial transmission technique.

All geometry conditions shown in Fig. 8.3 were maintained in each measurement at the different incident angles. For the scan, the transmitter was moved a distance of 10 mm along the axial direction of the bone sample at a step size of 0.1 mm. A sampling frequency of 500 MHz was selected this time to record the temporal signals received at every step (while moving the transmitter). After that, the acquired signals were averaged 1024 times by hardware. Additionally, a 3.0 mm spongy block was placed between the transducers. Only the Tube B sample was selected to be tested with the different soft-

tissue mimicking layers. The fabricated soft-tissue layers were placed carefully on top of the sample and covered a half of the external surface of the cylinder.

8.3 SIMULATION OF THE WAVE PROPAGATION

For the analysis of the wave propagation, 3D simulations based on the elastic FDTD method were implemented [8.8- 8.9]. The simulation geometries resemble the Tube B sample and are shown in Fig. 8.4 a) model of bare bone and b) model of bone with the soft-tissue layer. Wave propagation in complex materials can turn out to be too complicated. In order to consider a simplified but reliable model some assumptions were made. A three-dimensional hollow cylinder model was built to represent the cortical bone. The cylinder model and its surroundings, water and soft-tissue layer were considered isotropic and homogeneous mediums. The sound attenuation was not considered for the simulations. The transmitter and receivers consisted of a set of elements (of the simulation matrix) in a defined circumference of diameter 10 mm and 13 mm respectively (diameter of the transducers used in the experimental measurements). One set of elements as the transmitter and fifty sets of elements as receivers, in an axial transmission configuration, were positioned at angles of 15º, 30º, 45º and 60º. Each set of elements of the receiver were separated 0.3 mm from each other.
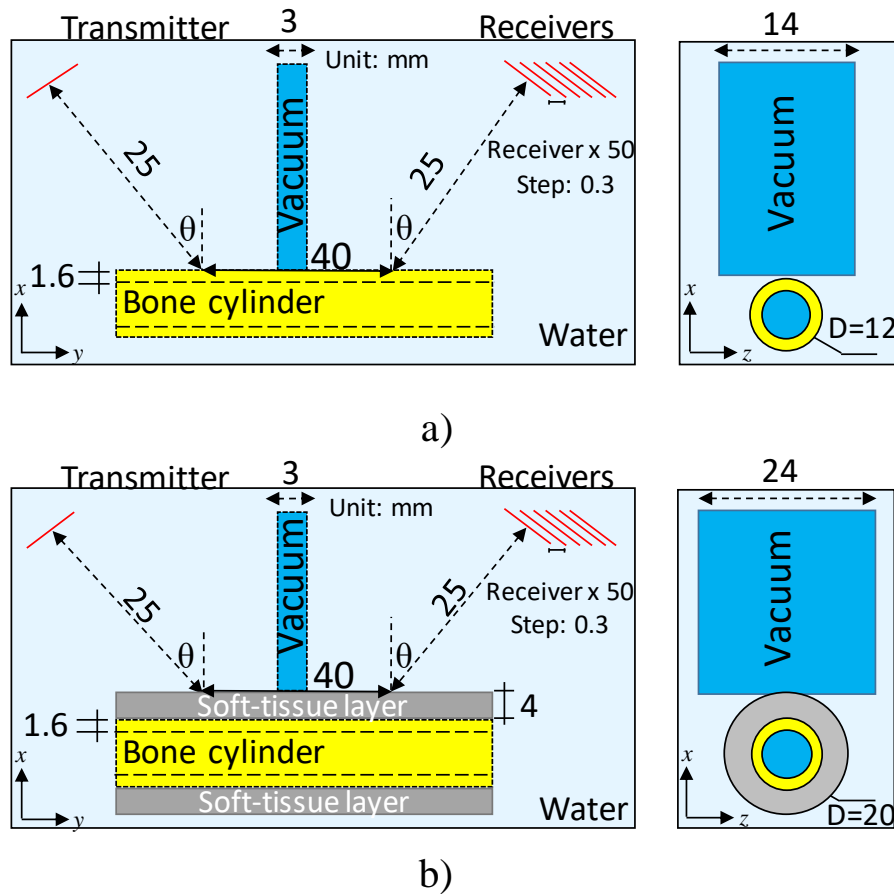
Figure 8.4 Simulation models and setup geometries of a) bare bone b) bone surrounded by the soft-tissue layer.

A single sinusoidal wave with a Hann window at 1 MHz was used as the transmitted signal. For the isotropic bone model, a longitudinal wave velocity of 4000 m/s and shear wave velocity of 1800 m/s was defined [8.10]. The bone density was defined using the same value measured experimentally in the Tube B sample, shown in Table 8.2. Additionally, the sound velocity in water was defined as 1500 m/s and a density of 1000 kg/m^3. This time, a 3.0 mm vacuum block was placed between the transducers in the model. In order to satisfy the Courant's stability condition [8.11] for the simulations, a spatial resolution of 74 μm and time resolution of 10.8 ns were determined. Higdon's boundary condition [8.12] was implemented. The simulation volume has a matrix size of $423 \times 1360 \times 204$ voxels for the case when the incident angle is 15° and similar matrix sizes in the other angle cases.

For experiments with the soft-tissue, an additional layer surrounding the bone tube was built. The thickness of the solid layer was 4.0 mm, similar to the used in the experiments. The soft-tissue layer had isotropic characteristics and, the wave velocity was defined as 1560 m/s, which is the averaged velocity of soft-tissue found in literature [8.13].

8.4   RESULTS AND DISCUSSION

In the first experiment of this section, measurements of the bare bone samples, Tube A and Tube B were performed using the proposed axial transmission method. In each sample, the experimental signals obtained from the measurement of the leaky waves at every step during the scan were stacked in a time-distance graph. These B-scans images at incident angles (θ) of 15º, 30º, 45º and 60º obtained from the Tube B sample are shown in Fig. 8.5 a) experiments and b) simulations. Additionally, the waveforms observed at 60° of same sample is presented in Fig. 8.6 for a) experiments and b) simulations.
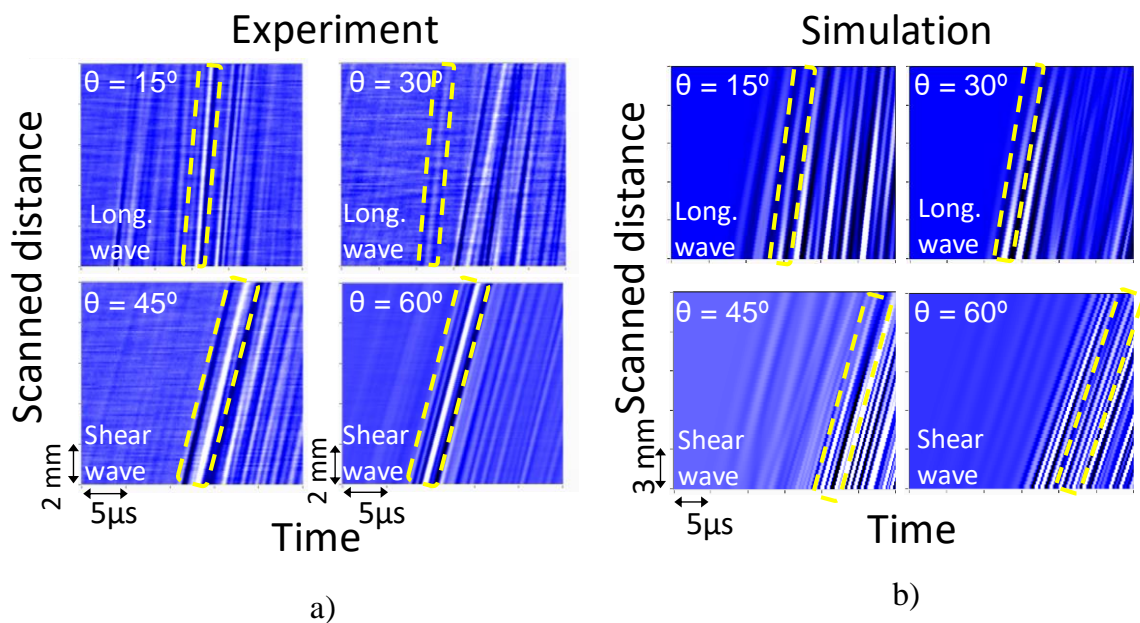
Figure 8.5 B-scan images obtained from a) experimental measurements and b) simulations of the bare bone (Tube B sample).
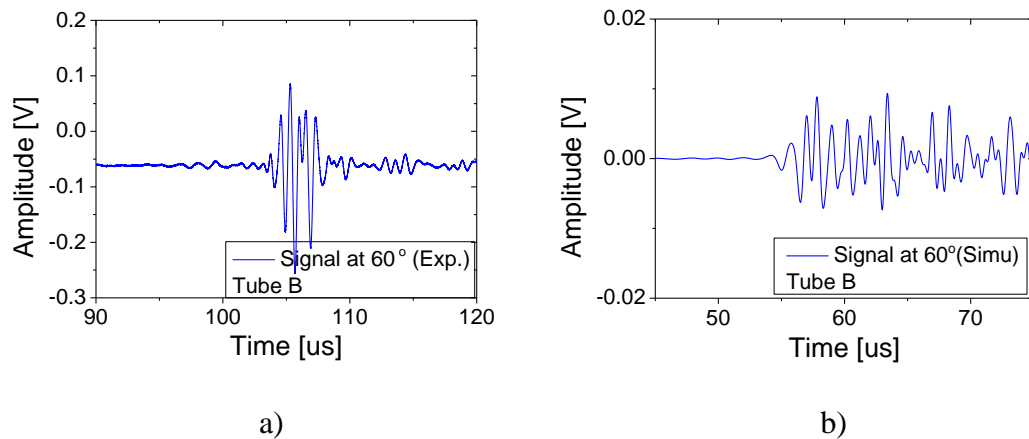
Figure 8.6 Waveforms obtained at 60° from a) experimental measurements and b) simulations of the bare bone (Tube B sample). *Experiments and simulations uses different transmitter-receiver distances and different sampling frequencies.

As observed in the previous measurements in plates, the angle dependence on the wave detection was confirmed in Tube A and Tube B samples. The angle dependence obeys Snell's law. Figure 8.5 shows a fast wave arriving at incident angles $\theta < 30°$ while a slower wave is detected at incident angles $\theta > 30°$. Interestingly, at incident angles closer to $\theta = 30°$ (close to longitudinal wave critical angle) these two waves could be observed (two slopes with different inclination). The detection of these waves was supported by simulations of a model resembling the Tube B sample. However, in all these cases, several signals were detected. At this step, a study on the wave propagation of the simulations was necessary to select correctly the characteristic wave at the corresponding incident angle. These are defined as the target waves, the waves that pass through the bone sample and are detected at the same incident angle. The selected waves are also indicated by the dashed lines in each case of Fig. 8.5. Consequently, these target waves found in the tube samples were used for wave velocity estimation and frequency analysis.

Wave velocity was determined at every incident angle, considering four peak points of the target waves. Wave velocities obtained from the experimental measurements in Tube A and Tube B samples and, simulations performed in the Tube B resembling model, are shown in Fig. 8.7. Supporting transverse transmission measurements in bone plate samples and Snell's law relations suggested that these values most likely correspond to

measurements of the apparent longitudinal and shear wave velocity [8.10] found in bovine bone.
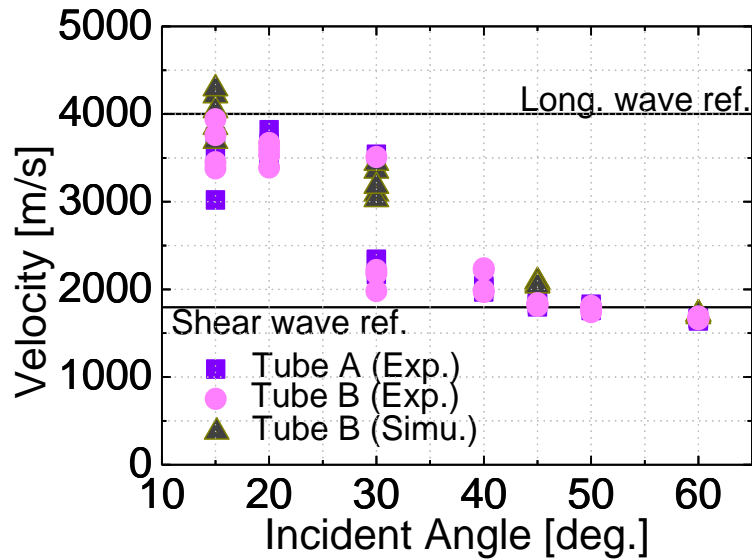
Figure 8.7 Apparent wave velocities from experimental measurements in Tube A and Tube B samples and simulations in Tube B sample.

For incident angles $\theta < 30°$, apparent longitudinal velocities in a range of (3020 – 3820 m/s) in sample A, and a range of (3380 – 3960 m/s) in sample B were measured. For incident angles $\theta = 30°$, an apparent longitudinal wave velocity of (3540 m/s) corresponding to the fastest signal and apparent shear velocities in the range of (2170 – 2340 m/s) corresponding to the second signal were measured in sample A. While in sample B, an apparent longitudinal wave velocity of (3510 m/s) and apparent shear velocities of (1980 – 2220 m/s) in the second signal were measured. For incident angles $\theta > 30°$, apparent shear velocities of (1640 – 1830 m/s) were measured in sample A. While in sample B, apparent shear velocities in a range of (1660 – 1810 m/s) was obtained. As is observed, apparent wave velocities measured in bare bone, Tube A and Tube B samples showed good agreement, these measurements strongly suggest the shear wave detection at incident angles $\theta > 30°$.

At the same time, these results in tubes were compared with measurements of wave velocity in bone plate samples (Table 7.3) of thickness $w = 1.6$ mm. Plate samples showed apparent longitudinal wave velocities in ranges of (3220 – 4070 m/s) and apparent shear

wave velocities of (1630 – 1800 m/s). Figure 8.8, shows a comparison between a) experimental measurements and b) simulations on Tube B and the plate sample. As can be observed, tube and plate samples also showed good agreement on the apparent wave velocities, especially closer to the shear wave critical angle 56°. In this case, incident angles greater than 50°, wave velocities showed high repeatability, therefore 50º and 60º are considered the effective angles for shear wave detection which is in agreement with Snell's Law.
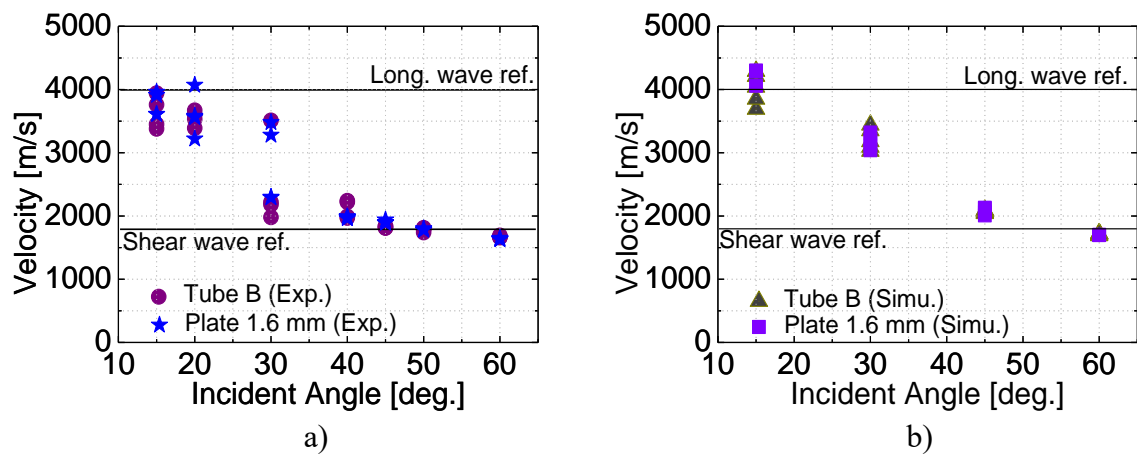
Figure 8.8 Apparent wave velocities in tube (Tube B) and plate samples from a) experimental measurements, and b) simulations.

On the other hand, plate and tube FDTD-simulations also showed a good prediction on the apparent wave velocities using the isotropic models resembling the bone plate and Tube B sample. In general, apparent longitudinal wave velocities were slightly higher than the ones obtained in the experiments while the apparent shear wave velocities showed good agreement. The apparent wave velocities obtained from the experiments and simulations of the Tube A and the Tube B are summarized in Table 8.3. In brief, these results showed that the bone curvature did not affect the shear wave measurements.

Table 8.3 Apparent wave velocities from experiments and simulation in bare bone samples Tube A and Tube B. Considering incident angles 15º – 20º (Long. wave) and 60º (Shear wave).

Wave velocity	Experiments		Simulation	
	Tube A	Tube B	Reference value	Tube B
Long. Wave [10^3 m/s]	3.02 – 3.82	3.38 – 3.96	4.00	3.69 – 4.29
Shear wave [10^3 m/s]	1.64 – 1.67	1.66 – 1.69	1.80	1.69 – 1.72

In the second experiment, the Tube B sample was tested with 2.2 mm, 4.0 mm, 7.0 mm soft-tissue mimicking layers on the top. Despite the addition of the soft-tissue layer, longitudinal and shear waves were detected as can be seen in the B-scan of the measurement with the 4.0 mm soft-tissue layer in Fig. 8.9. In the same way, an apparent longitudinal wave velocity was measured at incident angles $\theta < 30°$. and, at incident angles $\theta > 30°$, an apparent shear wave velocity was measured. Target waves were identified using the wave propagation simulations after that, the wave velocity was estimated. Waveforms observed in experimental measurements and simulations of bone sample Tube B with soft-tissue layer at 60° are shown in Fig. 8.10 a) and b), respectively.
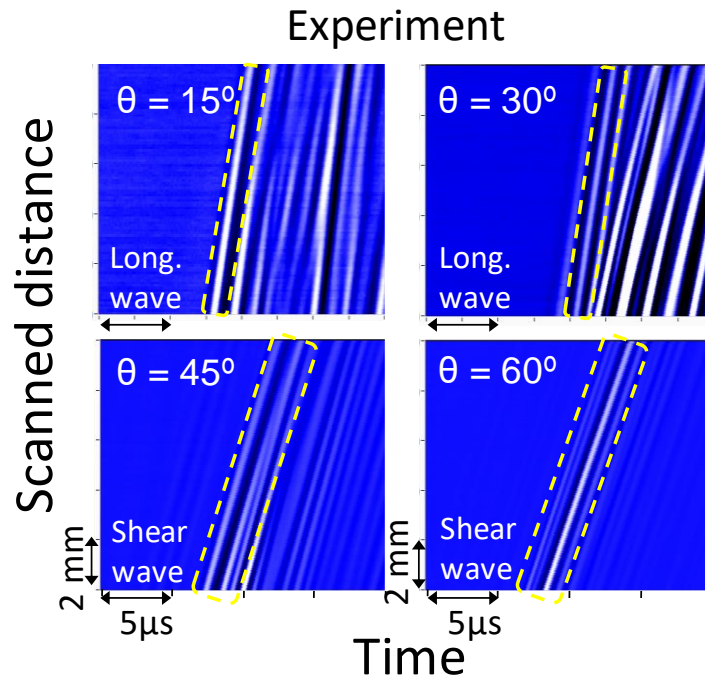
Figure 8.9 B-scan images from experimental measurements in bone tube samples with 4.0 mm of soft-tissue layer on the top.

a)   b)
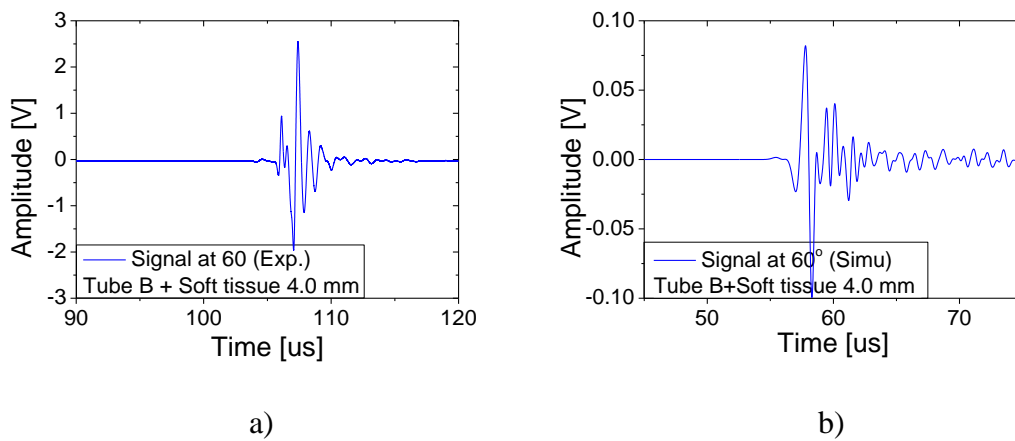
Figure 8.10 Waveforms obtained at 60° from a) experimental measurements and b) simulations of the bone (Tube B sample) with soft-tissue. *Experiments and simulations uses different transmitter-receiver distances and different sampling frequencies.

Signals acquired from the bone sample with soft-tissue layer, presented a larger amplitude (Fig. 8.10) compared to the signals acquired from the bare bone (Fig. 8.6). The reason is probably a superposition of the waves travelling on the soft-tissue, that leaked

immediately after the wave hit the soft-tissue layer, and the waves travelling through the bone. This was verified in the simulation and the consequently, the target waves were necessary to identify.

Apparent wave velocities of the bone sample covered by a) 2.2 mm, b) 4.0 mm, and c) 7.0 mm soft-tissue mimicking layers are shown in Fig. 8.11. Additionally, in the case of bone with the 4.0 mm soft-tissue layer, the simulation results are also depicted. Apparent wave velocities are summarized in Table 8.4.
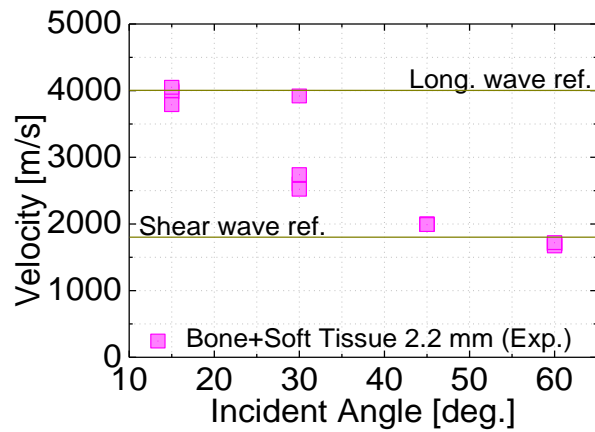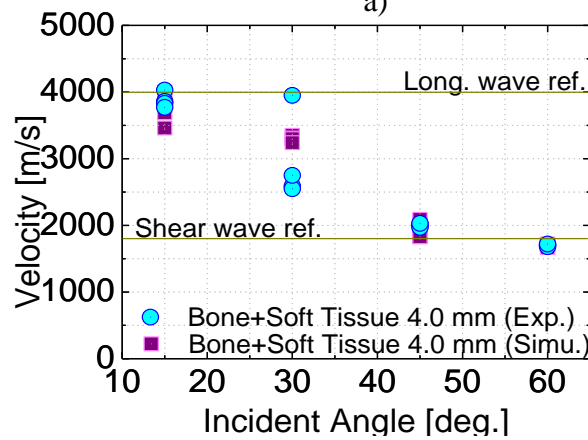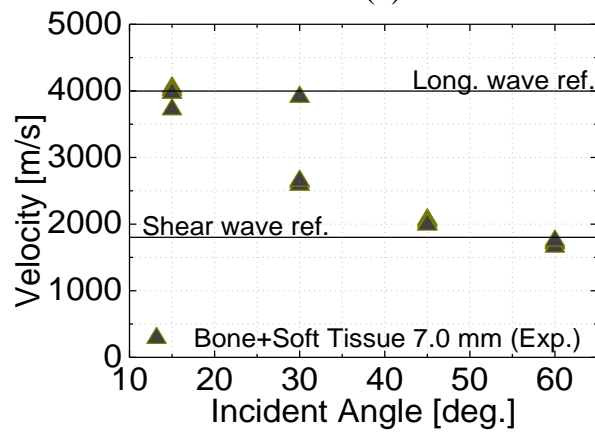
Figure 8.11 Apparent wave velocities in tube sample (Tube B) with a soft-tissue layer thickness of a) 2.2 mm b) 4.0 mm (experiments and simulations), and 7.0 mm.

Table 8.4 Apparent wave velocities from experiments and simulations in bone samples with 2.2 mm, 4.0 mm and 7.0 mm soft-tissue layers. Considering incident angles 15° (Long. wave) and 60° (Shear wave).

Wave velocity	Experiments			Simulations
	Soft-tissue (2.2 mm)	Soft-tissue (4.0 mm)	Soft-tissue (7.0 mm)	Soft-tissue (4.0 mm)
Long. Wave [10^3 m/s]	3.79 – 4.05	3.77 – 4.03	3.72 – 4.05	3.46 – 4.00
Shear wave [10^3 m/s]	1.67 – 1.72	1.68 – 1.72	1.66 – 1.75	1.67 – 1.72

This agreement on the apparent wave velocities, demonstrated that measurements of longitudinal and shear wave velocities and simulation at the corresponding angle according to Snell's Law were not affected by the soft-tissue layer on the top of the bone sample, for layers of thicknesses from 2.2 mm to 7.0 mm.

The elastic modulus of a typical soft-tissue is very low compared to the elastic modulus of bone and may be the reason why the velocity is not affected by the soft-tissue layer, this considering that mechanical stiffness and density of the material are deterministic in the wave velocity [8.14].

As the apparent longitudinal wave velocity is mainly measured at 15° and shear wave velocity is mainly measured at 60°, which are the effective incident angles for wave detection respectively. In the 45° case, it is believed that the resulting wave velocity may be a mixture of shear wave and weak traces of the S0 Lamb mode. S0 mode theoretically could be detected at this incident angle, according to Snell's Law. With a frequency of 1 MHz, the S0 mode velocity is closer to 2000 m/s, as shown in the theoretical dispersion curve (phase velocity - frequency) in Fig. 8.12. Therefore, the planar detector may be receiving these waves leaking at similar angles, and the resulting wave velocity could be slightly different (higher in this case) to the expected in the shear wave.
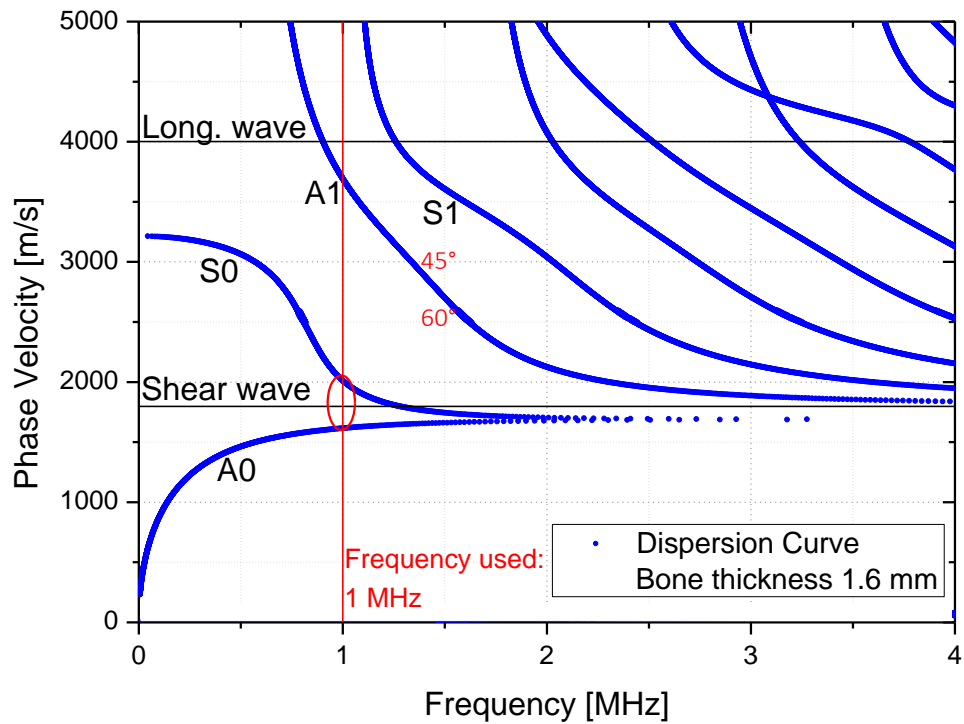
Figure 8.12 Theoretical dispersion curves (Frequency-Phase velocity)

Shear wave measurements were verified in the frequency domain. The frequency analysis based on the 2D-FFT method, considered the selected target waves in every case and the 2D-FFT maps confirmed the measurement of the shear wave in both cases, bare bone and bone surrounded by 4.0 mm of soft-tissue layer at the incident angle $\theta = 60°$ (the angle for an efficient shear wave detection) using the experimental and simulation data and the corresponding sampling frequency, 500 MHz (experiments), and 93 MHz (simulations). The relation between frequency and wavenumber is shown in Fig. 8.13. The data extracted from experiments and simulations are presented in an intensity graph, where the highest intensities are represented in white color. The results at 60° coincided with the reference value of the shear wave. Additionally, the extracted results were compared with theoretical dispersion curves calculated by finding the solutions of the Lamb's equations (Eq. 3.3, Eq. 3.4) [8.15].
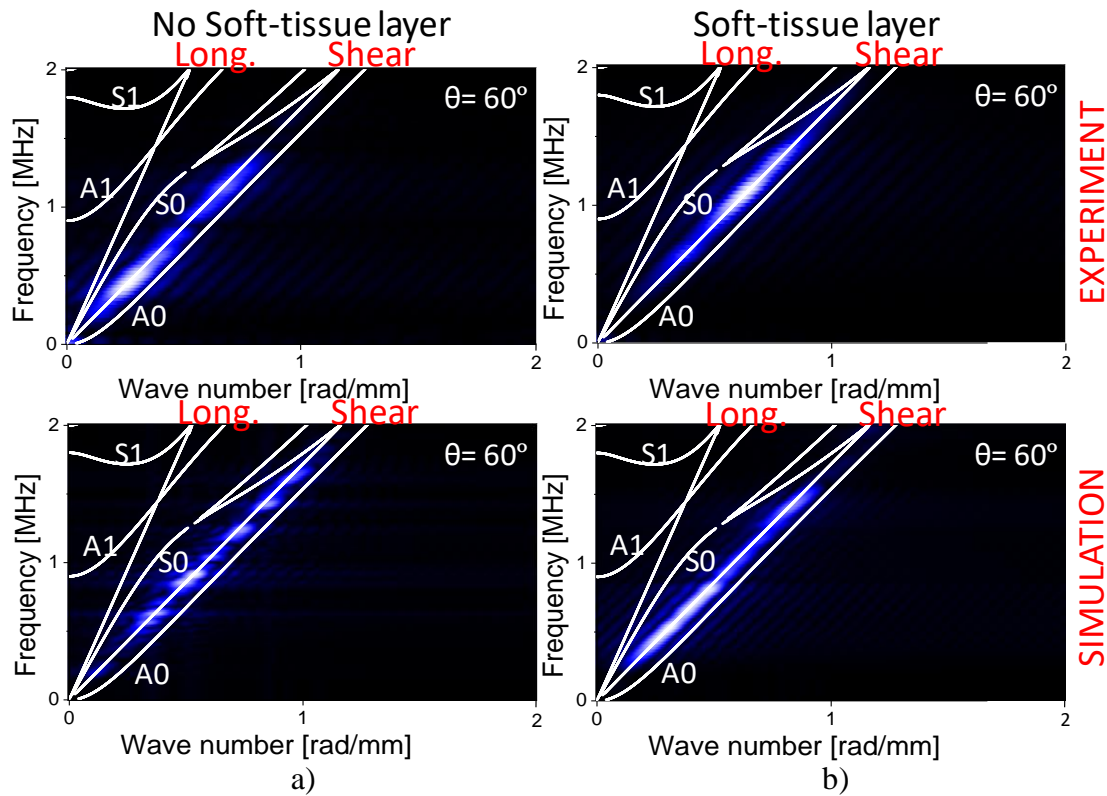
Figure 8.13 2D-FFT intensity maps in a) bare bone (experiments and simulations), b) bone with 4.0 mm soft-tissue layer (experiments and simulations).

Signs of Lamb modes were difficult to identify in the tubular samples even though detected signals showed additional waves propagating at different frequencies. The Lamb wave obtaining could be affected by the non-contact configuration of this experiment, where waves traveling through water could be attenuated. Lamb mode characterization is likely possible in in-contact measurements as has been demonstrated on several studies [8.16- 8.18]. Certainly, Lamb mode detection must be feasible when an isotropic model is considered, and absorption is neglected. However, as was mentioned in the method section, the incident angle configuration proposed here will emphasize the detection of the waves leaking at the approximated incident angle while attenuating the other waves. It is believed that at a frequency of 1 MHz (and probably due to the wavelength and cortical bone thickness relations described above) guided waves could be propagating along the sample but not as energetic as the surface waves (especially at the corresponding

critical angle of these waves). Considering simulations results at 60°, when shear wave detection is mainly emphasized, only traces of the other modes with similar wave velocity are possibly observed, however, the information obtained from the 2D-FFT is not enough to map the dispersion curve (in case of Lamb modes phase velocity changes with frequency) so the wave identification becomes difficult. But still, small frequency changes coming from these possibly Lamb waves are observed in the dispersion map in the same range of velocities.

8.5 SUMMARY

Considering the elongated and curved nature of most of the human bones and, its complex structure surrounded by biological tissues, this section of the thesis work proposed the application of an ultrasound axial transmission technique to investigate the impact of bone curvature and the surrounding soft-tissue on the shear wave velocity measurement of bone tube samples. Measurements were validated by 3D elastic-FDTD simulations of bone tube models. Shear wave observations were analyzed in time and frequency domains. In previous measurements on plate samples (thickness: 1~2 mm), shear waves were observed at large incident angles. Similarly, it was found that shear velocity measurements of tube samples were not affected despite the bone curvature and the mimicking soft-tissue layer on top of the samples.

8.6 CONCLUSIONS

Shear wave evaluation in cortical bone using the axial transmission technique was possible in bone tube samples with and without the soft-tissue mimicking layer. Apparent shear wave velocity measurements of bone tubes and plates showed good agreement. It was concluded that shear wave axial transmission detection and the apparent shear wave velocities were not affected despite the bone curvature and the soft-tissue layer on the top of the bone sample. In particular, incident angles (50º - 60º) closer to the shear wave critical angle, estimated employing Snell's law, showed good agreement and great repeatability on the wave velocity measurement.

Regarding to the waveforms observed at 60, where shear wave was measured, signals acquired from the bone sample with soft-tissue layer, presented a larger amplitude compared to the signals acquired from the bare bone. Waves travelling on the soft-tissue produced a superposition with the waves travelling through the bone. This, was also observed in the simulation. Target waves identification was necessary to extract the correct wave velocities.

It is thought that the reason why the soft-tissue mimicking layer did not produce a significant change on the shear wave velocity is that the elastic modulus of a typical soft-tissue is very low compared to the elastic modulus of bone. Wave velocities are substantially related to the mechanical stiffness of the material, and the mass density. Additionally, for finite bone models with dimensions compared to its wavelength, velocities are also related to geometric features such as thickness [8.14].

Simulations were useful for understanding the wave propagation in the complex medium of the cortical bone. Target waves were easily identified using these simulations. Moreover, results obtained from the 3D simulations of isotropic and homogeneous models of bone were comparable to measurements performed in the anisotropic medium of the bone, both showed good agreement and stand the reliability of the simulations for further bone property characterization.

Shear wave detection in bone tube samples was verified in the frequency domain using the 2D-FFT method. Although shear waves were identified and coincided with the theoretical dispersion curves, other Lamb modes were difficult to characterize due to the angle configuration which is mainly emphasizing the shear wave detection. However, small changes in the frequency map may be traces of attenuated Lamb waves with a wave velocity similar to the shear wave that is being detected at the same incident angle.

REFERENCES

[8.1] H. Sai, G. Iguchi, T. Tobimatsu, K. Takahashi, T. Otani, K. Horii, and K. Yoh, "Novel ultrasonic bone densitometry based on two longitudinal waves: significant correlation with pQCT measurement values and age-related changes in trabecular bone density, cortical thickness, and elastic modulus of trabecular bone in a normal Japanese population," *Osteoporosis international,* 21, (10), 1781-1790, 2010.

[8.2] M. O. Culjat, D. Goldenberg, P. Tewari and R. S. Singh, "A review of tissue substitutes for ultrasound imaging," *Ultrasound in medicine and biology*, 36, (6), 861-873, 2010.

[8.3] E. L. Madsen, M.A. Hobson, H. Shi, T. Varghese, and G. R. Frank, "Tissue-mimicking agar/gelatin materials for use in heterogeneous elastography phantoms," *Physics in medicine and biology*, 50, (23), 5597–5618, 2005.

[8.4] M. Burlew, E. Madsen, J. Zagzebski, R. Banjavic, and S. Sum, "A new ultrasound tissue-equivalent material," *Radiology*, 134, (2), 517-520, 1980.

[8.5] P. Moilanen, M. Talmant, V. Kilappa, P. Nicholson, S. Cheng, J. Timonen, and P. Laugier, "Modeling the impact of soft tissue on axial transmission measurements of ultrasonic guided waves in human radius," *The Journal of the Acoustical Society of America*, 124, (4), 2364-2373, 2008.

[8.6] E. Bossy, M. Talmant, P. Laugier, "Effect of bone cortical thickness on velocity measurements using ultrasonic axial transmission: A 2D simulation study," *The Journal of the Acoustical Society of America*, vol. 112, no.1, pp. 297-307, 2002.

[8.7] E. Bossy, M. Talmant, P. Laugier, "Three-dimensional simulations of ultrasonic axial transmission velocity measurement on cortical bone models," *The Journal of the Acoustical Society of America*, vol. 115, no. 5, pp. 2314-2324, 2004.

[8.8] Y. Nagatani, H. Imaizumi, T. Fukuda, M. Matsukawa, Y. Watanabe, and T. Otani, "Applicability of finite-difference time-domain method to simulation of wave

propagation in cancellous bone," *Japanese Journal of Applied Physics*, vol. 45, no. 9R, 2006.

[8.9] Y. Nagatani, K. Mizuno, T. Saeki, M. Matsukawa, T. Sakaguchi, H. Hosoi, "Numerical and experimental study on the wave attenuation in bone–FDTD simulation of ultrasound propagation in cancellous bone," *Ultrasonics,* vol. 48, no. 6-7, pp. 607-612, 2008.

[8.10] Y. Yamato, M. Matsukawa, T. Otani, K. Yamazaki, A. Nagano, "Distribution of longitudinal wave properties in bovine cortical bone in vitro," *Ultrasonics*, vol. 44, pp. e233-e237, 2006.

[8.11] R. Courant, K. Friedrichs, and H. Lewy, "On the partial difference equations of mathematical physics," *IBM Journal of Research and Development*, vol. 11, no. 2, pp. 215-234, 1967.

[8.12] R. L. Higdon, "Numerical absorbing boundary conditions for the wave equation. Mathematics of computation," *Mathematics of computation*, vol. 49, no. 179, pp. 65-90, 1987.

[8.13] M. O. Culjat, D. Goldenberg, P. Tewari and R. S. Singh, "A review of tissue substitutes for ultrasound imaging," *Ultrasound in medicine and biology,* 36, (6), 861-873, 2010.

[8.14] P. Laugier, G. Haiat eds., "Bone Quantitative Ultrasound", Dordrecht: Springer, vol. 576, 2011.

[8.15] H. Lamb, "On waves in an elastic plate," Proc. R. Soc. Lond. A, vol. 93, no. 648, pp. 114-128, 1917.

[8.16] P. Moilanen, "Ultrasonic guided waves in bone," *IEEE transactions on ultrasonics, ferroelectrics, and frequency control*, vol. 55, no. 6, pp. 1277-1286, 2008.

[8.17] J. Foiret, J. Minonzio, C. Chappard, M. Talmant, and P. Laugier, IEEE transactions on ultrasonics, ferroelectrics, and frequency control **61**, (9), 1478-1488, 2014.

[8.18] V. C. Protopappas, D. I. Fotiadis, and K. N. Malizos, "Guided ultrasound wave propagation in intact and healing long bones," *Ultrasound in medicine and biology*, vol. 32, no. 5, pp. 693-708, 2006.

CHAPTER IX EVALUATION OF WAVE VELOCITY IN LONG BONES

This section of the thesis work, proposes the implementation of the ultrasonic system with axial transmission measurement for the evaluation of shear waves propagating in the cortical layer of long bones surrounded by water. For this purpose, the diaphysis parts of two tibiae of swine were selected and tested along the axial direction of the bone. The main purposes of this measurement are to investigate the impact of bone shape, irregular cortical thickness, and medium, on the shear wave velocities. Additionally, understand the effects of the shear wave propagation by elastic FDTD simulations of the wave in models built from data of the HR-pQCT images that captured the bone heterogeneity. This data can be used to reflect the bone anisotropy of the long bone samples selected for this measurement.

To overcome the problem of the identification of the waves due to the complex interference of several waves pointed in [9.1], ultrasonic waves were characterized at different incident angles determined according to Snell's Law. Finally, wave velocities were determined in each case using a time-of-flight technique (ToF). Wave velocities were initially measured using a transverse transmission technique and verified later with measurements using the axial transmission technique and the proposed method.

To verify the efficacy of the FDTD method, bone models were compared and analyzed in each case, considering similar bone geometries and conditions used in the experiments.

This measurement presents a complete analysis and studies the viability of implementing shear wave measurements for in vivo bone evaluation.

9.1   SAMPLES

In order to represent a similar measurement to the actual bone in vivo measurement. The diaphysis part of two tibiae of swine, called bone B1 and B2, were selected and tested along the axial direction of bone using the axial transmission technique. Considering the anterior side of the bone samples as the measurement surface, sample B1 has a cortical thickness ranging from 3 mm to 6 mm and, sample B2 has a cortical thickness ranging from 3 mm to 7 mm. The length of the samples was 110 mm approximately. Fig. 9.1 a) - b), show images of the swine bone samples B1 and B2 respectively.

Figure 9.1 Tibia samples of swine bone used in the experiment a) sample B1 and b) sample B2.

9.2 EXPERIMENT DESCRIPTION

Bone samples (B1 and B2) were carefully degassed and immersed in water. The surface of the anterior part of the sample was aligned parallel to the horizontal as much as it was possible. The hollow part of the bone was filled with water. Transducers and samples were aligned to the axial direction and were separated 45 mm approximately. The lift-off distance was 50 mm, approximately. Experiments were performed with transducer at incident angles (θ) of 15º, 30º, 45º, and 60º. Fig. 8.2 shows an approximated representation of the bone geometries using the actual bone HR pQCT data and the configurations of the transducers for a) sample B1 and, b) sample B2. Again, these geometrical conditions were maintained in each measurement of the incident angle and specular reflection and waves traveling through water were avoided using the 10 mm spongy block between the transducers. In each case of the measurement, existing waves leaking at the same or close to the incident angle will be more easily detected while other

waves leaking at different angles will be attenuated. The same electronic equipment with the corresponding configuration were employed for the evaluation of the B1 and B2 samples. The scan along the anterior part of the bone sample in the axial direction was performed at a step size of 0.1 mm in a distance of 10 mm, as in previous cases. The temporal signals were received using a sampling frequency of 100 MHz. A total of 100 time-amplitude signals were recorded during the scan.
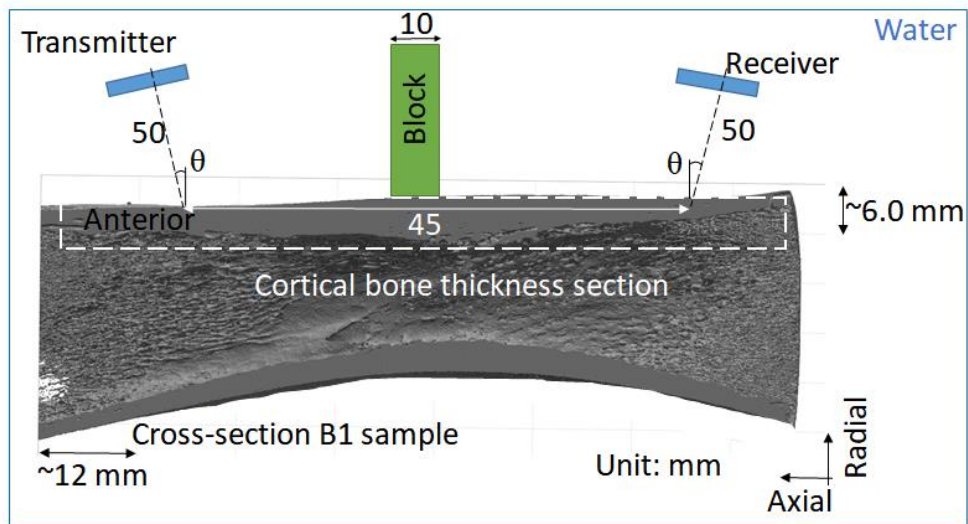
a)
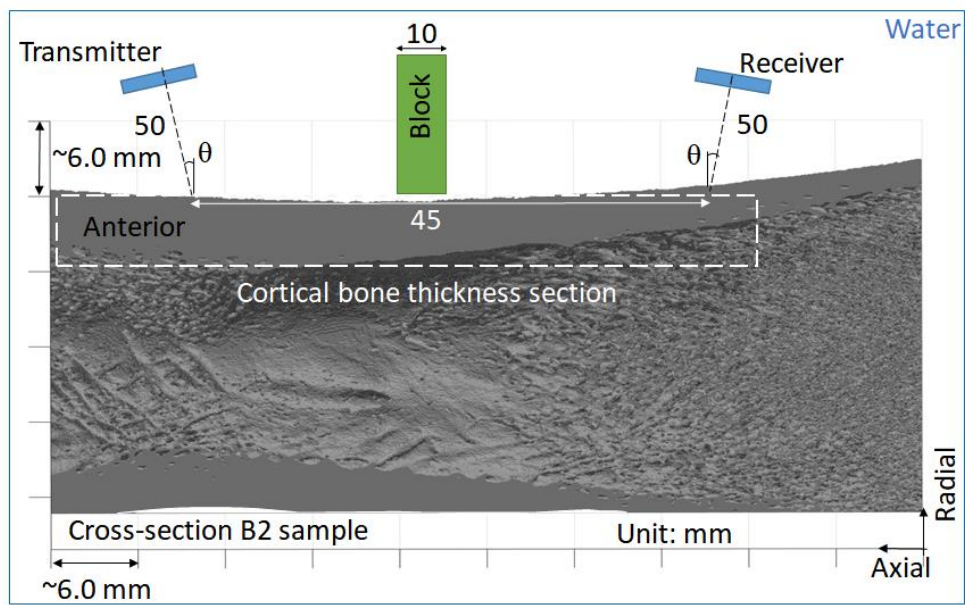
b)

Figure 9.2 Bone geometries and experimental system using AT configuration of a) sample B1 and b) sample B2.

9.2.1   ADDITIONAL EXPERIMENTS

A transverse transmission measurement was carried out in each bone sample (B1 and B2) in order to verify the wave velocity values obtained from the axial transmission measurement. For the determination of the shear wave velocity, the anterior part of the bone was placed between the transmitter and receiver at an initial angle of $\alpha = 54°$ (sample B1) and $\alpha = 50°$ (sample B2) approximately. The transducers were vertically and horizontally aligned and fixed, after that, the sample was rotated around the y-axis as is shown in Fig. 9.3. Measurements were performed every 1° from 54° to 60° in the case of sample B1 and from 50° to 60° in the case of sample B2. Shear wave velocity was calculated by relations of the total time in the water, time in bone, and geometrical relations of the distance traveled.
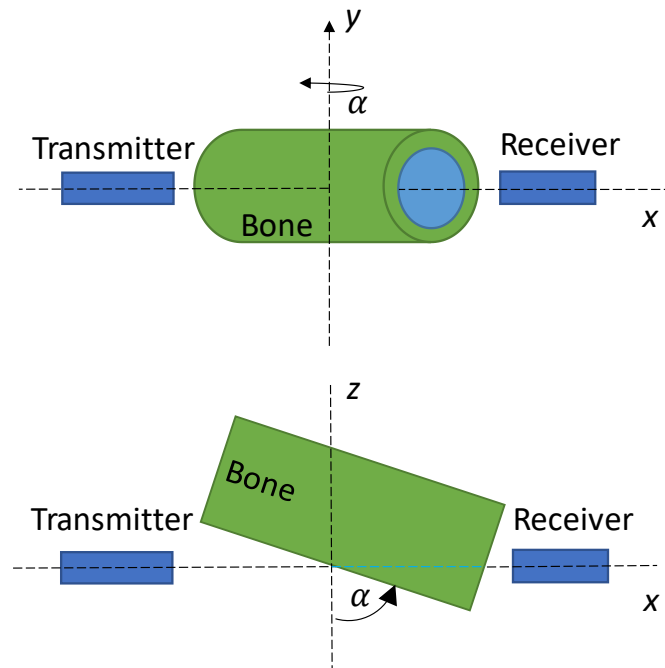
Figure 9.3 Transverse transmission configuration for measurement of shear wave.

9.3   SIMULATION OF THE WAVE PROPAGATION

9.3.1   CONSTRUCTION OF THE MODEL

3D-bone models were reconstructed from the bone CT data obtained by HR pQCT. To reflect the bone heterogeneity, the average of the bone mass density was assumed to be 2000 kg/m^3, the same value found for bovine femur bone [9.2]. After that, the value of the bone mass density of each voxel of the 3D model matrix was calculated from the calibration data of the BMD. Bone mass density was set in a range of 1400 – 2400 kg/m^3 approximately. The simulation volume of the sample B1 has a matrix size of 590×1580×470 voxels (36 mm × 96.4 mm × 28.7mm) and sample B2, 510×1590×580 voxels (31.1 mm × 97 mm × 35.4 mm) in the x, y, and z directions for the case when the incident angle is 60° and similar matrix sizes in the other angle cases. Due to the large size of the bone sample, only the anterior part of the model was considered for the simulation, approximately a half of the entire bone shell, additionally, the lift-off distance of the transducers with respect to the top of the bone surface was reduced to 25 mm. The simulation geometries are shown in Fig. 9.4 a) for bone B1 b) for model B2.
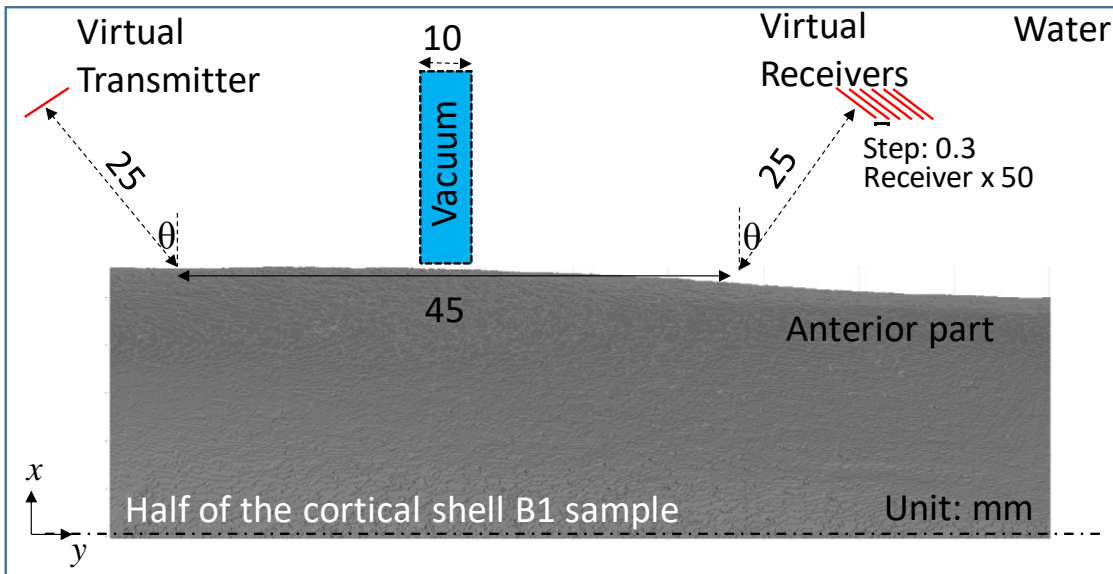
a)
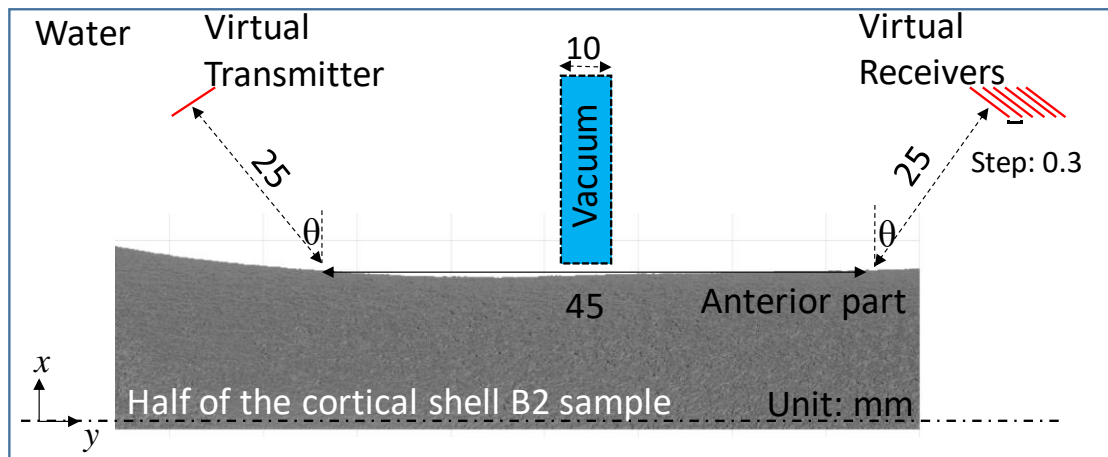
b)

Figure 9.4 Simulation models and geometries of the AT configuration of a) sample B1 and b) sample B2.

The transmitter and receivers were modeled considering sets of voxels (of the simulation matrix) in a defined circumference of diameter 10 mm and 13 mm, the same diameter of the transducers used in the experimental measurements, respectively. One set

of voxels as the transmitter and fifty sets of voxels as receivers separated 0.3 mm from each other, in an axial transmission configuration. Each model of the transmitter and receiver were positioned at angles of 15º and 60º, which are the most representative angles in this experiments. A 10.0 mm vacuum block was placed between the transducers in the model. For simulation purposes, some considerations were made. The surrounding medium, water was considered isotropic and homogeneous. Additionally, the sound velocity in water was defined as 1500 m/s and a water density of 1000 kg/m^3. A single sinusoidal wave with a Hann window at 1 MHz was used as the transmitted signal.

The simulation has a spatial resolution of 61 μm and a time resolution of 8.8 ns, both values satisfied the Courant's stability condition [9.3]. Cortical bone and cancellous bone are considered to be transversally isotropic in its material symmetry [9.4]. Shear wave velocities were estimated assuming uniaxial anisotropy and a Poisson's ratio of 0.33 in the isotropic plane [9.5- 9.6]. A transversally isotropic bone has five independent elastic constants. The matrix of the elastic coefficients would have the form described in Eq. (2.2).

According to the sample model developed by Van Buskirk et al. [9.7] for measurement of longitudinal and transverse velocities, the elastic coefficients were calculated. c_{13} and c_{66} were obtained assuming transverse isotropy from the Eq. (9.1) and Eq. (9.2).

$$c_{13} = c_{23} \qquad (\mathbf{9.1})$$

$$c_{66} = \frac{1}{2}(c_{11} - c_{12}) \qquad (\mathbf{9.2})$$

On the other hand, c_{13} was estimated by fitting experimental measurements of longitudinal wave velocities in all propagation directions of a bovine cortical bone ball sample reported by Nakatsuji et al. [9.8] using the least-squares method [9.9].

c_{33} was calculated from the longitudinal wave velocity as shown in Eq. (9.3):

$$c_{33} = \rho v_{13} \qquad (\mathbf{9.3})$$

Whereas c_{44} and c_{55} were calculated from the shear wave velocity considering the

bone mass density of each voxel in the model. c_{11} was calculated from the longitudinal wave velocities in the radial and tangential directions.

9.3.2   ELASTIC- FDTD METHOD

In order to simulate longitudinal and shear wave propagation along the bone, an elastic FDTD simulations in anisotropic medium were implemented [9.10- 9.11]. In this case, the sound attenuation was not considered in the simulations. To avoid reflections coming from the end faces of the simulation volume, a Higdon's second order absorption boundary condition [9.12] was implemented. During the simulation, the values taken by the voxels in each receiver were averaged at every loop and then recorded.

9.4   RESULTS AND DISCUSSION

The evaluation of the long bone samples B1 and B2 was performed experimentally using the proposed axial transmission method. In each sample, the signals obtained from the measurement of the waves at the incident angle (θ) during the scan along the sample were stacked in a time-distance graph. The resulting B-scans images at incident angles (θ) of 15º, 30º, 45º, and 60º obtained from sample B1 are shown in Fig. 9.5 and, B-scans images of the sample B2 are shown in Fig. 9.6. In Fig. 9.7 the waveforms observed at 60º in samples B1 and B2 are shown.
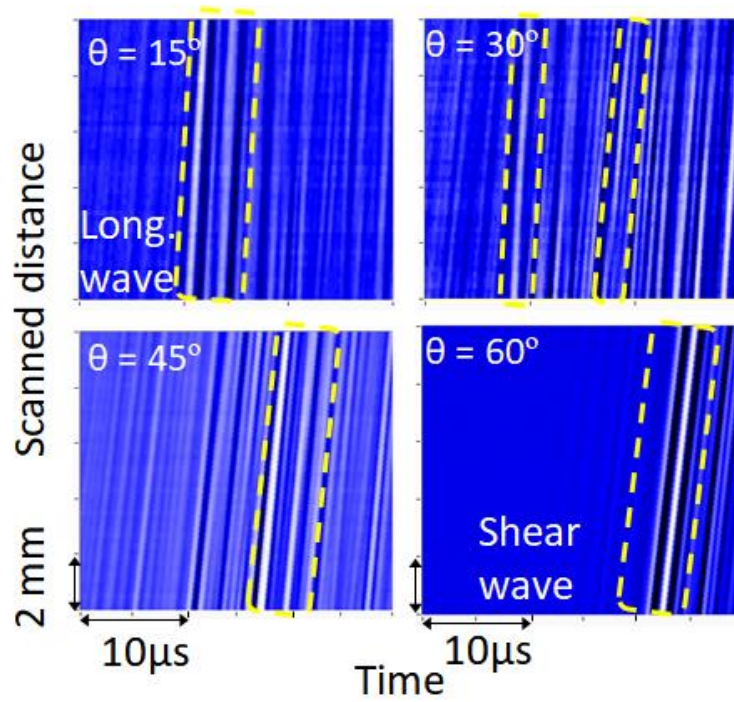
Figure 9.5 B-scan images obtained from experimental measurements of sample B1 at incident angles of 15º, 30º, 45º, and 60º. Dashed lines indicate the selected target waves.
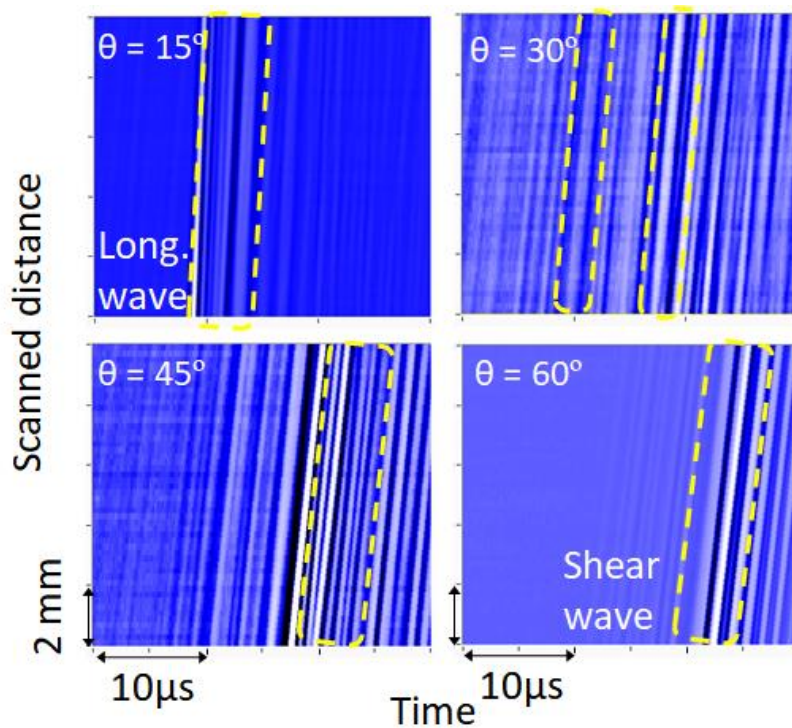
Figure 9.6 B-scan images obtained from experimental measurements of sample B2 at incident angles of 15º, 30º, 45º, and 60º. Dashed lines indicate the selected target waves.

a)   b)
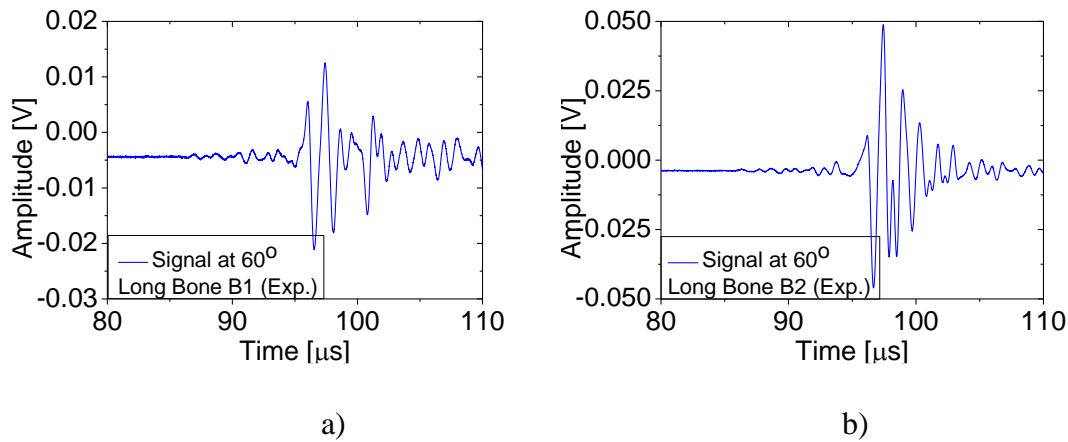
Figure 9.7 Waveforms obtained from experimental measurements at incident angle 60º
of sample a) B1 and b) B2.

As has been reported in the previous measurements in bone plates and bone tubes, an angle dependence on the wave detection is observed in samples B1 and B2. Depending on the incident angle of the ultrasound radiation, the corresponding wave leaking at the same or approximated incident angle is more likely to be detected. These angle dependence obeys Snell's law and can be determined using Eq. (3.8) as was explained in the method section. In general, in both samples the fastest waves arrive at incident angles $\theta < 30°$ while slower waves are detected at incident angles $\theta > 30°$, being $\theta_c = 28°$ the approximated critical angle for detection of longitudinal wave (calculated with values of velocity found in the literature [9.13]). Additionally, at incident angles close to $\theta = 30°$ (close to longitudinal wave critical angle), two waves could be observed in Fig. 9.5 and Fig. 9.6 (two slopes with a different inclination that are formed by two types of waves traveling at different velocity and are detected at different times). These observations were more clear in the previous samples that consider a regular cortical surface (plates and tubes). Nevertheless, measurements in the limit of 30° when these two waves are close enough to affect their propagations, the wave velocity is modified.

On the other hand, results of the simulations considering the HR pQCT data of samples B1 and B2 and similar experimental conditions showed concordance with experimental observations. The B-scan images of samples B1 and B2 at the incident angle

$\theta = 60°$ are shown in Fig. 9.8 a) and b) respectively, where a slow wave is observed. The waveforms obtained from the simulations in sample B1 and B2 are shown in Fig. 9.9.
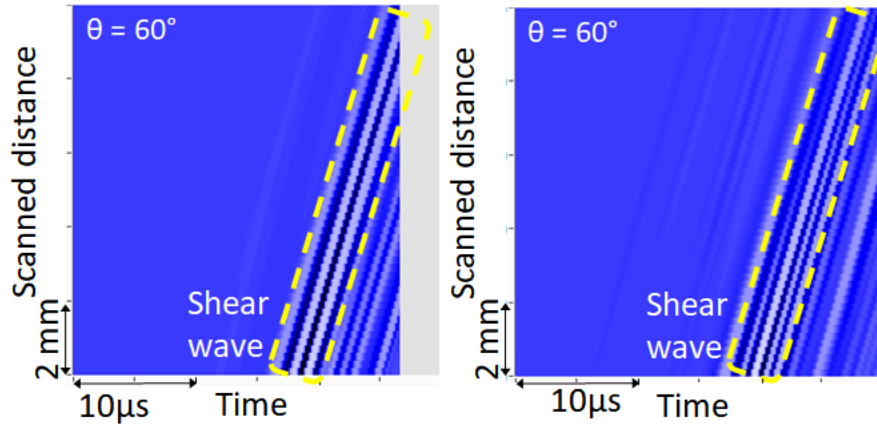
Figure 9.8 B-scan images obtained from simulations of a) sample B1 and b) sample B2 at the effective angle for shear wave detection, (60°). Dashed lines indicate the selected target waves.
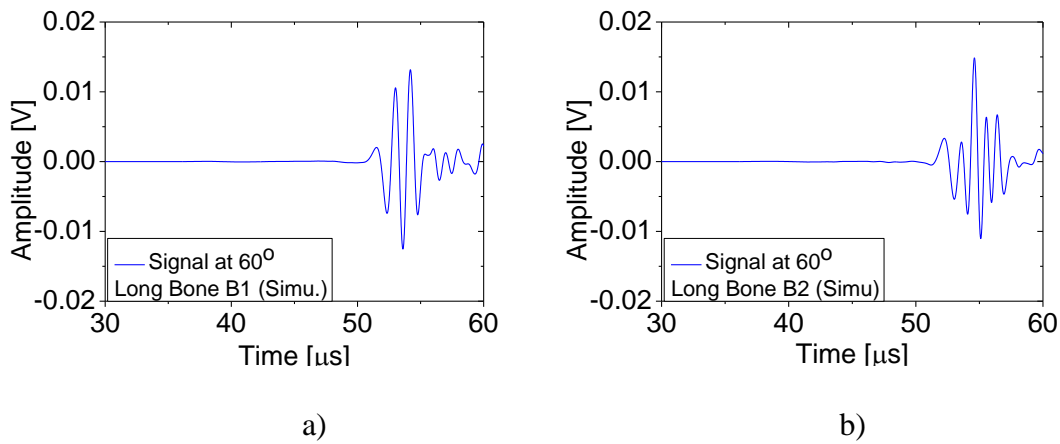
Figure 9.9 Waveforms obtained from simulation calculations at incident angle 60° of sample a) B1 and b) B2. *Simulations consider a shorter distance between the transducers and the sample compared to the experimental measurements.

Waveforms observed in the experiments and anisotropic simulations of sample B1 and B2, show similar characteristics. The amplitudes were very approximated especially, in the case of sample B1. In previous simulations of the bone plate and tube samples that

considered bone as an isotropic material, waveforms were less similar to the experimental ones. This could be an indicator of a good representation of anisotropic properties of bone for simulations, and a good performance of the FDTD code for simulations of the wave propagation.

Wave detection, especially in the experimental measurements, is affected by noise and multiple reflections originated in an irregular solid medium, producing several signals difficult to identify. At this step, an analysis of the wave propagation along the sample using the corresponding simulation was necessary to select correctly the characteristic wave at the corresponding incident angle. Fig. 9.10 shows different instants of the simulation of the wave propagation at $\theta = 60°$ (sample B1).
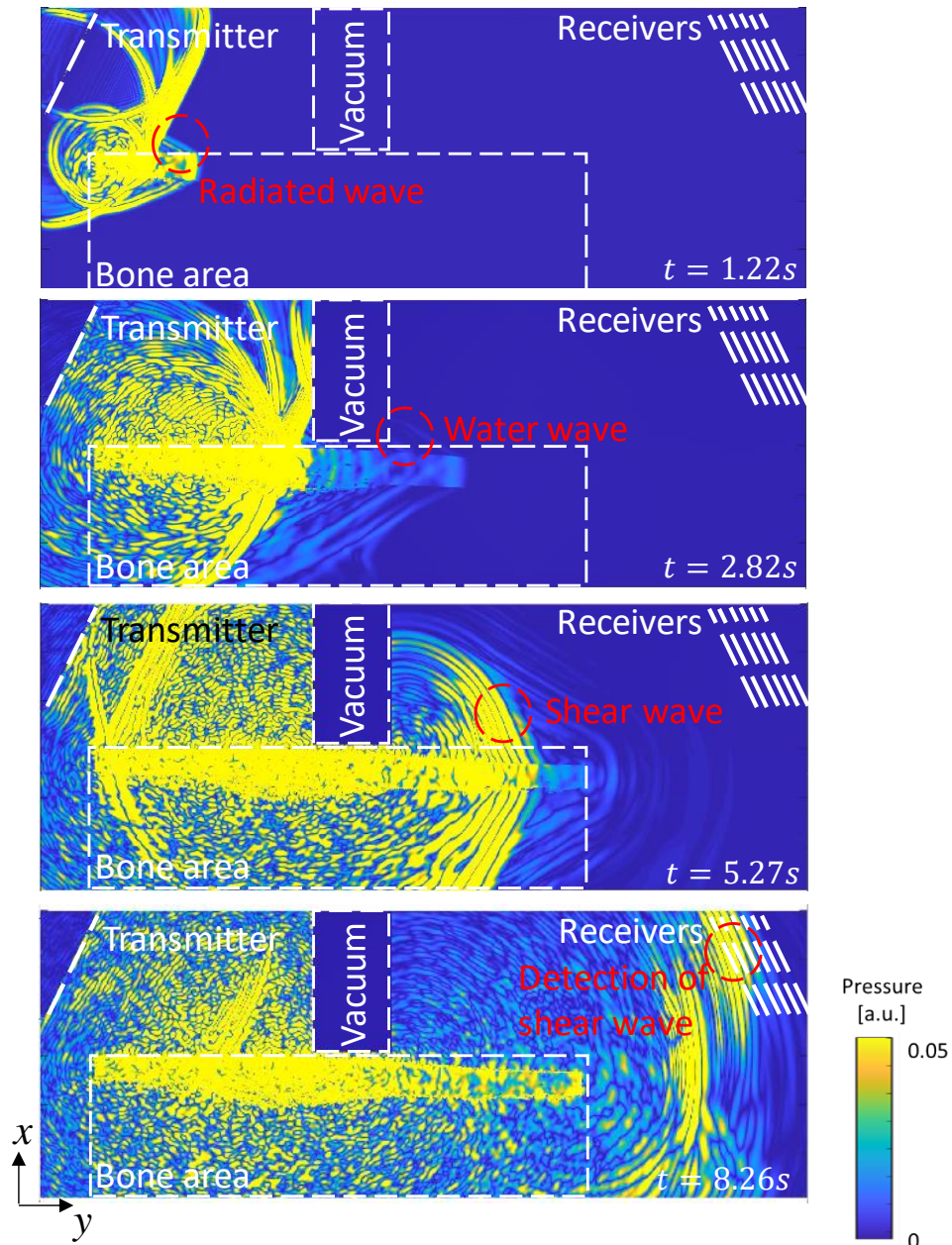
Figure 9.10 Analysis of the wave propagation in the simulation of the sample B1 at incident angle $\theta = 60°$.

At the beginning of the simulation, Fig. 9.8 (a) when the wave hits the surface, a radiated wave is produced. This radiated wave reflects on the surface, (b) leaks immediately into the water and starts to propagate through the water medium. Passing under the thin space of water between the block and the sample that simulates a soft-tissue

layer, (c) an attenuated part of this signal is the first wave to be detected. After that (d) an energetic wave that has traveled through the cortical surface of the bone leaks into the water at the same initial incident angle, is detected in second place. This wave corresponds to the measurement of the target wave that in this case is theoretically, the measurement of the shear wave. Therefore, the waves that pass through the bone sample and are detected at the same incident angle are defined here as the target waves. These target waves are indicated by dashed lines in each case of each sample in Fig. 9.5, Fig. 9.6, and Fig. 9.8. Consequently, these target waves were used for wave velocity estimation. Target waves can also be identified without simulations by an analysis in frequency. Waves could be characterized using a 2D-FFT method, and the phase velocity of each one can be compared to theoretical values or dispersion curves. Shear wave will show a constant velocity independently of the frequency. If the phase velocity changes depending on the frequency, then this wave corresponds to one of the guided modes.

Wave velocities determined from the experimental axial transmission measurements of samples B1 and B2 were estimated using the ToF technique at incident angles (θ) of 15º, 30º, 45º, and 60º. Considering four peak points of the target waves, estimated wave velocities are shown in Fig. 9.11 a) sample B1 and b) sample B2.
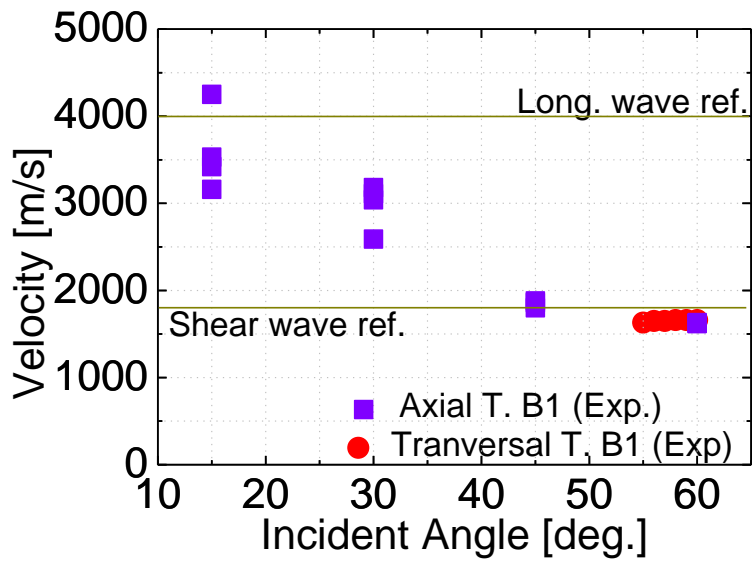
(a)
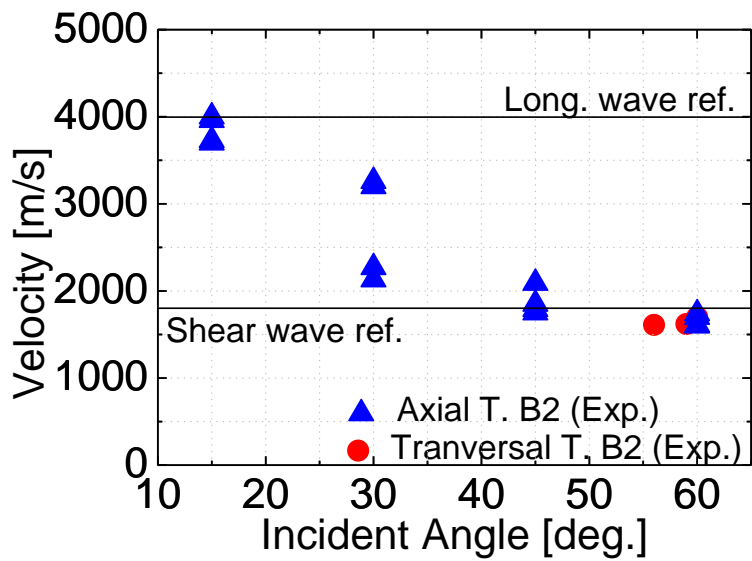
(b)

Figure 9.11 Apparent wave velocities in a) sample B1 and b) sample B2 found in experimental measurements using axial and transverse transmission techniques.

These wave velocity values agreed with measurements of the longitudinal and shear wave velocity found commonly in the bone [9.13]. For incident angles $\theta < 30°$, apparent longitudinal velocities in a range of 3160 – 4250 m/s in sample B1, and velocities in a

range of 3700 – 4000 m/s in sample B2 were estimated. For incident angles $\theta > 30°$, apparent shear velocities in a range of 1620 – 1630 m/s were measured in sample B1. Whereas in sample B2, apparent shear velocities in a range of 1600 – 1740 m/s were obtained. Additionally, supporting transverse transmission measurements for the determination of the shear wave velocity were compared with the measurements of the wave velocity using the axial transmission technique. The results of these measurements are also shown in Fig. 9.11. As is observed, experimental measurements of the shear wave velocity using the transverse transmission technique showed good agreement with measurements of the apparent shear wave velocity determined with the axial transmission technique. For sample B1 a shear wave velocity of 1660 m/s at $\alpha = 60°$ was measured and, at the same angle, a shear wave velocity of 1700 m/s was found in sample B2.

At the same time, FDTD-simulations also showed a good prediction of the apparent wave velocities using the bone HR pQCT data and the proposed method. In sample B1 an apparent longitudinal wave velocity in the range of 3210 – 4270 m/s was estimated. Shear wave velocity estimations in sample B1 and B2 using the effective incident angle $\theta = 60°$ showed wave velocities in a range of 1630 – 1650 m/s and 1640 – 1680 m/s for sample B1 and sample B2, respectively. Shear wave velocities determined in the simulations and wave velocities obtained from experimental measurements using the axial transmission technique were compared in Fig. 9.12 a) sample B1 and b) sample B2. As is observed in Fig. 9.12, at incident angles close to 60°, wave velocities showed high repeatability, the same was observed in previous studies. Here, it is concluded that incident angles between 50º and 60º are the effective angles for shear wave detection which is in agreement with Snell's Law. These concordances in the measured wave velocities confirmed the detection of shear waves in the bone samples.
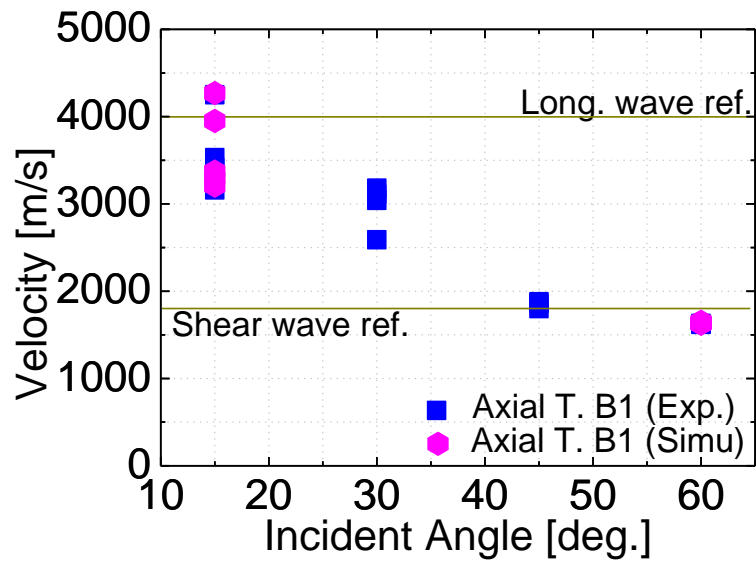
(a)
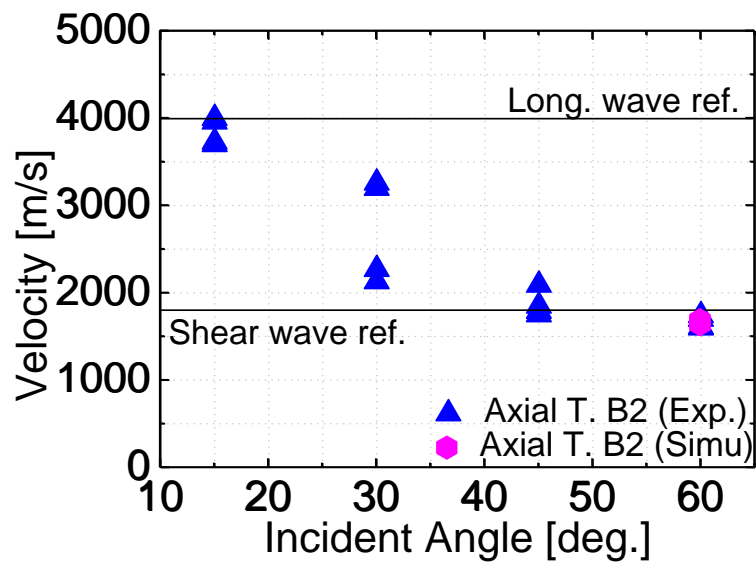
(b)

Figure 9.12 Comparison between apparent wave velocities measured in the AT experiment and velocities estimated from the simulations of a) sample B1 and, b) sample B2.

In general, apparent longitudinal and shear wave velocities obtained from the simulations were slightly higher than the ones obtained in the experiments. This, since attenuation, is not being considered in the simulations. Additionally, since measurements of the wave velocity in both samples are mainly determined by the density characteristic of each bone sample, sample B2 seemed to have higher velocities than sample B1, this coincided in all the wave velocity values found in the samples including transverse transmission measurements and simulations. Apparent wave velocities obtained from the experiments using the axial and transverse transmission techniques and simulations of the sample B1 and sample B2, are summarized in Table 9.1.

Table 9.1 Apparent Longitudinal and Shear Wave Velocities from Experiments (Axial - Transverse) and Simulations of Sample B1 and Sample B2.

| Wave velocity | Experiments | | Simulation | | |
	Sample B1	Sample B2	Ref. value	HR pQCT data Sample B1	HR pQCT data Sample B2
Long. Wave [10^3 m/s]	3.16 – 4.25	3.38 – 3.96	4.00	3.21 – 4.27	-
Shear wave [10^3 m/s]	1.62 – 1.63	1.60 – 1.74	1.80	1.63 – 1.65	1.64 – 1.68
	1.66 *	1.70*			

*Observed data by transverse transmission.

These results demonstrated that the bone irregular shape and cortical thickness did not significantly modify the wave propagation and using the proposed method, shear wave measurements were not affected. On the other hand, measurements of the apparent longitudinal wave velocity, mainly measured at 15º, have shown more sensitivity to changes in the cortical bone thickness and were found in a large range of values.

Additionally, in the 45º case, it is believed that the resulting wave velocity may be a mixture of shear wave and traces of the S0 Lamb mode. S0 mode theoretically could be detected at this incident angle and dispersion curve maps [9.14- 9.15]. At 1 MHz, the S0

mode has a velocity close to 2000 m/s and changes in other frequencies, as shown in the theoretical dispersion curve in Fig. 9.13. Therefore, the planar detector may be receiving waves leaking at the similar angles, and the resulting wave velocity could be slightly different from the expected. The same can be concluded from intermediate cases of the incident angle.
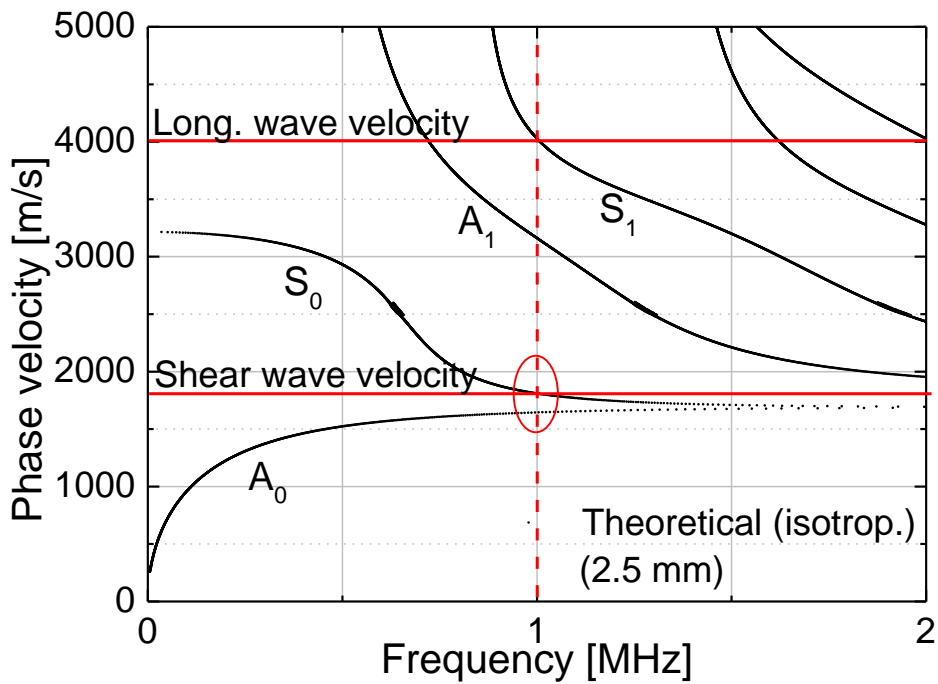
Figure 9.13 Theoretical dispersion curve (phase velocity vs. frequency).

9.5   SUMMARY

In this section of the thesis work, QUS techniques with axial transmission measurements were applied for the evaluation and characterization of shear waves propagating along the axial direction of the cortical layer of swine tibiae samples. The aim of this measurement was to investigate the impact of irregular shape and thickness of the cortical bone layer and the surrounding medium on the shear wave velocity by the proposed experimental method. Additionally, to understand the wave propagation, simulations in digital models of the bone samples were implemented using the elastic

FDTD method. It was found that wave characterization depends on the incident angle at which the ultrasound was radiated. Shear waves were consistently observed with this method at angles larger than 50° and its velocities showed great repeatability independently of the bone irregular thickness. Wave velocities were also in good agreement to those observed by transverse transmission measurements. Simulations in anisotropic and heterogeneous models showed to be a reliable approximation to the actual bone measurement.

9.6   CONCLUSIONS

This experiment proposed an ultrasonic method with axial transmission measurement for the evaluation of shear waves propagating in the cortical layer of long bone samples with irregular shape and cortical thickness and surrounded by water.

Results demonstrated that shear wave detection was possible using the axial transmission technique and our methods. The corresponding incident angle, for wave detection could be estimated by Snell's law. Ultrasound radiation at incident angles of (60º), close to the shear wave critical angle, showed good agreement with theoretical values and great repeatability on the shear wave velocity measurements. Additionally, these values were confirmed and in concordance with transverse transmission measurements of the wave velocity.

Signals recorded by the simulation of the wave propagation in the respective bone's HR pQCT data, taking into account bone anisotropy and heterogeneity, verified experimental measurements and confirmed the detection of the shear wave in cortical bone. In general, sample B2 presented higher wave velocities than sample B1, this is mainly related to the bone density characteristic of each bone. The complicated geometry and bone structure produced complicated waveforms that were easy to identify by analyzing the wave propagation along the bone. Here, the simulations of the wave propagations were helpful for the identification of the shear waves.

The agreement between simulation and experimental measurements verified the reliability of the simulations and the 3D models of the HR pQCT data of the bone that can be used for further bone property characterization.

Shear wave velocities did not significantly change and were not affected despite the irregular bone shape, cortical thickness, and the water surrounding. However, apparent longitudinal wave velocities were estimated in a larger range of values that suggested that longitudinal waves may show more sensitivity to changes in the cortical bone thickness.

REFERENCES

[9.1]   E. Bossy, M. Talmant, P. Laugier, "Effect of bone cortical thickness on velocity measurements using ultrasonic axial transmission: A 2D simulation study," *The Journal of the Acoustical Society of America*, vol. 112, no.1, pp. 297-307, 2002.

[9.2]   M. Saeki, L. Bustamante, T. Misaki, K. Chiba, I. Mano, Y. Nagatani, M. Matsukawa, "FDTD simulation study of ultrasonic wave propagation in human radius model generated from 3D HR-pQCT images," *Physics in Medicine*, 100029, 2020.

[9.3]   R. Courant, K. Friedrichs, and H. Lewy, "On the partial difference equations of mathematical physics," IBM Journal of Research and Development, vol. 11, no. 2, pp. 215-234, 1967.

[9.4]   R. B. Ashman, S. C. Cowin, W. C. Van Buskirk, J.C. Rice, "A continuous wave technique for the measurement of the elastic properties of cortical bone," *Journal of biomechanics*, vol. 17, no. 5, pp. 349-361,1984.

[9.5]   A. Hosokawa, "Numerical analysis of variability in ultrasound propagation properties induced by trabecular microstructure in cancellous bone," *IEEE transactions on ultrasonics, ferroelectrics, and frequency control*, 56(4), 738-747, 2009.

[9.6]   T. H. Smit, J. M. Huyghe, S.C. Cowin, "Estimation of the poroelastic parameters of cortical bone," *Journal of biomechanics*, vol. 35, no. 6, pp. 829-835, 2002.

[9.7]   Van Buskirk, W. C., "The elastic moduli of bone," *Trans Am Soc Mech Eng*, vol. 45, pp. 131-143, 1981

[9.8]   T. Nakatsuji, K. Yamamoto, D. Suga, T. Yanagitani, M. Matsukawa, K. Yamazaki, Y. Matsuyama, "Three dimensional anisotropy of ultrasonic wave velocity in bovine cortical bone: effects of hydroxyapatite crystallites orientation and microstructure," *Japanese Journal of Applied Physics*, vol. 50, no. 7S, 2011.

[9.9] K. Takano, Y. Nagatani, and M. Matsukawa, "Simulation study of axial ultrasound transmission in heterogeneous cortical bone model," *Japanese Journal of Applied Physics*, vol. 56, no. 7S1, 2017.

[9.10] Y. Nagatani, H. Imaizumi, T. Fukuda, M. Matsukawa, Y. Watanabe, and T. Otani, "Applicability of finite-difference time-domain method to simulation of wave propagation in cancellous bone," *Japanese Journal of Applied Physics*, vol. 45, no. 9R, 2006.

[9.11] Y. Nagatani, K. Mizuno, T. Saeki, M. Matsukawa, T. Sakaguchi, H. Hosoi, "Numerical and experimental study on the wave attenuation in bone–FDTD simulation of ultrasound propagation in cancellous bone," *Ultrasonics*, vol. 48, no. 6-7, pp. 607-612, 2008.

[9.12] R. L. Higdon, "Numerical absorbing boundary conditions for the wave equation. Mathematics of computation," *Mathematics of computation*, vol. 49, no. 179, pp. 65-90, 1987.

[9.13] Y. Yamato, M. Matsukawa, T. Otani, K. Yamazaki, A. Nagano, "Distribution of longitudinal wave properties in bovine cortical bone in vitro," *Ultrasonics*, vol. 44, pp. e233-e237, 2006.

[9.14] H. Lamb, "On waves in an elastic plate," Proc. R. Soc. Lond. A, vol. 93, no. 648, pp. 114-128, 1917.

[9.15] N. Bochud, Q. Vallet, J. G. Minonzio, and P. Laugier, "Predicting bone strength with ultrasonic guided waves," *Scientific reports*, vol. 7, no. 43628, 2017.

CHAPTER X GENERAL CONCLUSIONS

Shear wave detection and characterization were possible in plate and tube samples of bovine cortical bone, as well as, long bone samples of swine using the proposed axial transmission system and method. Various samples of regular and irregular thicknesses, densities, and bone shapes were successfully evaluated considering the bone surrounding medium.

It was demonstrated that the sample position in the axial transmission configuration does not affect the shear wave velocity. However, it showed a significant impact on the longitudinal wave velocity. This suggested that bone evaluation must include measurements of both waves.

Wave detection depended on the angle of the ultrasound radiation. The effective incident angle was estimated using theoretical values of the wave velocities and the Snell's law equation. Ultrasound radiation at incident angles between (50º - 60º), close to the shear wave critical angle, showed great repeatability on the shear wave velocity measurements.

Velocity measurements in bone tubes (with and without soft-tissue mimicking layer) and bone plates with regular cortical thickness showed good agreement with the estimated shear wave velocities. It was concluded that shear wave velocity was not affected despite the bone curvature and the additional soft-tissue layer on the top of the bone tube sample. Since the elastic modulus of a typical soft-tissue is very low compared to the elastic modulus of bone, the wave propagation was not sufficiently affected.

In the same way, shear wave velocities were not significantly affected by long bones with an irregular shape, irregular cortical thickness, and actual features of a human bone. Estimated shear wave velocities showed good repeatability, and are approximated to values estimated in regular samples of bovine bone as well.

Estimated shear wave velocities by axial transmission techniques were in concordance with transverse transmission measurements of the wave velocity.

On the other hand, it was demonstrated that longitudinal waves are very sensitive to changes in the cortical bone thickness, bone shape, the sample position, a has been demonstrated in various studies. The estimated velocities varied in a large range of values.

Target waves were easily identified using these simulations of the wave propagation. In general, wave velocities found in simulations were in concordance with the experimental measurements. However, wave velocity values from simulations that consider isotropic conditions were slightly higher than the ones predicted by the experiments. On the other hand, wave velocities values from simulations that consider the bone heterogeneity and bone anisotropy more precisely agreed the values observed in the experiments. Nevertheless, isotropic simulations with simplified bone geometries showed good reliability on the prediction of the wave velocities and could be used as an alternative when needing an easy and fast simulation. Complicated geometries are much more difficult to represent and using the bone's HR pQCT data could not be possible in many cases.

The analysis in the frequency domain using the 2D-FFT method verified the measurement of the shear wave. Additionally, the wave characterization showed the detection of Lamb modes that were well observed in the bone plate samples, in the other cases, the complicated structures originated several additional waves that were difficult to identify.

The presented system offers an accurate and reliable bone diagnosis that integrates an axially transmitted shear wave evaluation and could be implemented for in vivo bone assessment of osteoporotic bone and for bone mechanical property estimation.

APPENDIX

PUBLICATIONS, PROCEEDINGS AND CONFERENCES

JOURNALS

[1] L. Bustamante, M. Saeki, and M. Matsukawa, "Characterization of shear waves in cortical bone using the axial transmission technique", *Japanese Journal of Applied Physics*, vol. 58, art. no. SGGE20.

[2] L. Bustamante, M. Saeki, T. Misaki, M. Matsukawa, "Effects of soft-tissue layer on shear wave velocity measurements in cortical bone tubes", *Japanese Journal of Applied Physics*, vol. 59, art. no. SKKB05.

[3] M. Saeki, L. Bustamante, T. Misaki, K. Chiba, I. Mano, Y. Nagatani, M. Matsukawa, "FDTD simulation study of ultrasonic wave propagation in human radius model generated from 3D HR-pQCT images", *Physics in Medicine*, vol. 10, art. no. 100029.

[4] T. Makino, T. Nakamura, L. Bustamante, Shinji Takayanagi, Yosuke Koyama, and M. Matsukawa, "Piezoelectric and inversely piezoelectric responses of bone tissue plates in the MHz range", *IEEE Transactions on Ultrasonics, Ferroelectrics, and Frequency Control*, vol. 67, no. 8, pp. 1525-1532, 2020.

[5] L. Bustamante, T. Misaki, M. Matsukawa, "Shear wave evaluation in long bones using axial transmission technique: Experiments and FDTD simulations", *IEEE Transactions on Ultrasonics, Ferroelectrics, and Frequency*. (Submitted)

[6] L. Bustamante, J. Natarajan, C. H.Yang, "Evaluation of defect detection in aluminium, CFRP and epoxy resin pates using non-contact Air-coupled ultrasonic waves", *International Journal of Precision Engineering and Manufacturing*, (Accepted)

INTERNATIONAL CONFERENCES

[1]   L. Bustamante, C. H. Yang, "A hybrid system employing laser generation and air coupled detection for characterization of mechanical properties of metallic plates", The 18th Non-Destructive Testing Technology Seminar SNTCT (2016.11).

[2]   L. Bustamante, M. Saeki, M. Matsukawa, "Evaluation of axially transmitted shear waves in cortical bone: experimental and simulation study", 176th Meeting of the Acoustical Society of America (2018.11).

[3]   N. Murashima, L. Bustamante, M. Matsukawa, "Ultrasonic evaluation of anisotropic structure of swine skull", 176th Meeting of the Acoustical Society of America (2018.11).

[4]   M. Saeki, L. Bustamante, Y. Nagatani, K. Chiba, I. Mano, M. Matsukawa, "Study on the ultrasonic wave convergence in the medium with bone", 176th Meeting of the Acoustical Society of America (2018.11).

[5]   L. Bustamante, M. Saeki, T. Makino, M. Matsukawa, Y. Nagatani, "Experimental and 3D-simulations of shear wave in cortical bone tubes using axial transmission technique", 8th International Symposium on Ultrasonic Characterization of Bone (2019.6).

[6]   M. Saeki, L. Bustamante, Y. Nagatani, K. Chiba, M. Matsukawa, "FDTD simulation study on ultrasonic wave convergence in heterogeneous bone", 2019 International Congress on Ultrasonics (2019.9).

[7]   L. Bustamante, M. Saeki, M. Matsukawa, Y. Nagatani, "Shear wave measurements in cortical bone tubes with soft tissue-mimicking layers: experiments and 3D-simulations", IEEE International Ultrasonics Symposium 2019 (2019.10).

[8]   M. Saeki, <u>L. Bustamante</u>, Y.i Nagatani, I. Mano, K Chiba, M. Matsukawa, "Study on the effective ultrasonic wave convergence in bone for fracture healing", IEEE International Ultrasonics Symposium 2019 (2019.10).

DOMESTIC CONFERENCES

[1]   <u>L. Bustamante</u>, K. Takano, M. Matsukawa, "Experimental evaluation for the shear axial transmission wave in in vivo bone", 第 65 回応用物理学会春季学術講演会 (2018.3).

[2]   <u>L. Bustamante</u>, M. Saeki, M. Matsukawa, "Evaluation of shear wave in cortical bone plates using axial transmission technique", 日本音響学会 2018 年秋季研究発表会 (2018.9).

[3]   村島和, <u>L. Bustamante</u>, 安井寛和, 松川真美, "超音波法による頭蓋骨内の異方性評価", 日本音響学会 2018 年秋季研究発表会 (2018.9).

[4]   <u>L. Bustamante</u>, M. Saeki, M. Matsukawa, "Characterization of ultrasonic waves in cortical bone using axial transmission technique", 第 39 回超音波エレクトロニクスの基礎と応用に関するシンポジウム (2018.10).

[5]   牧野大輝, 中村司, <u>L. Bustamante</u>, 小山大介, 高柳真司, 松川真美, "皮質骨から放射される縦波超音波", 第 39 回超音波エレクトロニクスの基礎と応用に関するシンポジウム (2018.10).

[6]　L. Bustamante, M. Saeki, M. Matsukawa, "Axially transmitted ultrasonic waves in plate and tube cortical bone samples", 圧電材料・デバイスシンポジウム 2019 (2019.1).

[7]　村島和, 道本樹, L. Bustamante, 安井寛和, 松川真美, "ブタ頭蓋骨内における超音波伝搬の評価", 電子情報通信学会 超音波研究会 (2019.1).

[8]　L. Bustamante, 佐伯誠哉, 松川真美, "Application of ultrasonic axial transmission technique for the evaluation of cortical bone tubes", 日本音響学会 2019 年春季研究発表会 (2019.3).

[9]　佐伯誠哉, L. Bustamante, 千葉恒, 長谷芳樹, 真野功, 松川真美, "ヒト橈骨の 3D CT データを用いた骨中の音波集束シミュレーション", 電子情報通信学会超音波研究会 (2019.7).

[10]　L. Bustamante, M. Saeki, M. Matsukawa, "Effects of soft-tissue layer on shear wave velocity measurements in cortical bone tubes", 第 40 回超音波エレクトロニクスの基礎と応用に関するシンポジウム (2019.11).

[11]　見崎貴史, 佐伯誠哉, L. Bustamante, 新実信夫, 千葉恒, 松川真美, "ヒト大腿骨の CT データを用いた大腿骨頸部の超音波集束シミュレーション", 第 40 回超音波エレクトロニクスの基礎と応用に関するシンポジウム (2019.11).

[12]　佐伯誠哉, 見崎貴史, <u>L. Bustamante</u>, 長谷芳樹, 千葉恒, 松川真美, "長骨中の
超音波照射制御シミュレーション", 第 40 回超音波エレクトロニクスの基
礎と応用に関するシンポジウム (2019.11).

OTHERS

[1]　<u>L. Bustamante</u>, M. Matsukawa, "超音波の音速測定方法および装置", 特願
2020-089270.